NASA Technical Memorandum 78747

# SAM II GROUND-TRUTH PLAN -
# CORRELATIVE MEASUREMENTS FOR THE STRATOSPHERIC AEROSOL MEASUREMENT-II (SAM II) SENSOR ON THE NIMBUS G SATELLITE

(NASA-TM-78747) SAM-2 GROUND-TRUTH PLAN: CORRELATIVE MEASUREMENTS FOR THE STRATOSPHERIC AEROSOL MEASUREMENT-2 (SAM 2) SENSOR ON THE NIMBUS G SATELLITE (NASA) 118 p HC A06/MF A01 CSCL 04A G3/46 N78-27689 Unclas 25225

P. B. RUSSELL, M. P. MCCORMICK, L. R. MCMASTER, T. J. PEPIN, W. P. CHU, AND T. J. SWISSLER

JUNE 1978

National Aeronautics and Space Administration

Langley Research Center
Hampton, Virginia 23665

CONTENTS

## ILLUSTRATIONS

TABLES

**ACKNOWLEDGEMENTS**

We are grateful to a number of individuals who have assisted in developing this Plan William Cross of the Office of Naval Research, Minneapolis Branch, compiled an extensive data base on meteorological conditions at many high latitude sites. Edward Harrison, William Fuller, and Samuel Sokol, all of NASA Langley Research Center, provided support for SAM-II mission analysis, airborne lidar analysis, and aircraft procurement and flight planning, respectively. Todd Cerni of the University of Wyoming developed the model atmospheres used in simulating instrument and data processing performance. John Livingston of SRI International ran the lidar performance simulations Gerald Grams of Georgia Institute of Technology and Benjamin Herman of the University of Arizona, both members of the SAM-II Nimbus Experiment Team, reviewed the manuscript and provided helpful comments

Linda Jones and Vivian Griswold of SRI International prepared the text and tables and provided invaluable coordination

# 1. INTRODUCTION

## 1.1. SAM-II Measurements and Ground Truth Requirements

The SAM-II (Stratospheric Aerosol Measurement) sensor is scheduled for launch on the Nimbus G satellite in August 1978. Its mission is to measure vertical profiles of aerosol extinction in high latitude bands of the Northern and Southern Hemispheres. The sensor is a one-channel sunphotometer, centered at wavelength 1.0 $\mu$m, which views the sun through the earth's atmosphere during spacecraft sunrise and sunset events, as shown in Figure 1. (The instrument is described in more detail in Appendix A.) The time-dependent radiance thus measured during each event will be combined with spacecraft ephemeris data and a local atmospheric density profile, and then numerically inverted to yield a vertical profile of aerosol extinction above the earth tangent point. (Details of the inversion process are given by McCormick et al., 1976, GSFC, 1976, and Chu et al., 1977.) The expected Nimbus G orbit is such that the tangent points are confined to the latitude bands 64° - 80° N and S, as indicated in Figures 1 and 2.

The SAM-II data products (vertical profiles of aerosol extinction and inferred number density) will be archived (GSFC, 1975) and made available for use in scientific investigations. However, before being released, the data must be validated by comparisons with correlative measurements made by sensors of appropriate accuracy, resolution, and reliability. To avoid confusion and compromising the integrity of the SAM-II data, the accuracy and resolution of correlative sensors should, if possible, be equal to or better than that expected from SAM-II.

The expected performance of SAM-II is indicated by Figures 3-5, which show results of inversions using a typical SAM-II inversion algorithm with simulated radiance data and simulated errors of the magnitude expected for a typical measurement cycle. (The errors arise both from the instrument and from the molecular density estimation process. Instrumental errors, which include both radiometric measurement and pointing, are described in Appendix A.) The aerosol models used in Figures 3 and 4 are representative of high-latitude nonvolcanic conditions, having been derived (Pepin and Cerni, 1978) from 2-channel dustsonde measurements made at Pt. Barrow, Alaska (71°N) in November 1973, and at McMurdo, Antarctica (78°S) in January, 1975, respectively (Rosen et al., 1975). Nonvolcanic aerosol conditions have been most prevalent during the past 15 years (e.g. Hofmann et al., 1976, Russell and Hake, 1977), and thus the models in Figures 3 and 4 approximate the most probable stratospheric aerosol conditions to be encountered by SAM-II. On the other hand, the model used in Figure 5 is representative of moderate volcanic conditions, having been derived from coordinated measurements made over Kansas City (39°N) in July 1975 (e.g., Pepin, 1977) about 9 months after the 1974 major eruption of the volcano Fuego in Guatemala. Because a similar eruption may increase stratospheric aerosol concentrations during the SAM-II mission, it is important to simulate SAM-II performance under such conditions. (Note that the January 1975 antarctic observations, although made three months after the Fuego eruption, were apparently unaffected by it, because of the great intervening distance, the short intervening time, and the lack of cross-hemispheric circulation during the season just after the eruption.)

The results shown in Figures 3-5 indicate the resolution and accuracy to be expected from SAM-II inversions. Notice first that the vertical resolution of each inverted profile is about 1 km. This resolution is achieved by virtue of two factors: (1) the narrow field of view - 0.6 arc min - of the radiometer and (2) the sharply peaked weighting functions for the limb-viewing geometry. The limb weighting functions do, in fact, depend on aerosol conditions, which can produce significantly poorer vertical resolution at certain times and heights. Nevertheless, a vertical resolution of 1 km is a useful target specification for ground-truth measurements. Notice further that, even for nonvolcanic or background aerosol conditions (which are highly likely), the expected relative error in extinction coefficient is less than or equal to 10% over virtually all of the region where particulate extinction exceeds about 50% of gaseous Rayleigh extinction. (The error bars in Figures 3-5 were derived by performing the inversion for 10 different cases of simulated random errors and taking the standard deviation of the resulting set of solutions.)

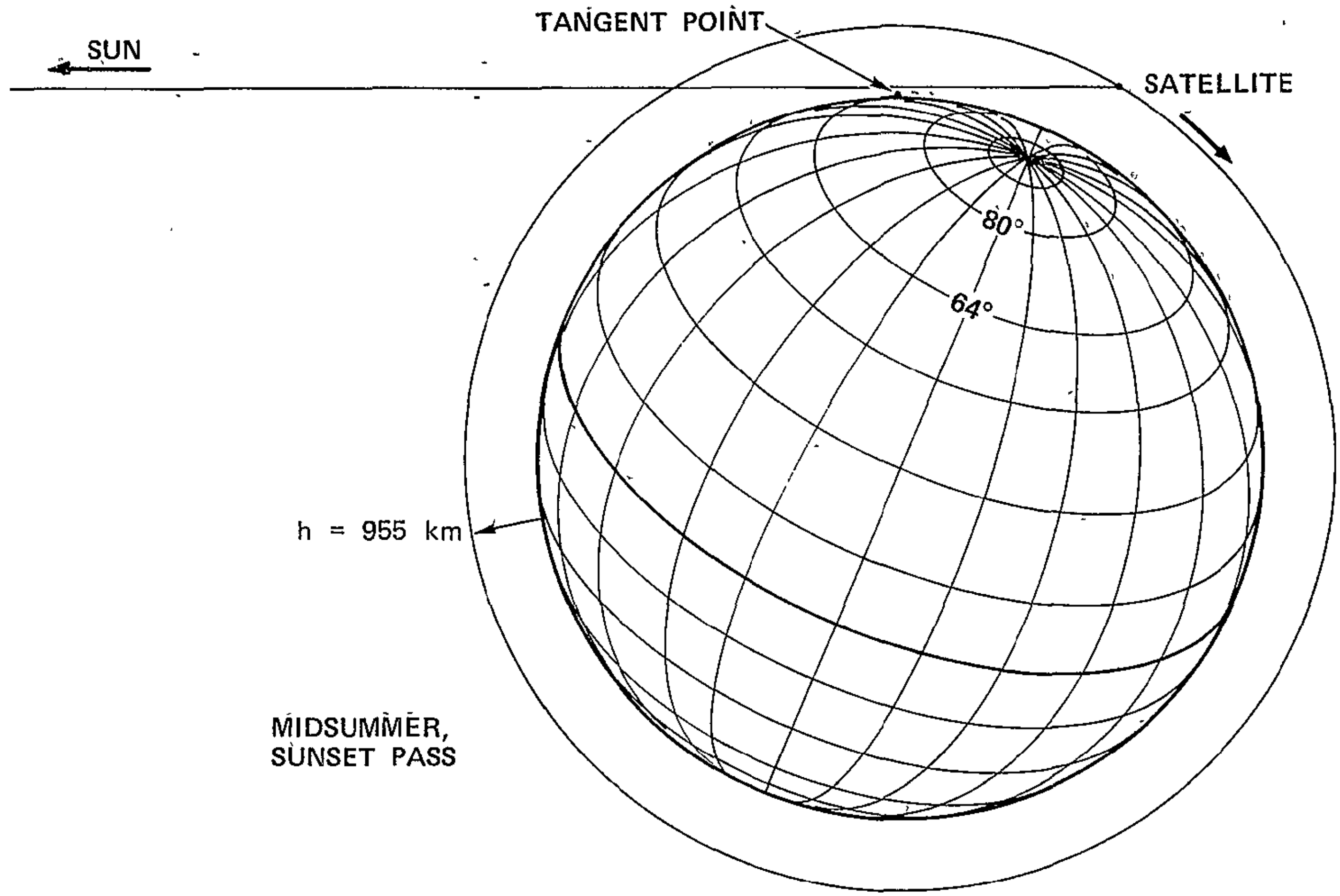


SA-5557-6

FIGURE 1 SAM-II ORBITAL AND VIEWING GEOMETRY

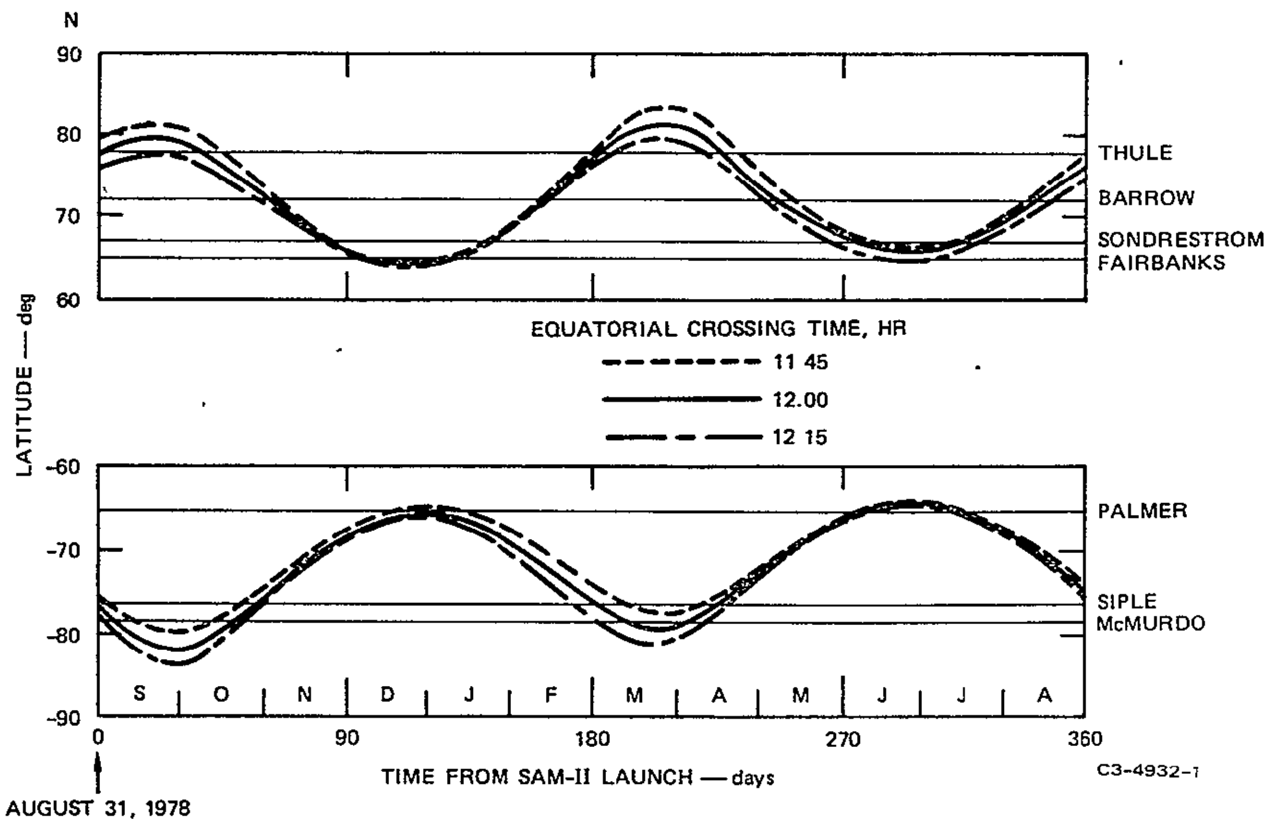


FIGURE 2 LATITUDE COVERAGE OF SAM-II TANGENT POINTS FOR SUN-SYNCHRONOUS HIGH-NOON ORBIT. Effect of changing equatorial crossing time on tangent location dates is shown by dashed curves

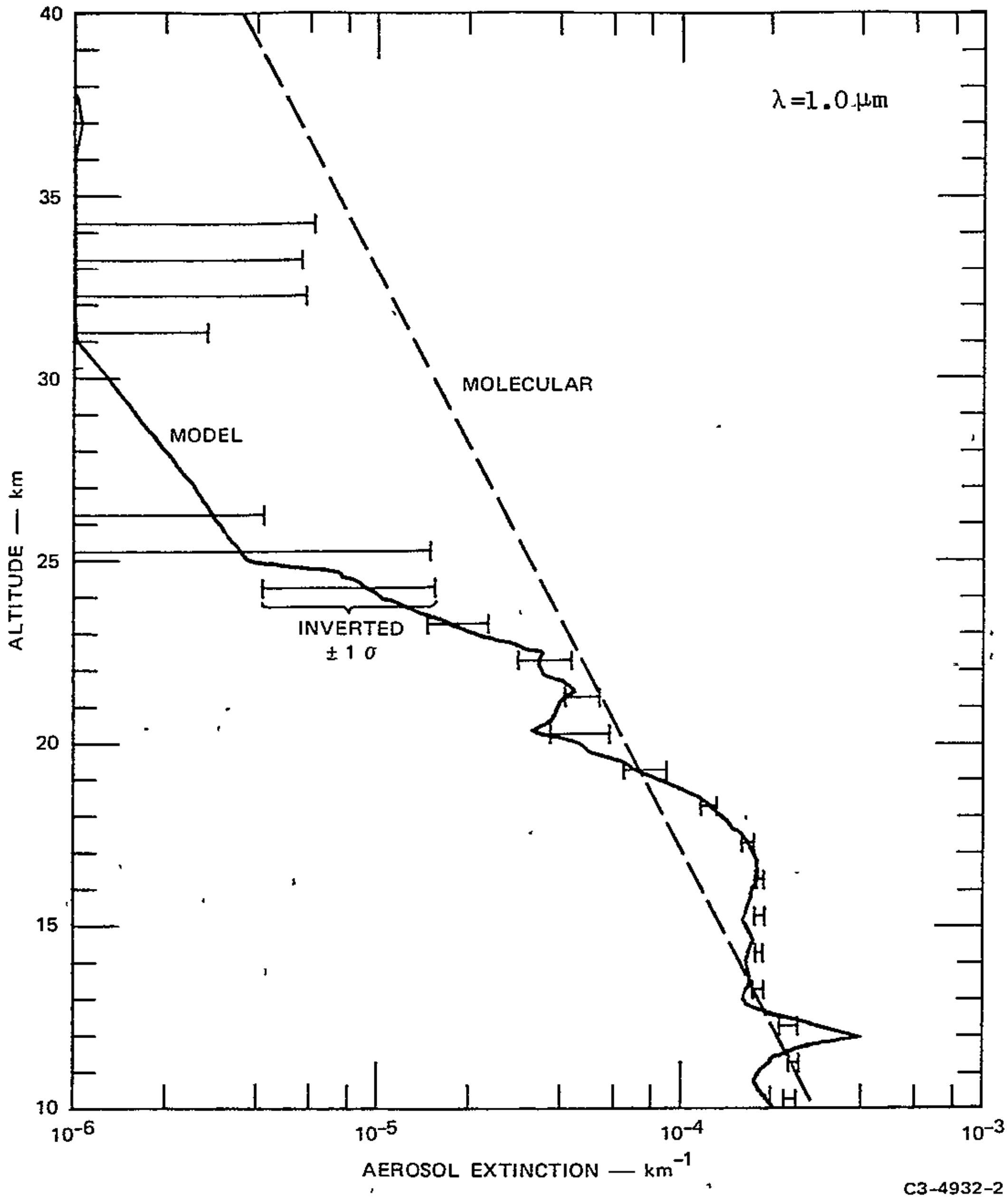


FIGURE 3 COMPARISON OF B-10 (ARCTIC NONVOLCANIC) MODEL PROFILE OF PARTICULATE EXTINCTION WITH RESULTS INVERTED FROM SIMULATED SAM-II RADIANCE DATA AND MOLECULR DENSITY DATA Error bars show ± one standard deviation about the mean of inverted solutions for ten independent simulations with different random errors All simulations assumed probable errors of 3% for molecular density, 3 arc seconds for pointing, and 0.5% (of signal) for radiometric measurement All radiometric data were quantized to 10-bit A/D accuracy

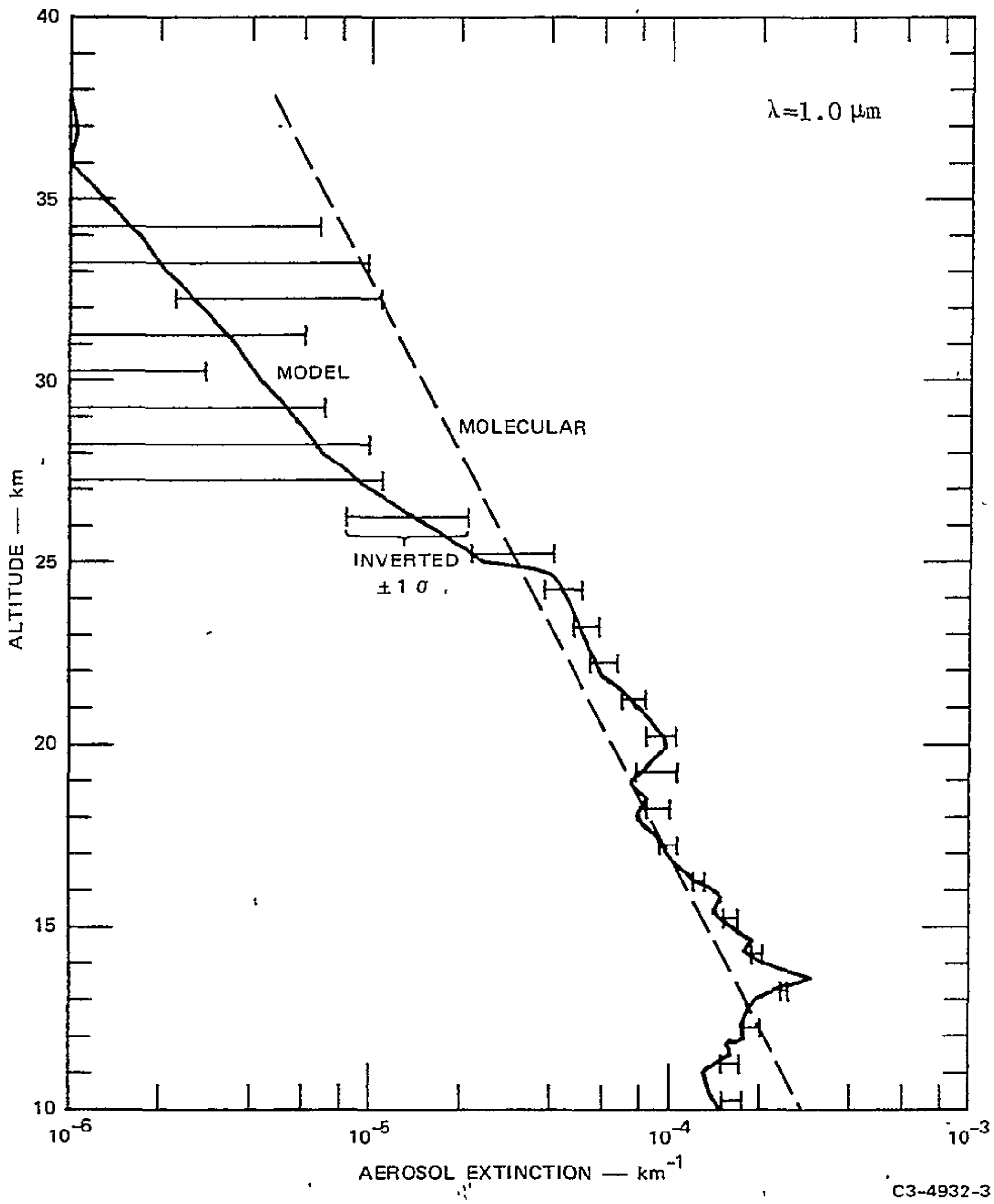


FIGURE 4 AS IN FIGURE 3, BUT FOR THE A-14 (ANTARCTIC NONVOLCANIC) MODEL ATMOSPHERE

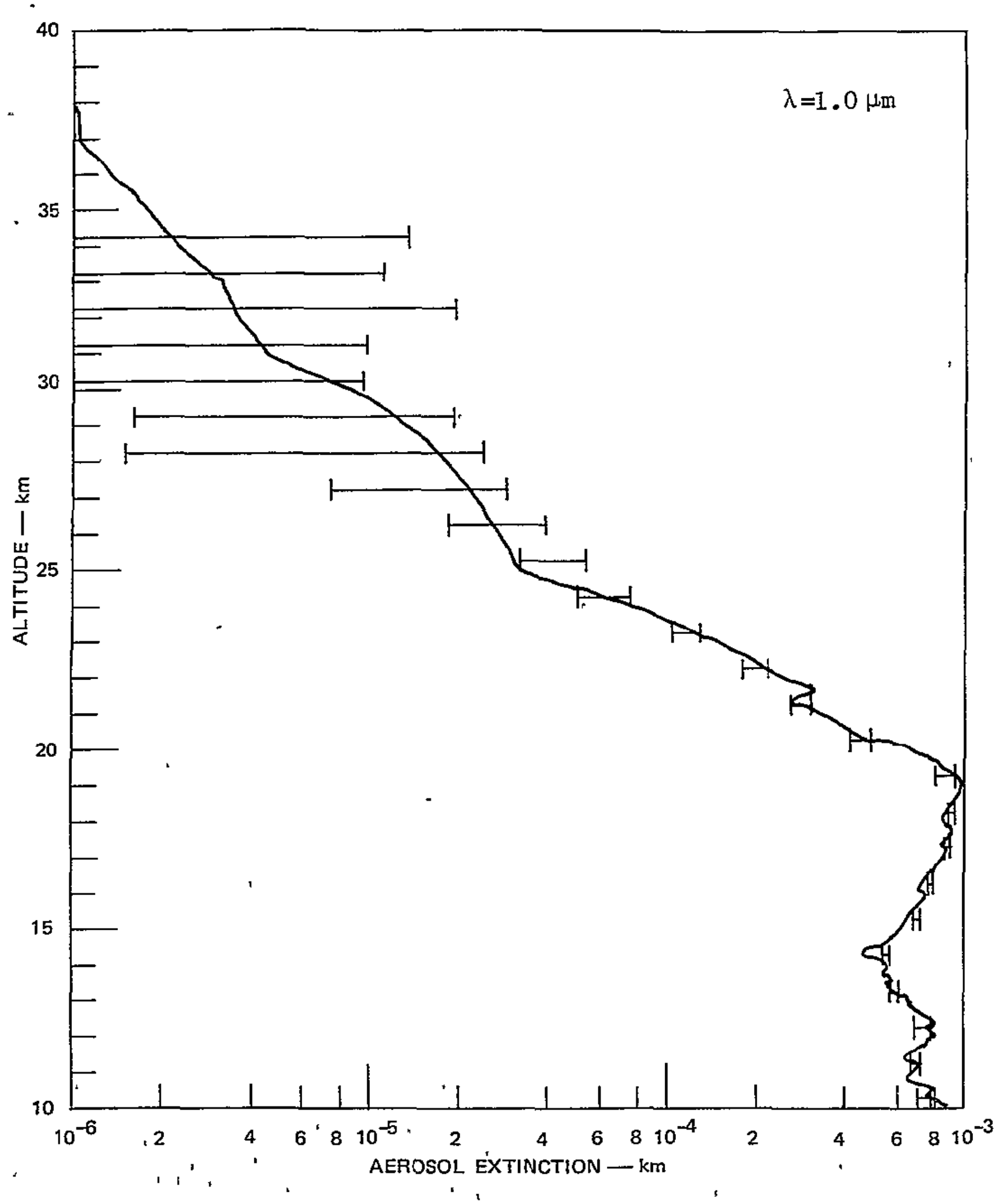


FIGURE 5 AS IN FIGURE 3, BUT FOR THE ASTP (MIDLATITUDE MODERATE VOLCANIC) MODEL.

From the above it can be seen that ground-truth measurements for SAM-II data validation must provide a vertical profile of an aerosol parameter (preferably, particulate 1 0-$\mu$m extinction) at the time and tangent point of SAM-II scans The profile should extend from cloud tops (below which SAM-II cannot view) to heights of 40 km (and above, if possible). The measurements should have a vertical resolution of 1 km or better, and the particulate parameter measured should be accurate to 10% or better over the height range where particulate 1 0-$\mu$m extinction exceeds about 50% of molecular 1 0-$\mu$m extinction (For nonvolcanic conditions this includes approximately the 10-23 km range, depending on latitude.) Moreover, for ground-truth sensors that do not directly measure particulate extinction at a wavelength of 1 0 $\mu$m, the quantity measured should be such that uncertainties in converting to 1 0-$\mu$m extinction are as small as possible (In some cases ground-truth measurements themselves can be used to assess and reduce these uncertainties) It would also be desirable to check aerosol horizontal homogeneity along the SAM-II viewing path, since this homogeneity is assumed by the SAM-II inversion algorithms In addition, data should be obtained in both the Northern and Southern Hemispheres, because of a basic difference in the way SAM-II measurements are made in each hemisphere--i.e all Northern Hemisphere measurements are sunset measurements, and all Southern Hemisphere measurements are sunrise measurements

One further prerequisite of the ground-truth measurements is that they must have a very high probability of data capture at the times and locations of SAM-II tangent scans This prerequisite stems from the facts that (1) the SAM-II tangent points move from day to day, making it difficult to repeat missed opportunities, and (2) the SAM-II data must be validated and archival begun within six months after the launch date As will be seen, this prerequisite of high data capture probability strongly impacts ground-truth planning, because of the limited ground sites and frequent adverse weather in the 64° - 80° latitude bands covered by SAM-II

## 1.2. Overview of Ground Truth Plan

On the basis of the prerequisites listed in the preceeding section, the members* of the SAM-II Nimbus Experiment Team (NET) have assigned the following priorities (in decreasing order) to each element of the ground-truth plan

1. Airborne Lidar (development and use)
2. Dustsondes (use)
3. Balloonborne Sunphotometer (development and use)
4. Practice Comparative Experiment (using the above three sensors)
5. Airborne Polar Nephelometer and Impactors (use)

Development and use of an airborne lidar has been assigned top priority because

- No other technique can give an exact ground point comparison with SAM-II vertical profiles
- No other technique can provide data over the same atmospheric path that SAM-II measures
- Airborne lidar permits a measurement regardless of cloud cover (below airplane) or ground weather conditions.
- Airborne lidar allows quick reaction to targets of opportunity (e g volcanic injections)

* The members are Dr M P McCormick (leader), NASA Langley Research Center, Dr G W Grams, Georgia Institute of Technology, Dr B M Herman, University of Arizona, Dr T J Pepin, University of Wyoming, and Dr P B Russell, SRI International

- Southern hemisphere (antarctic) measurements can be made with the same advantages as listed above.
- Airborne lidar provides the same capabilities for SAGE* ground-truth over oceans or remote areas.

As described in Section 2 2 1, a suitable airborne lidar is now being developed at the Langley Research Center.

Dustsondes (balloonborne optical particle counters) are well-developed and tested instruments that have been flown from many sites by the University of Wyoming and collaborators for many years (e g Rosen, 1974; Pinnick and Hofmann, 1973, Hofmann et al, 1975; Rosen and Hofmann, 1975) Dustsondes have the required vertical resolution and accuracy (up to about 25 km, see also Section 2 1.1.) and have in fact provided the largest data set of stratospheric aerosol vertical profiles yet available from a single sensor design

A balloonborne sunphotometer is now being developed by Dr. T J. Pepin at the University of Wyoming It is the only correlative sensor that will provide a direct measurement (albeit not entirely out of the atmosphere) of 1.0 $\mu$m extinction, which is the quantity measured by SAM-II Its expected performance is described in Section 2 2.3.

A practice comparative experiment, using the airborne lidar, a dustsonde, and the balloonborne sunphotometer, is scheduled for August 1978 at Laramie, Wyoming The objectives are to.

- Provide a test for the newly-developed sensors
- Establish and practice multi-sensor and multi-platform coordination procedures.
- Provide a test for ground-truth data-reduction procedures and algorithms
- Practice data-intercomparison procedures

More detailed plans for the practice comparative experiment are given in Section 3 1.

Optical properties of the stratospheric aerosol, including size distribution and complex refractive index (and ideally particle shape), must be known in order to convert the SAM-II extinction profiles to profiles of particle number (an archived quantity) and also to convert the various correlative measurements to 1.0-$\mu$m extinction profiles The purpose of the airborne polar nephelometer and impactor measurements is to supply information on these optical properties The reason that these airborne measurements have been given a rather low priority is that they do not very easily yield vertical profile information, which is a fundamental prerequisite for the SAM-II corroborative data set. Moreover, recent measurements (some of which are continuing) have provided appreciable information on stratospheric aerosol optical properties, at least for nonvolcanic conditions. (For example, a predominant composition of about 75% sulfuric acid and 25% water seems rather stable for nonvolcanic conditions, and the continuing dustsonde flights provide a two-channel measurement which yields some size information.)

For these reasons only limited SAM-II funds have been allocated for nephelometer and impactor flights. However, the investigators who fly these instruments routinely, such as Gerald Grams of Georgia Institute of Technology, David Woods of LRC, and Guy Ferry of NASA Ames Research Center, have been encouraged to coordinate their flights with SAM-II measurements whenever their schedules and funding permit For example, Gerald Grams has been granted NCAR sabreliner flight time to conduct polar nephelometer and other in-situ measurements at Sondrestrom during the November 1978 Sondrestrom experiment, and has requested NCAR sabreliner time for the July 1979 experiment (see Table 15) Any data acquired in this manner will be used as part of the SAM-II correlative data set and in converting SAM-II extinction profiles to particulate number profiles

---

* SAGE (Stratospheric Aerosol and Gas Experiment) is a multichannel, later-generation version of SAM-II It will measure aerosol and ozone profiles in the approximate latitude band 79° N to 79° S Launch is tentatively scheduled for January 1979 See McCormick et al, 1976

In addition to the nephelometer and impactor programs, several other ongoing measurement programs are expected to provide stratospheric and mesospheric aerosol information in the high-latitude bands during SAM-II's lifetime These programs and the expected use of their data are described in Section 2 1

Table 1 shows the overall schedule for development and execution of the ground-truth plan The results of completed milestones of this schedule are presented at appropriate points in the remainder of this report

Detailed schedules, flight plans, and the site-selection rationale for all ground-truth measurements are given in Section 3 2 Here we present a brief overview Following the practice comparative experiment, the initial ground-truth experiment, to employ the airborne lidar, the balloonborne sunphotometer, and dustsondes is planned for late November 1978 at Sondrestrom, Greenland (67° N, 51° W, cf SAM-II's expected latitude in Figure 2) Subsequent ground-truth experiments are planned for other times and locations, including the Southern Hemisphere in mid-December 1978 and again at Sondrestrom in late May or early June, 1979 The second Sondrestrom experiment will occur after the launch of SAGE and will constitute the first SAGE/SAM-II comparison with ground-truth support

Table 1

SCHEDULE FOR DEVELOPMENT AND EXECUTION OF SAM-II GROUND-TRUTH PLAN

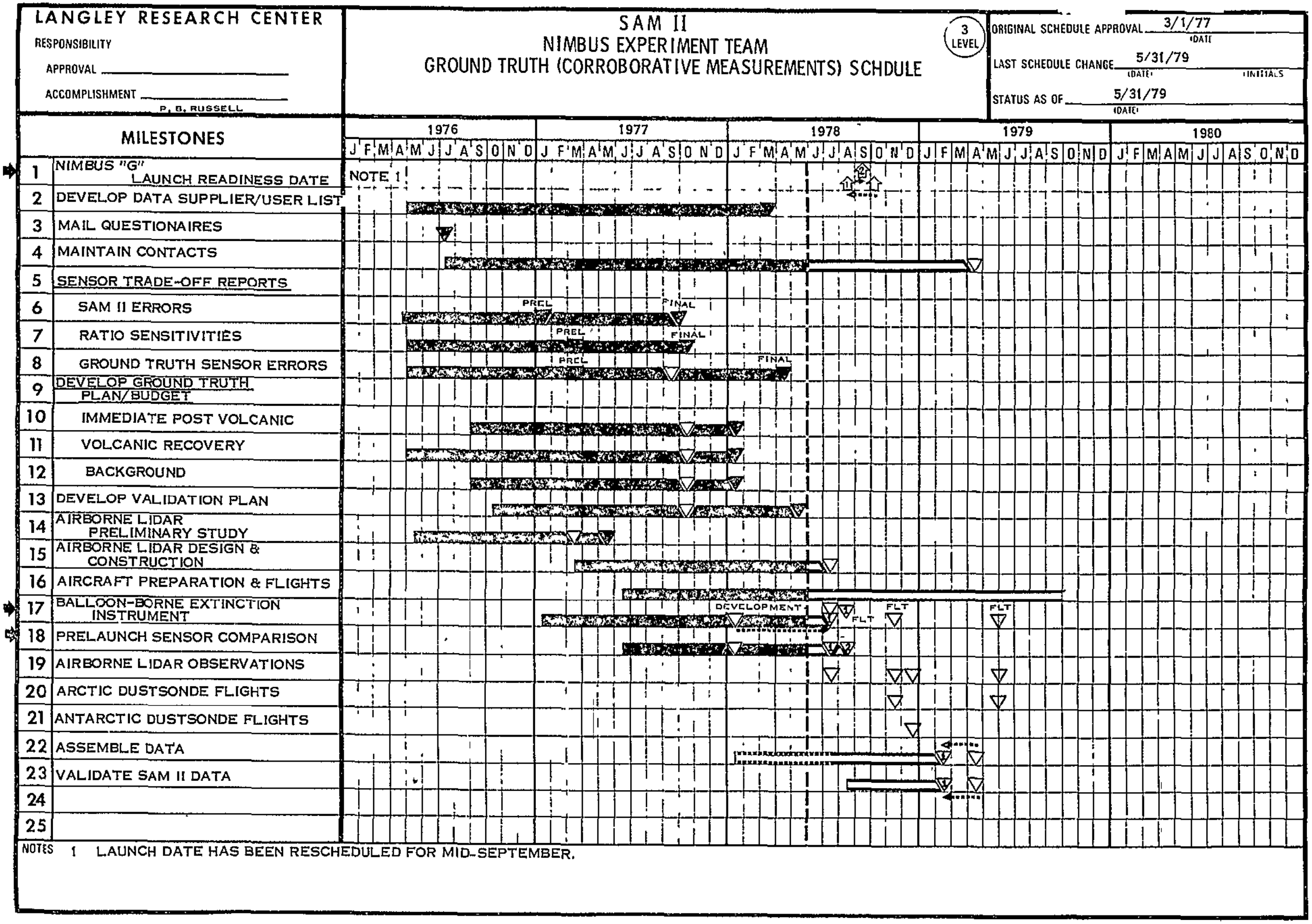

## 2. GROUND TRUTH SENSORS AND PROGRAMS

### 2.1. Existing Facilities and Programs

A mail survey was conducted in 1976 and 1977 to locate existing or planned programs that could provide data suitable for validating the SAM-II measurements. The rationale was to provide cost savings by using measurements that would already be available, thus ensuring that SAM-II ground-truth funds would support only collection of essential data unavailable from other sources. The survey letter, questionnaire, and results are shown in Appendix B. As those results show, the near-polar SAM-II latitudinal coverage (64° - 80° N and S) greatly reduces the global set of stratospheric and mesospheric aerosol observations to a very small subset that would be of limited use for SAM-II data validation This subset is described in the remainder of this section.

#### 2.1.1. Antarctic Dustsonde Measurements

Professor James Rosen of the University of Wyoming is conducting a program of dustsonde observations in the antarctic with support from the Atmospheric Research Section of the National Science Foundation The program continues through 1979 and is expected to provide several aerosol concentration profiles that will be useful for validation of SAM-II measurements Balloon launch sites currently in use are at McMurdo (77° 51'S, 166° 37'E) and the South Pole (90°S) Launches are scheduled between December and January. These sites and times, however, do not coincide with SAM-II coverage.

*Instrument and Operation Procedure*

Figure 6 shows a schematic drawing of the University of Wyoming balloonborne dustsonde that is planned for ground-truth in the SAM-II program Its mode of operation is as follows Air sampled on balloon ascent and parachute descent is pumped at approximately 0 75 liters/minute in a well defined stream through the focal point of the condenser lens in the 2 5-liter scattering chamber where the individual stratospheric aerosol particles scatter light into the microscopes. The light pulses that can be observed with the microscope are detected and amplified by the photomultipliers By pulse height discrimination and careful laboratory calibration with aerosols of known size and index of refraction the integral concentration of aerosol particles with radii greater than 0.15 and 0 25 $\mu$m can be determined

Two photomultipliers are used to enhance the signal-to-noise ratio by counting only coincident events from the two detectors. The background noise for the system is mainly due to Rayleigh scattering from air molecules in the chamber at low altitude and from cosmic ray scintillation in the photomultiplier glass at high altitude The coincidence of events from the two detectors removes the contribution due to the cosmic ray scintillation The background is measured approximately every fifteen minutes during the flight by passing filtered air through the chamber The background produced by the Rayleigh scattering is negligible above a 10 km altitude Below this altitude the measured corrections for the background are employed The dustsonde is also equiped with rawinsonde temperature elements for recording the vertical temperature profile

*Resolution and Accuracy*

Figure 7 shows a typical dustsonde-measured profile of particle number density. Notice that, below about 28 km, the vertical resolution is better than 1 km in both particle-size channels Professor Rosen has performed an analysis of the accuracy of dustsonde measurements (e g Hofmann et al., 1975) The major sources of error are counting statistics and possible variations in particle refractive index. The counting method and sensor channels are designed to minimize these errors, they result in typical uncertainties, in the stratosphere below 25 km, of about 8% for both Channels I and II ($r \geqslant 0$ 15 and 0 25 $\mu$m, respectively). Above 25 km, these errors tend to increase significantly, because of poorer counting statistics and less accurate measurement of the sampled air volume

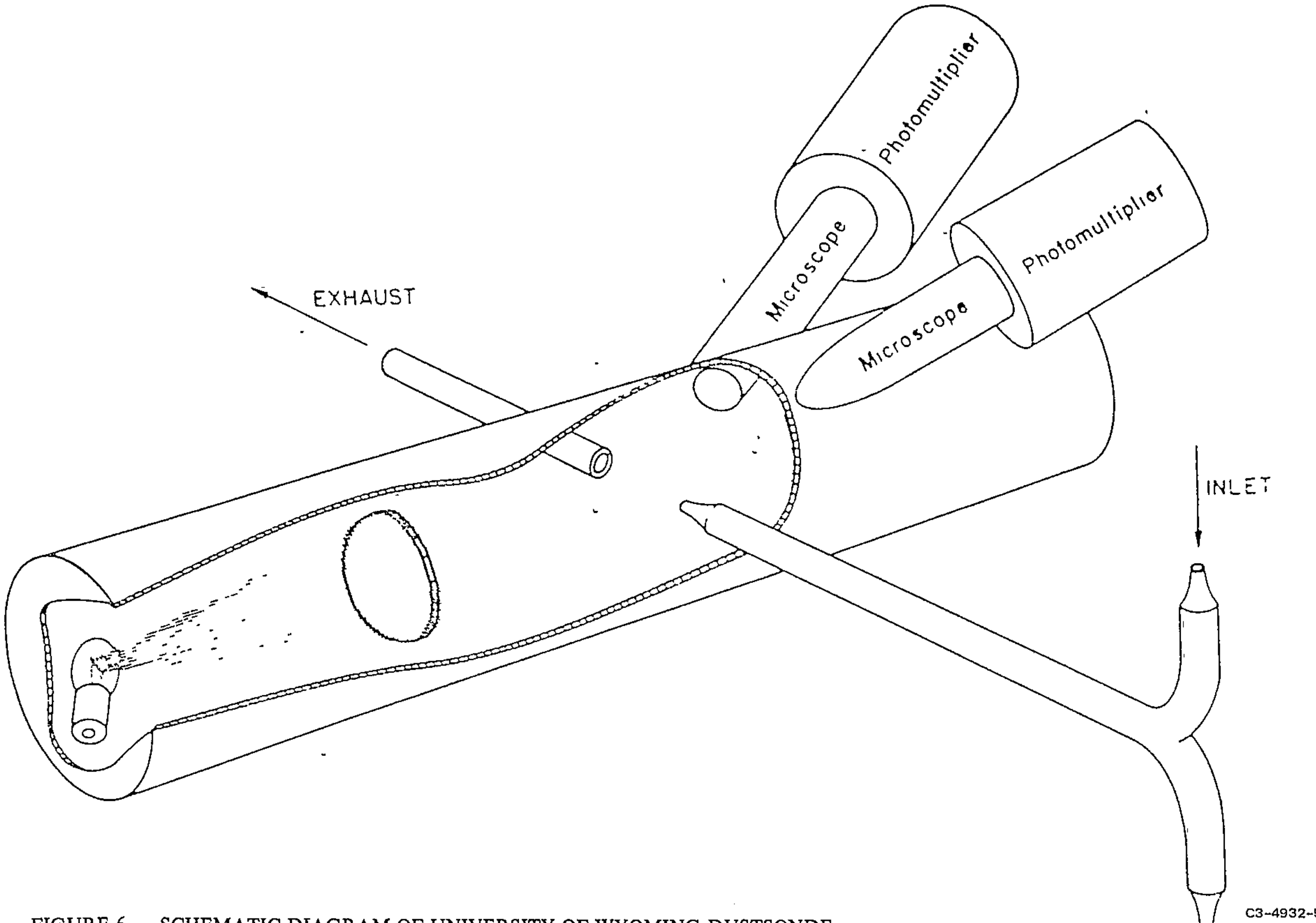


FIGURE 6 SCHEMATIC DIAGRAM OF UNIVERSITY OF WYOMING DUSTSONDE

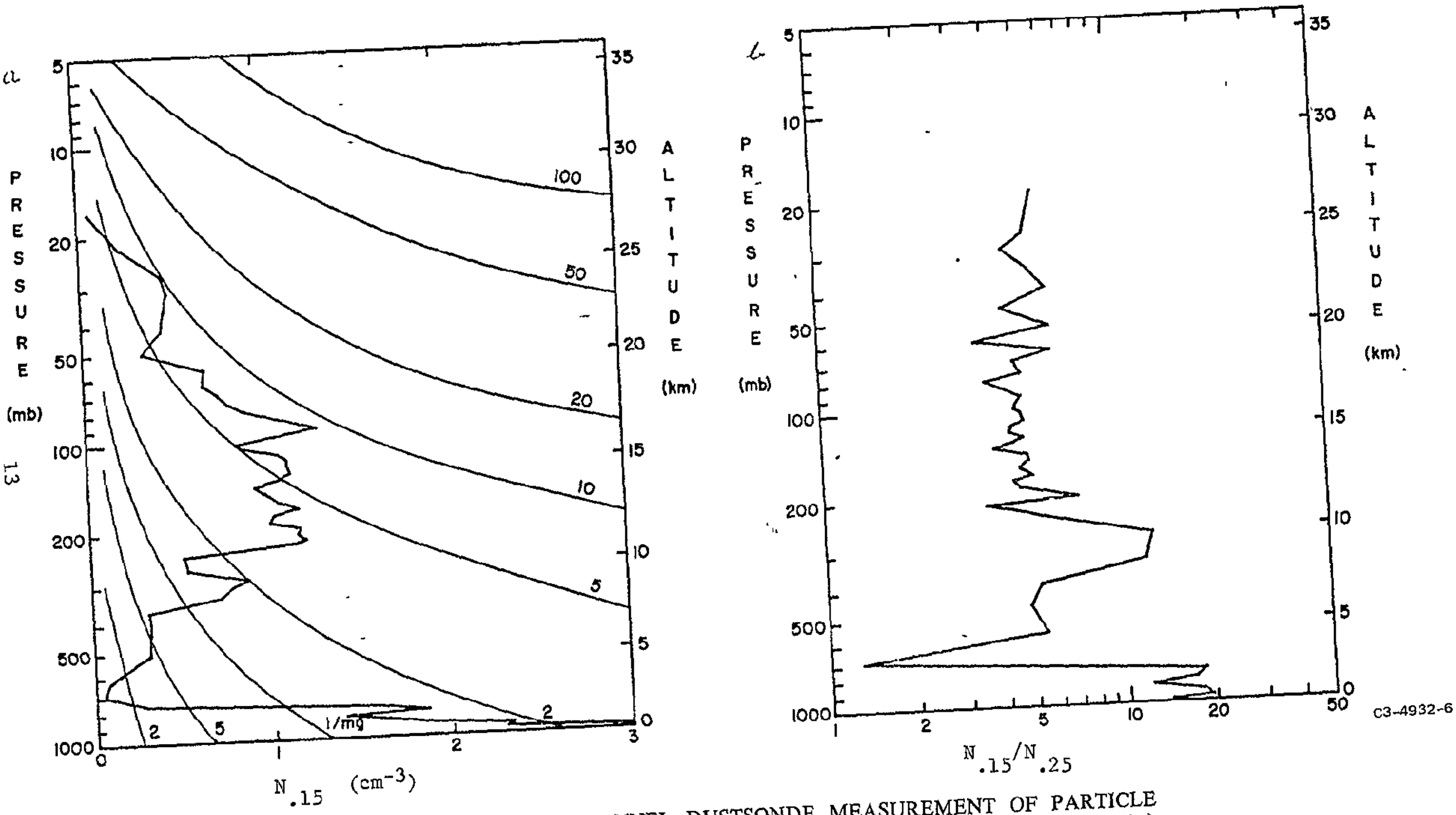


FIGURE 7 EXAMPLE OF 2-CHANNEL DUSTSONDE MEASUREMENT OF PARTICLE NUMBER DENSITY, OBTAINED AT MCMURDO STATION (78°S, 167°E) DURING NONVOLCANIC CONDITIONS (12 JANUARY 1973). a) Number of particles with radius ⩾0.15 μm ($N_{.15}$, measured by Channel I) Curves are lines of constant mixing ratio (particle number per mg of air) b) Ratio of numbers of particles measured by channels I and II $N_{.25}$ is number of particles with radius ⩾0.25 μm, and is measured by Channel II. Ratio data are plotted at heights where Channel II data are available. $N_{.15}$ data are interpolated at these heights in computing ratios

Dustsonde measurements can be converted to an estimated particulate 1 0-$\mu$m extinction coefficient by using an assumed refractive index and a two-parameter size distribution fitted to the two-channel dustsonde data Figure 8 shows the dependence of the conversion ratio on optical model properties. (The size distribution functions and refractive indices shown have been derived from measurements by various investigators--e g Hofmann et al., 1975; Toon and Pollack, 1976, Harris and Rosen, 1976, Swissler and Harris, 1976 However, to generate the complete range of values shown for each curve, parameters were varied, sometimes beyond the range of observations Note that observations of $N_{15}/N_{25}$ less than 2 are very rare, and average values for stratospheric layers several km thick are typically between 3 and 5.) In a given dustsonde measurement, the channel ratio, $N_{15}/N_{25}$, is known, but the particle size model and refractive index can in general only be estimated on the basis of previous measurements. Thus the uncertainty in conversion ratio is given by the vertical spread in the curves above the measured value of $N_{15}/N_{25}$ As can be seen, the uncertainty in converting a two-channel dustsonde measurement to 1.0-$\mu$m extinction is thus about ±25% if particle composition is unknown, and about ±15% if the refractive index is known to be one of the two values shown in Figure 8 (i e either silicate or aqueous sulfuric acid composition) A similar conclusion was obtained by Pepin and Cerni (1977)

### 2.1.2. Noctilucent Cloud Sightings

The International Noctilucent Cloud (NLC) Program, in cooperation with the World Meteorological Organization, records and collates observations of noctilucent clouds (particulate layers in the 73-95 km altitude region) Mr. E J Truhlar of the Canadian Atmospheric Environment Service (AES) collects observations from 60 Canadian and 16 U.S. stations, and Dr D H McIntosh of the University of Edinburgh (UE) collects them for western Europe We have made arrangements to receive tabulations of sightings (with about one month's delay) from the AES and UE and will attempt to make similar arrangements with others. Sample tabulations, relevant correspondence, and a description of the observation charactersitics are given in Appendix C.

*Resolution and Accuracy*

Bronshten and Grishiken (1975) estimate that the height accuracy of the "best" NLC measurements is better than 1 km (see also Appendix C) Presumably the "best" measurements are those made with aligned cameras or visually with theodolites Many sightings are made with the unaided eye, and their height accuracy is probably considerably worse than 1 km Uncertainties in the size distribution and shape of NLC particles, together with the uncalibrated brightness scale of observations, make conversion of sightings to 1.0-$\mu$m extinction coefficients extremely approximate at best The purpose of the NLC sightings will be to provide time and location data for comparison with any layers detected by SAM-II in the 73-95 km region Because of the paucity of other particulate data in this height region, the NLC data are considered an important source of ground-truth information

(An attempt will also be made to obtain useful lidar data in the 73-95 km region See Section 2 1 4.)

### 2.1.3. NOAA Point Barrow Lidar

Dr Ronald Fegley of the NOAA Wave Propagation Laboratory (Boulder, CO) is developing a dye lidar for installation at Point Barrow, Alaska (71° 20' N, 156° 38' W) as part of NOAA's Geophysical Monitoring for Climatic Change Program. Starting in Spring 1978, observations extending into the stratosphere are planned on a weekly basis, cloud cover permitting We intend to include such data as are made available in the SAM-II ground-truth data set when this is appropriate. However, the high probability of cloud cover at Point Barrow makes the probability of data capture within the time window of a SAM-II overflight smaller than is acceptable for a primary ground-truth sensor. Moreover, the short wavelength (585 nm) of the lidar yields expected errors in measured particulate backscattering of greater than ±30% throughout the stratosphere during nonvolcanic background conditions. (These errors result

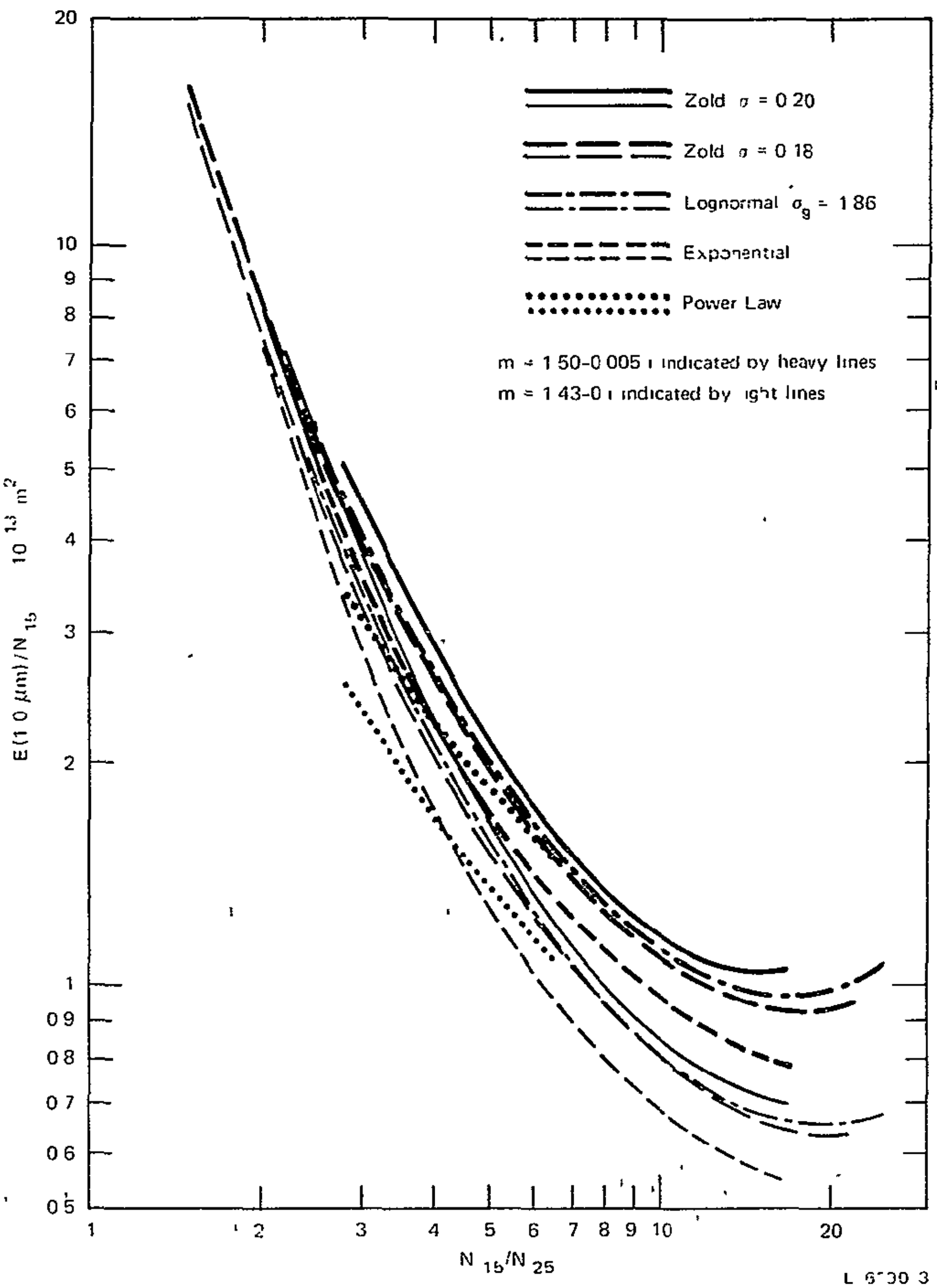


FIGURE 8 DEPENDENCE OF EXTINCTION-TO-NUMBER RATIO [E(1 0 $\mu$M)/$N_{.15}$] ON CHANNEL I/II RATIO ($N_{.15}/N_{.25}$), PARTICLE SIZE MODEL, AND REFRACTIVE INDEX

primarily from molecular density uncertainties, see also Section 2 2 1.) It is for these reasons that an airborne lidar of longer wavelength (694 or 1060 nm) is being developed specifically for SAM-II ground-truth measurements

### 2.1.4. CNRS Heyss Island Lidar

Dr. M L Chanin of France's Centre National de la Recherche Scientifique (CNRS) will conduct a program of noctilucent cloud observations by dye lidar techniques from Heyss Island (80.5°N), where a lidar station has been set up since 1975 for sodium measurements The observations, part of a joint Franco-Soviet program, are planned to start in June 1978, prior to the SAM-II launch. Dr. Chanin has agreed to make available to the SAM-II ground-truth program any NLC observations that are near to SAM-II scans in space and time

## 2.2. Facilities and Measurements Planned Especially for SAM-II

### 2.2.1. Airborne Lidar

An airborne lidar for SAM-II ground-truth measurements is now being developed at NASA Langley Research Center (LRC) The lidar design is based on a study by Evans (1977), with appropriate modifications by LRC personnel. Table 2 shows the design parameters (The decision to use a ruby or Nd-YAG laser--or both--has not yet been made, see below) Table 3 shows the organization of the airborne lidar project, and Table 4 shows the project schedule.

Several aircraft were considered for the lidar flights, including the NASA WFC P-3, the NASA JSC C-130, the NASA ARC CV990, the NCAR Electra, the NOAA C-130 and the NOAA WP-30 For various programatic reasons, the NASA WFC P-3 was chosen as the appropriate platform for the ground-truth program Costs and other logistic aspects of operating the P-3 at various ground-truth sites are described in Appendix D.

*Resolution and Accuracy*

Measurements with the NASA Langley 48" ruby system, the SRI 16" ruby-dye system, and the NCAR system, among others, have shown that stratospheric aerosol measurements can be made with a vertical resolution of 1 km or better (up to about 30 km) by accumulating photons for reasonable amounts of time The accuracy of the particulate backscattering coefficients derived from such measurements is a strong and complicated function of the laser wavelength, other lidar parameters, skylight background, aerosol concentration, proximity of nearest radiosonde sounding, validity of normalization procedures, and even the uncertainty in the ozone vertical profile To assess this accuracy for realistic situations, we have developed a computer program that simulates the measurement and data analysis process, as shown in Figure 9. (A parameter shown in Figure 9 is the scattering ratio, R, a central quantity derived in the analysis of stratospheric lidar data. It is defined as $R \equiv (B_p + B_g)/B_g$, where $B_p$ and $B_g$ are respectively the particulate and gaseous backscattering coefficients)

At each appropriate step of the simulation, the program computes the relative uncertainty in each derived quantity by using an analytical expression The sources of error include (1) photon counting error, (2) molecular density uncertainty, (3) aerosol and ozone transmission uncertainty, and (4) normalization uncertainty. As a check on the analytical expressions for error propagation, random number generators (symbolized by circles in Figure 9) are used to inject random errors from sources (1)-(3) at appropriate points of the simulation (Error (4), normalization, affects the whole derived profile in a systematic way, and should not be simulated by different random errors at each data point) Table 5 lists the sizes of the error sources used in the simulations. (Justification for the chosen error sizes is given by Russell et al, 1976a,b)

Lidar measurement and data processing errors were simulated for the same three model atmospheres as were used in simulating SAM-II performance (See Figures 3-5 and accompanying discussion) Figure 10 shows the first model atmosphere. The molecular density and particulate extinction profiles are as derived by Pepin and Cerni (1978) from the B-10

Table 2

DESIGN PARAMETERS OF AIRBORNE LIDAR

| *TRANSMITTER* | *RUBY* | *Nd:YAG* |
|---|---|---|
| WAVELENGTH($\mu$m) | 0.6943 | 1 06 |
| ENERGY PER PULSE (J) | 1.0 | 0.5 |
| REP RATE (pps) | 1 0 | 20 |
| PULSE WIDTH (n sec) | 30 | 20 |
| BEAM DIVERGENCE (mr) | 1.0 | 1 0 |
| BEAM DIAMETER (cm) | 8 | 7 6 |
| *RECEIVER* | | |
| DIAMETER (cm) | 36 | 36 |
| FIELD OF VIEW (mr) | 2 | 2 |
| FILTERBANDWIDTH (Å) | 10 | 10 |
| OPTICAL EFF TO PMT | 0.35 | 0 35 |
| PMT QUANT EFF. | 0 10 | 0 03 |
| *SKYLIGHT BACKGROUND* [w/(m² srÅ)]* | 2 x $10^{-4}$ | 1.3 x $10^{-5}$ |
| *DATA ACQUISITION* | | |
| BANDWIDTH | 1 - 2 5 MHZ | |
| ADC RATE | 10 MHZ (MAX) | |
| ADC RESOLUTION | 10 BIT | |
| ADC MEMORY | 2048 WORDS | |
| COMPUTER MEMORY | 32 K 16-BIT WORDS | |
| MAG TAPE | 45 IPS, 800 CPI, 9 TRACK | |

* For zenith-viewing lidar flying above 6 km, with sun near horizon

Table 3

ORGANIZATION OF AIRBORNE LIDAR PROJECT

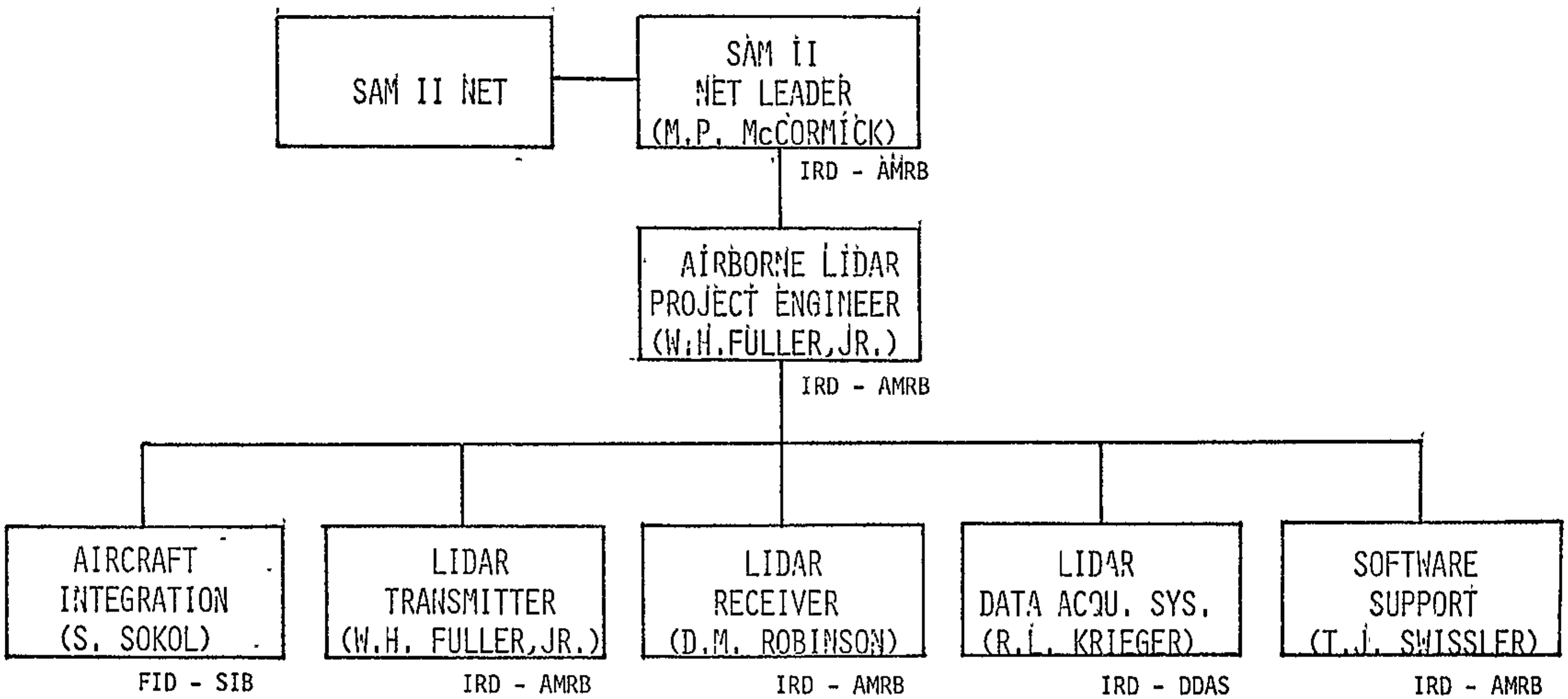


FID - FLIGHT INSTRUMENTATION DIVISION
IRD - INSTRUMENT RESEARCH DIVISION
AMRB - AEROSOL MEASUREMENTS RESEARCH BRANCH
DDAS - DIGITAL DATA ACQUISITION SECTION
SIB - SPACECRAFT INSTRUMENTATION BRANCH

Table 4

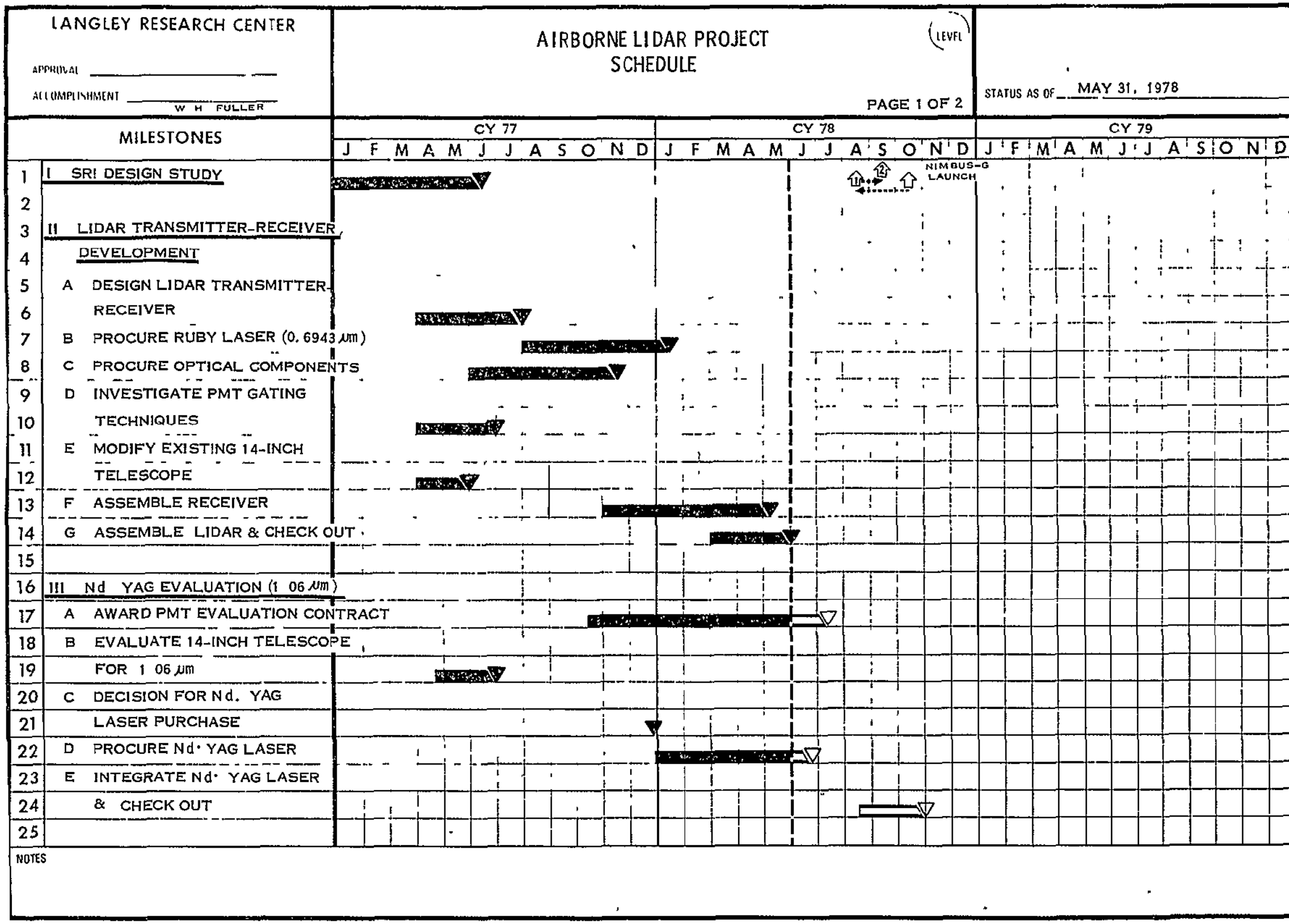
LANGLEY RESEARCH CENTER
APPROVAL
ACCOMPLISHMENT
W H FULLER
AIRBORNE LIDAR PROJECT SCHEDULE
LEVEL
PAGE 1 OF 2
STATUS AS OF MAY 31, 1978
MILESTONES
CY 77
CY 78
CY 79
J F M A M J J A S O N D
NIMBUS-G LAUNCH
1 I SRI DESIGN STUDY
2
3 II LIDAR TRANSMITTER-RECEIVER
4 DEVELOPMENT
5 A DESIGN LIDAR TRANSMITTER-
6 RECEIVER
7 B PROCURE RUBY LASER (0.6943 μm)
8 C PROCURE OPTICAL COMPONENTS
9 D INVESTIGATE PMT GATING
10 TECHNIQUES
11 E MODIFY EXISTING 14-INCH
12 TELESCOPE
13 F ASSEMBLE RECEIVER
14 G ASSEMBLE LIDAR & CHECK OUT
15
16 III Nd YAG EVALUATION (1 06 μm)
17 A AWARD PMT EVALUATION CONTRACT
18 B EVALUATE 14-INCH TELESCOPE
19 FOR 1 06 μm
20 C DECISION FOR Nd. YAG
21 LASER PURCHASE
22 D PROCURE Nd· YAG LASER
23 E INTEGRATE Nd· YAG LASER
24 & CHECK OUT
25
NOTES

Table 4 (Concluded)

LANGLEY RESEARCH CENTER

APPROVAL ____________

ACCOMPLISHMENT ____________ W. H. FULLER

# AIRBORNE LIDAR PROJECT SCHEDULE (Continued)

LEVEL

PAGE 2 OF 2

STATUS AS OF MAY 31, 1978

CY 77: J F M A M J J A S O N D — CY 78: J F M A M J J A S O N D — CY 79: J F M A M J J A S O N D

| | MILESTONES |
|---|---|
| 1 | IV DATA ACQUISITION SYSTEM |
| 2 | A DESIGN SYSTEM & WRITE SPECS |
| 3 | B PROCURE DATA SYSTEM |
| 4 | COMPONENTS |
| 5 | C ASSEMBLE SYSTEM & DEBUG |
| 6 | D INTEGRATE DATA SYSTEM |
| 7 | & DEBUG |
| 8 | E ACQUIRE LIDAR DATA & |
| 9 | DEVELOP SOFTWARE |
| 10 | |
| 11 | V AIRCRAFT INTEGRATION & |
| 12 | OPERATIONS |
| 13 | A DEFINE REQUIREMENTS & |
| 14 | SELECT AIRCRAFT |
| 15 | B MAKE NECESSARY MODIFICATIONS |
| 16 | C DESIGN & CONSTRUCT |
| 17 | AIRCRAFT MOUNT |
| 18 | D INSTALL LIDAR SYSTEM |
| 19 | E TEST FLIGHT & DEBUG |
| 20 | |
| 21 | |
| 22 | |
| 23 | |
| 24 | |
| 25 | |

NOTES

SIMULATION PROCEDURE

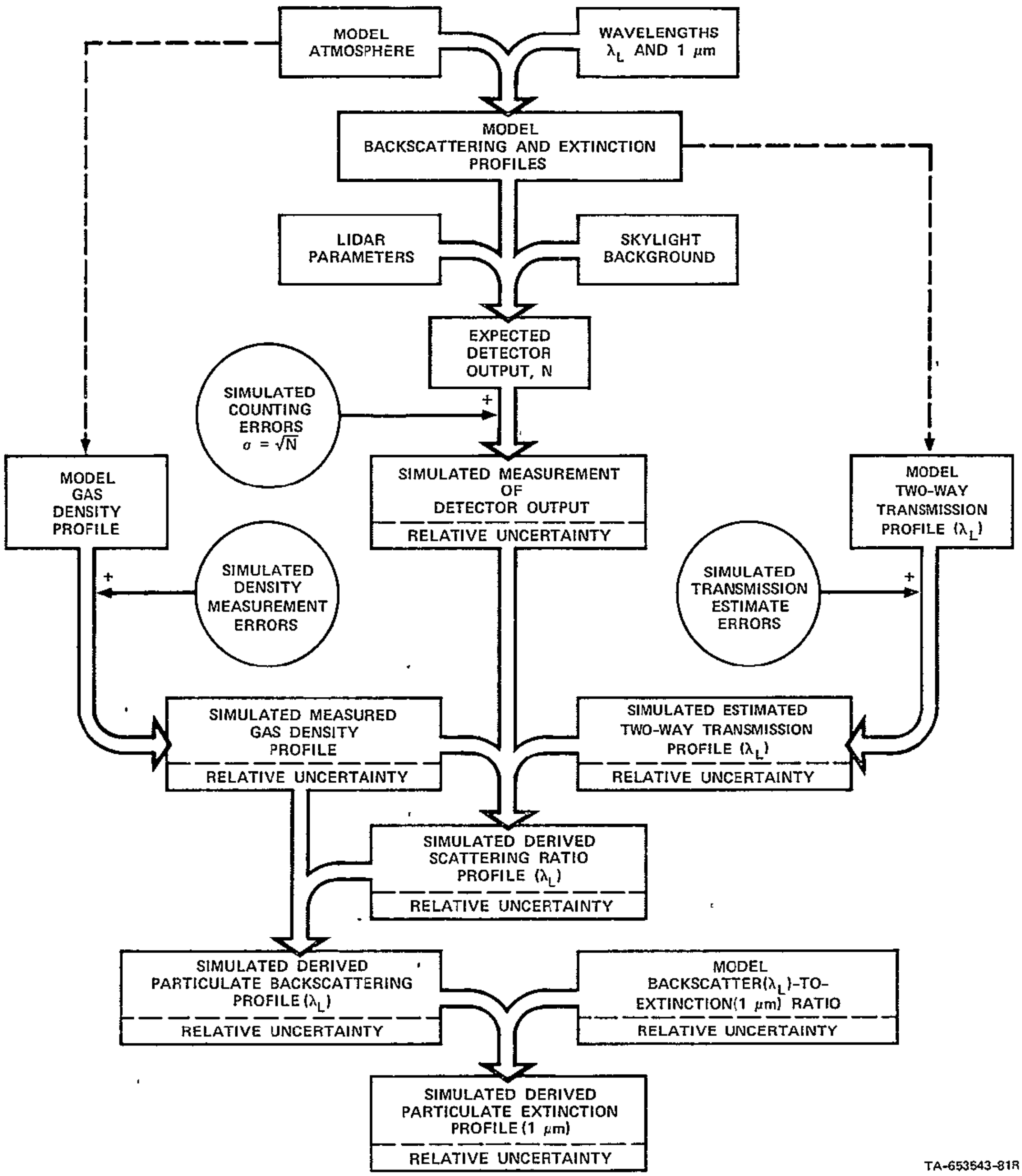


FIGURE 9 SIMULATION PROCEDURE FOR EVALUATING LIDAR MEASUREMENT ERRORS $\lambda_L$ is the lidar wavelength. Each simulation is also performed for the SAM-II wavelength, 1.0 $\mu$m Circles symbolize random number generators that inject simulated errors into derived quantities at appropriate steps of the computation

Table 5

ASSUMED SIZES OF ERROR SOURCES IN LIDAR DATA ANALYSIS

| Source | Relative Uncertainty |
| --- | --- |
| Detector Signal, S | $\frac{\sigma_S}{S} = \frac{\sqrt{S + B + I}}{S}$ |
| Molecular Density, D | $\frac{\sigma_D}{D} =$ 1% below 30 km* <br> 3% above 30 km |
| Two-way Transmission, $T^2$ | $\frac{\sigma_{T^2}}{T^2} = 0.4\ \tau_3^{+} + \tau_p$** |
| Normalization Constant, K | $\frac{\sigma_K}{K} = \mathrm{Min}\ [0.05(R_{max}-1),\ 0.025\ (\lambda_L/0.69\mu m)^{4.08-b}]$ ‡ |

Notes: B, I = Detector output resulting from background light and internal noise, respectively.

$\tau_3, \tau_p$ = One-way optical thickness of ozone and aerosol particles, respectively, between normalization altitude and altitude of analysis.

$R_{max}$ = Maximum scattering ratio in lidar profile being analyzed.

$\lambda_L$ = Lidar wavelength

b = Exponent of power-law approximation to wavelength dependence of particulate backscattering between 0.69 μm and $\lambda_L$. For most practical purposes $b \approx 1.8$.

---

* Assumes radiosonde density profile available within about 100 km and 6 hours of lidar measurement, and no intervening frontal activity.

† Assumes ±20% uncertainty in $\tau_3$.

** Assumes ±50% uncertainty in $\tau_p$.

‡ Based on typical aerosol concentration present at height of minimum mixing ratio in a long series of nonvolcanic and postvolcanic dustsonde measurements at Laramie, Wyoming, and on several ruby lidar-vs-dustsonde comparison experiments. The error sizes shown apply to the case in which the scattering ratio profile is normalized to force its minimum to equal the value expected from previous dustsonde measurements, rather than the value 1.00 commonly used. If instead $R_{min}$=1.00 is forced, the expected errors become asymmetric (always negative) and roughly twice as large.

B-10 MODEL ATMOSPHERE
(ARCTIC NONVOLCANIC CONDITIONS)

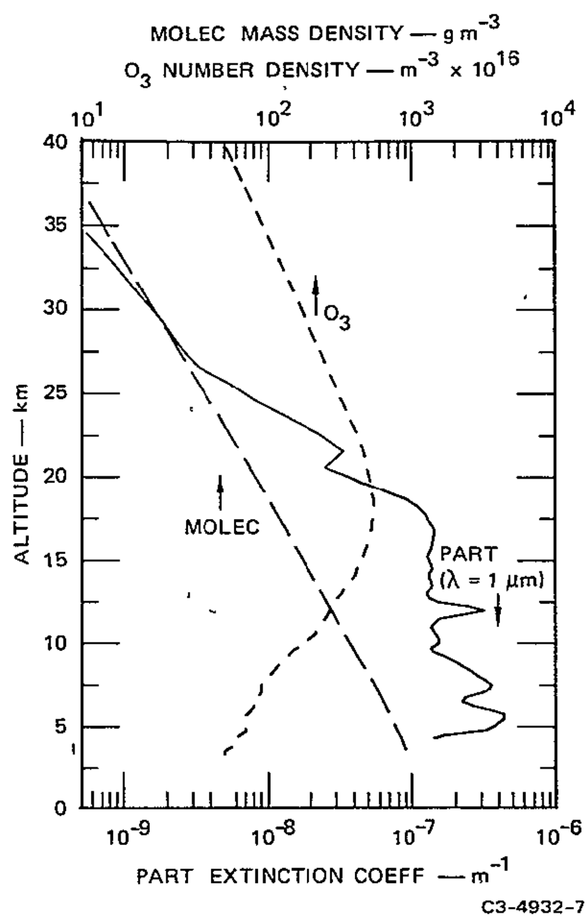


FIGURE 10 MOLECULAR DENSITY, PARTICULATE EXTINCTION, AND OZONE CONCENTRATION PROFILES FOR THE B-10 (ARCTIC NONVOLCANIC) MODEL ATMOSPHERE

November 1973 dustsonde measurement; the ozone profile is from an average of winter high-latitude observations compiled by Wu (1973) Figure 11 shows ruby ($\lambda$ = 0.69 $\mu$m) and Nd ($\lambda$ = 1.06 $\mu$m) profiles of scattering ratio, R, derived from the B-10 dustsonde measurement by Pepin and Cerni (1978) by fitting a two-parameter size distribution to the two-channel particle number data and assuming a composition of 75% $H_2SO_4$ and 25% $H_2O$ (refractive index 1.42-0i) Three points of Figure 11 are worthy of note First of all, the major peak in scattering ratio occurs rather low, at about 17 km, because of the high latitude of the observation (see e g Hofmann and Rosen, 1975) Second, because of this low height and the denser air there, the peak value of (R-1) for each wavelength is only about two-fifths as large as it would be if the peak were at 21 km (a typical midlatitude height) and about three-quarters as large as if the peak were at 19 km (a typical height for 67° N latitude, where the first ground-truth lidar flights will be made). And, third, note that all values of (R-1) for the Nd profile are about three times as large as for the ruby profile As will be seen, this latter factor tends to make the Nd measurement considerably more accurate than the ruby measurement, at least for the lidar parameters assumed in Table 2 and for high-latitude nonvolcanic model atmospheres (For model atmospheres with higher aerosol peaks or greater aerosol concentrations, some of the Nd advantage is lost, as will be shown.)

Figure 12 shows the expected scattering-ratio error bars derived by the simulation program (Figure 9) for the assumed ruby and Nd lidar parameters and the B-10 model atmosphere The simulations assume that both lidars are flying at a height of 4 km, a skylight background appropriate for zenith viewing from 4 km with the sun on the horizon (as it will be during SAM-II scans), and an integration time of one minute (For an airplane speed of 600 km/hr, this yields a horizontal resolution of 10 km ) Vertical range bins of 0 25 km are used, except at high altitudes where combining bins is necessary to reduce photon counting uncertainty (The lidar being built will be capable of range bins as small as 0 15 km, however, range bins of 0 25 km are more comparable to SAM-II's vertical resolution.)

Figure 13 shows how uncertainties in scattering ratio propagate to error bars in particulate backscattering coefficient. In addition, the dots show simulated measurements with all four sources of random error included, as a check on the error bar computation The scatter of simulated data points is approximately the same as the range of error bars, indicating that the error bar computation is at least approximately correct However, a closer look at the model (solid line), the simulated measurements (dots), and the error bars reveals two noteworthy points First, it can be seen that the error bars actually span a range that is slightly greater than the $\pm 1\sigma$ scatter of data points This occurs because the error bars include a contribution caused by normalization uncertainty, and normalization errors do not introduce scatter among different range bins, but instead affect all range bins systematically. Second, the simulated data points for each wavelength are systematically underestimated, such that most data points are less than the model, and by an amount that is slightly greater than one error bar Close inspection of this particular simulation revealed that this systematic underestimation was caused by the fact that the simulated density measurements at the normalization height (29-35 km) contained positive errors of greater than 1%, which, after normalization, were reflected as negative errors of the same size in all other range bins This type of density-induced normalization error was not included in the error bar calculations used to obtain the results shown, but the simulation program (Figure 9) does have the capability of including it at the user's option The question of whether or not to include this density-normalization uncertainty in all lidar error bars is a subtle one, and we have not yet resolved it (The normalization uncertainty included in all our lidar error bar calculations is the uncertainty in the amount of particulate backscattering at the normalization height The results shown also include photon-counting uncertainties at the normalization height as part of the normalization uncertainty.) We note these points to emphasize some of the subtleties in lidar error analysis, and the value of introducing random errors into simulated measurements as a way of checking the validity of analytical error expressions. (Further discussion follows below )

It can be seen from Figure 13 that the relative errors in the Nd backscattering coefficient profile are about half as large as the relative errors for the ruby profile. The relative size and

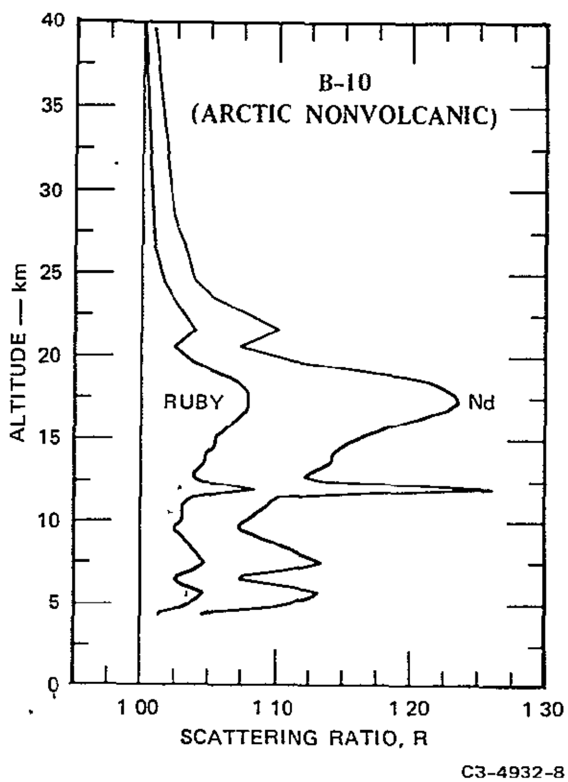


FIGURE 11 RUBY AND Nd SCATTERING RATIO PROFILES FOR THE B-10 (ARCTIC NONVOLCANIC) MODEL ATMOSPHERE

B-10 (ARCTIC NONVOLCANIC) MODEL
SUN ON HORIZON
1-MINUTE INTEGRATION

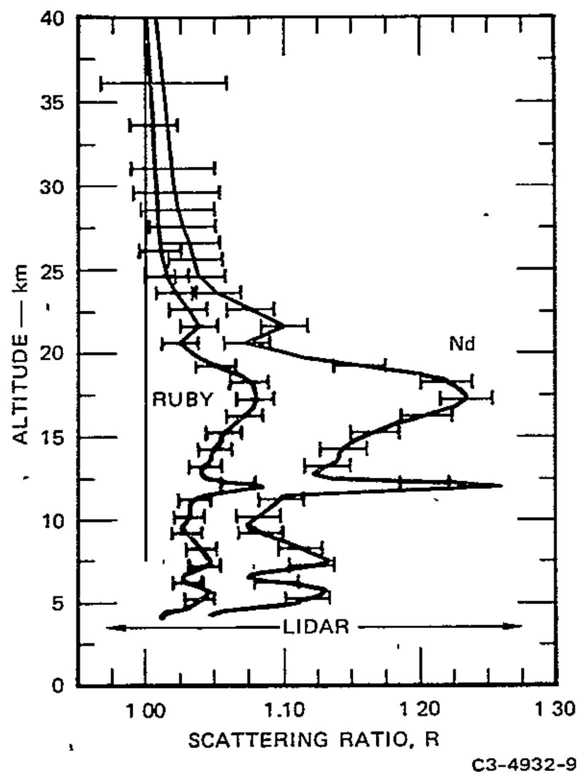


FIGURE 12 EXPECTED LIDAR-MEASUREMENT ERROR BARS FOR RUBY AND Nd SCATTERING RATIOS WITH THE B-10 (ARCTIC NONVOLCANIC) MODEL ATMOSPHERE Error calculation assumes the lidar parameters of Table 2, error sources of Table 5, lidar flight altitude of 4 km, sun on the horizon, and integration for one minute

B-10 (ARCTIC NONVOLCANIC) MODEL
SUN ON HORIZON
1-MINUTE INTEGRATION

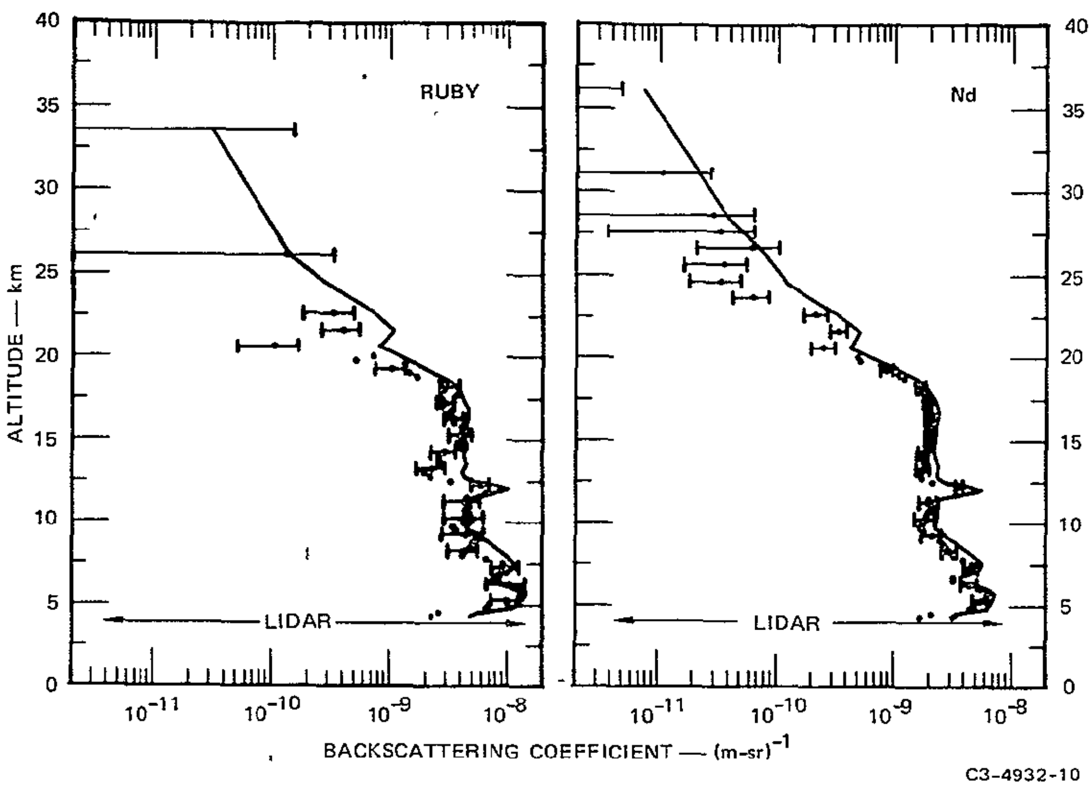


FIGURE 13 EXPECTED LIDAR-MEASUREMENT ERROR BARS FOR RUBY AND Nd PARTICULATE BACKSCATTERING COEFFICIENTS WITH THE B-10 (ARCTIC NONVOLCANIC) MODEL ATMOSPHERE Error calculations are as described in Figure 12 Dots show simulated measurements with all four sources of random error included, as a check on the error bar computation. Systematic underestimations in simulated measurements are caused by a type of normalization error that is not included in the error bar computations See text for discussion

height dependence of these errors can be seen more clearly in Figure 14, which also shows how the four sources of uncertainty (density, transmission, normalization, and counting) contribute to the total. Identifying the sources of uncertainty aids in roughly predicting the effect of varying certain lidar parameters Note, for example, that the major source of uncertainty for the ruby measurement, at all altitudes, is the uncertainty in the molecular density profile This uncertainty cannot be reduced by using higher laser energy, a larger receiver, a more efficient detector, longer counting, coarser vertical resolution, or flying closer to the aerosol peak. In fact, the only way of reducing this uncertainty is by determining the relative molecular density profile above the lidar to an accuracy of better than 1% (cf Table 5). The measurement errors and horizontal drift of radiosondes make reduction of this error very unlikely (see, e g. Lenhard, 1973, Hoxit and Henry, 1977) However, there is hope that simultaneous measurements with a frequency-doubled ruby transmitter ($\lambda$ = 0 347 nm) could provide significantly reduced density errors (Fuller et al , 1976), especially when an iterative scheme is used to correct for particulate backscattering in the doubled-frequency channel For present purposes, however, it should be noted that the current SAM-II airborne lidar design does not allow for transmission of frequency-doubled laser output or for simultaneous two-wavelength signal detection and processing

As shown by Figure 14, density errors are also the dominant source of error for the Nd backscattering measurement, at least below 25 km Above this height, photon-counting errors do become significant, and the expected total uncertainty is sensitive to transmitted power, detector efficiency, aircraft height, vertical resolution, and received signal integration time. In this connection we note that Nd counting errors would be reduced somewhat by flying at a higher altitude, say 8 km However, we do not recommend this procedure, because normalization errors increase significantly if the lidar profile excludes the height of minimum mixing ratio, which is frequently found several km below the tropopause. (The minimum mixing ratio does not occur below the tropopause in the B-10 model--possibly because of upper tropospheric dust from the Mongolian Desert--and it usually does not occur there after volcanic eruptions However, analyses of dustsonde data (Russell et al., 1976b) have shown that the minimum mixing ratio does tend to occur below the tropopause for nonvolcanic midlatitude conditions We also note that another reason for flying low is that the minimum height of the lidar data profile will be 1 or 2 km above the airplane, because of the distance required for transmitter-receiver convergence )

Regarding the relative size of ruby and Nd measurement uncertainties shown in Figure 14, it should be noted that including the density type of normalization error (discussed above) would not decrease the advantage of the Nd system In fact, including density-normalization uncertainties has the same effect (on total uncertainty) as multiplying the density-induced uncertainties shown in Figure 14 by a factor of $\sqrt{2}$, for both lidars Thus the relative increase in total uncertainty would be greater for the ruby than for the Nd lidar, actually increasing the difference in measurement uncertainties between the two systems

We also note that the 1 0-$\mu$m detector quantum efficiency of 3% assumed in Table 2 is a fairly conservative value, being somewhat less than the value of 4% recently measured at SRI International for a tube of the type intended for use in the airborne lidar (Evans, 1978) However, these values do apply to a new photomultiplier tube (PMT) that is known to be delicate and to require continuous cooling Moreover, it has not yet been used for lidar measurements For these reasons Langley Research Center has recently contracted with William Evans of SRI International to purchase one of these PMT's and test its specifications and other aspects of suitability for airborne lidar use The decision of whether to use a ruby or Nd laser in the lidar that is actually flown for SAM-II ground-truth measurements will hinge critically on the outcome of these tests

Figures 15 and 16 summarize the results of simulations for the two remaining model atmospheres A-14 (antarctic nonvolcanic) and ASTP (midlatitude moderate volcanic) The results for model A-14 are very similar to those for model B-10. (Compare Figures 14 and 15c,d ) Specifically, they show that, for high-latitude nonvolcanic conditions, the Nd system

B-10 (ARCTIC NONVOLCANIC) MODEL
SUN ON HORIZON
1-MINUTE INTEGRATION

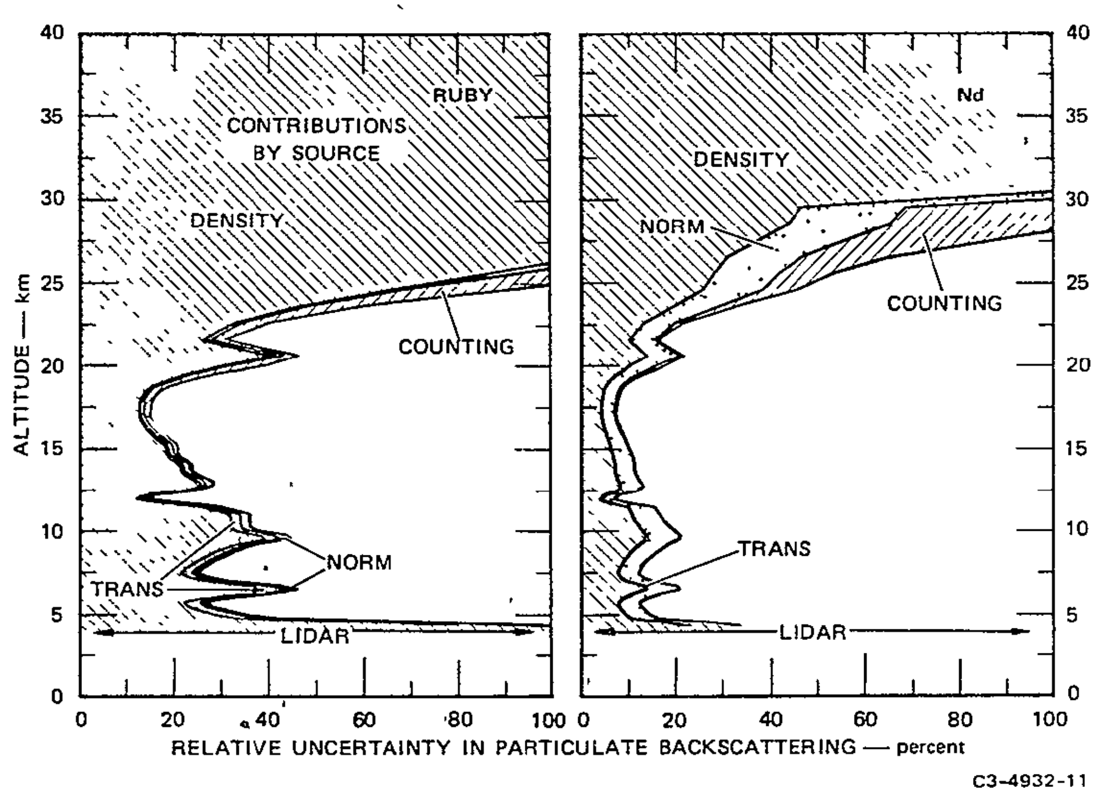


FIGURE 14 HEIGHT DEPENDENCE OF EXPECTED UNCERTAINTY IN LIDAR-MEASURED PARTICULATE BACKSCATTERING FOR THE B-10 (ARCTIC NONVOLCANIC) MODEL ATMOSPHERE, SHOWING CONTRIBUTIONS BY SOURCE Assumed parameters as in Figure 12

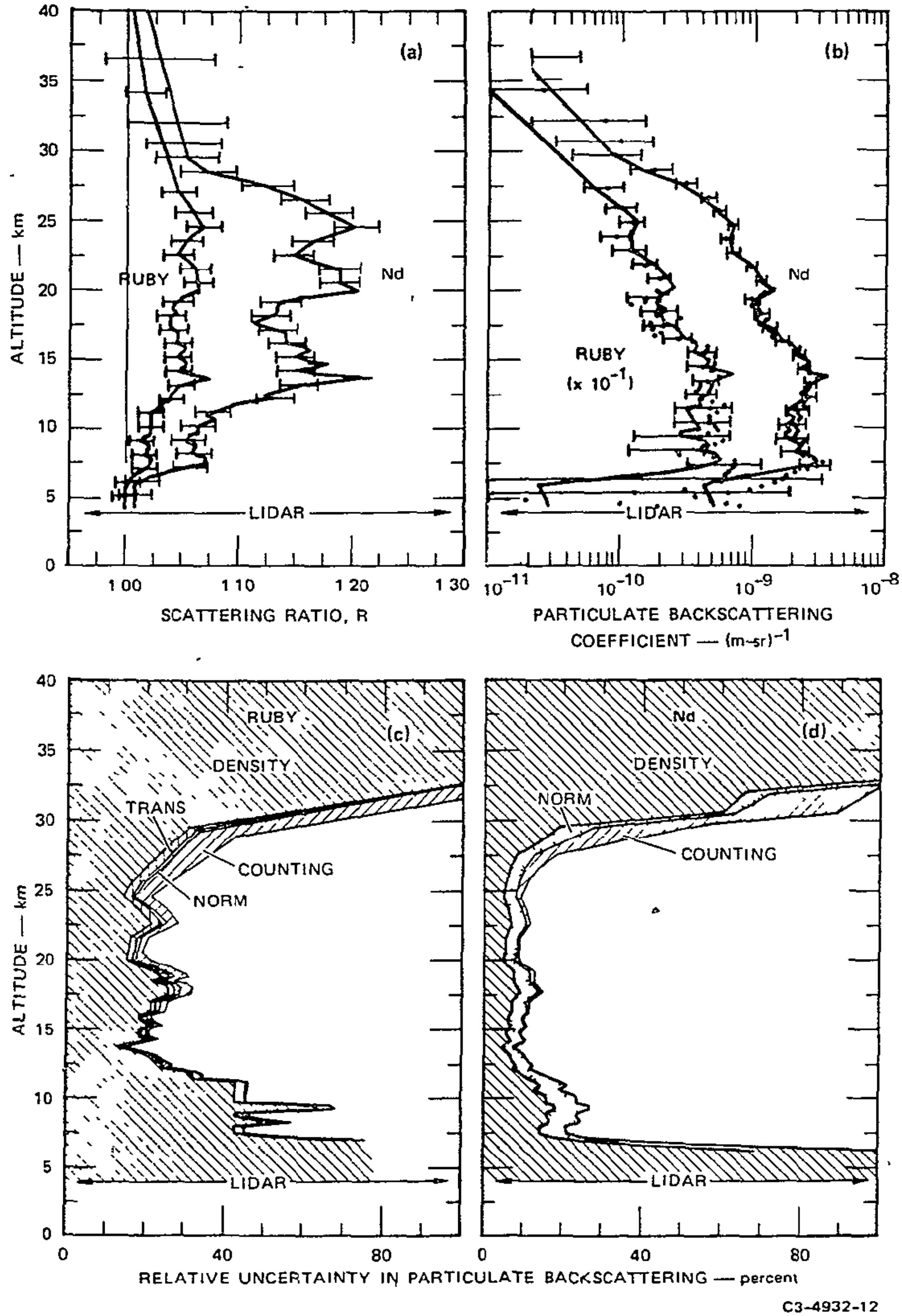


FIGURE 15 LIDAR MEASUREMENT UNCERTAINTIES AND SIMULATED MEASUREMENTS FOR THE A-14 (ANTARCTIC NONVOLCANIC) MODEL ATMOSPHERE. (a) Model scattering ratios and expected error bars. (b) Model backscattering coefficients, simulated measurements (dots), and expected error bars. (c) Relative uncertainty in particulate backscattering, showing contributions by source.

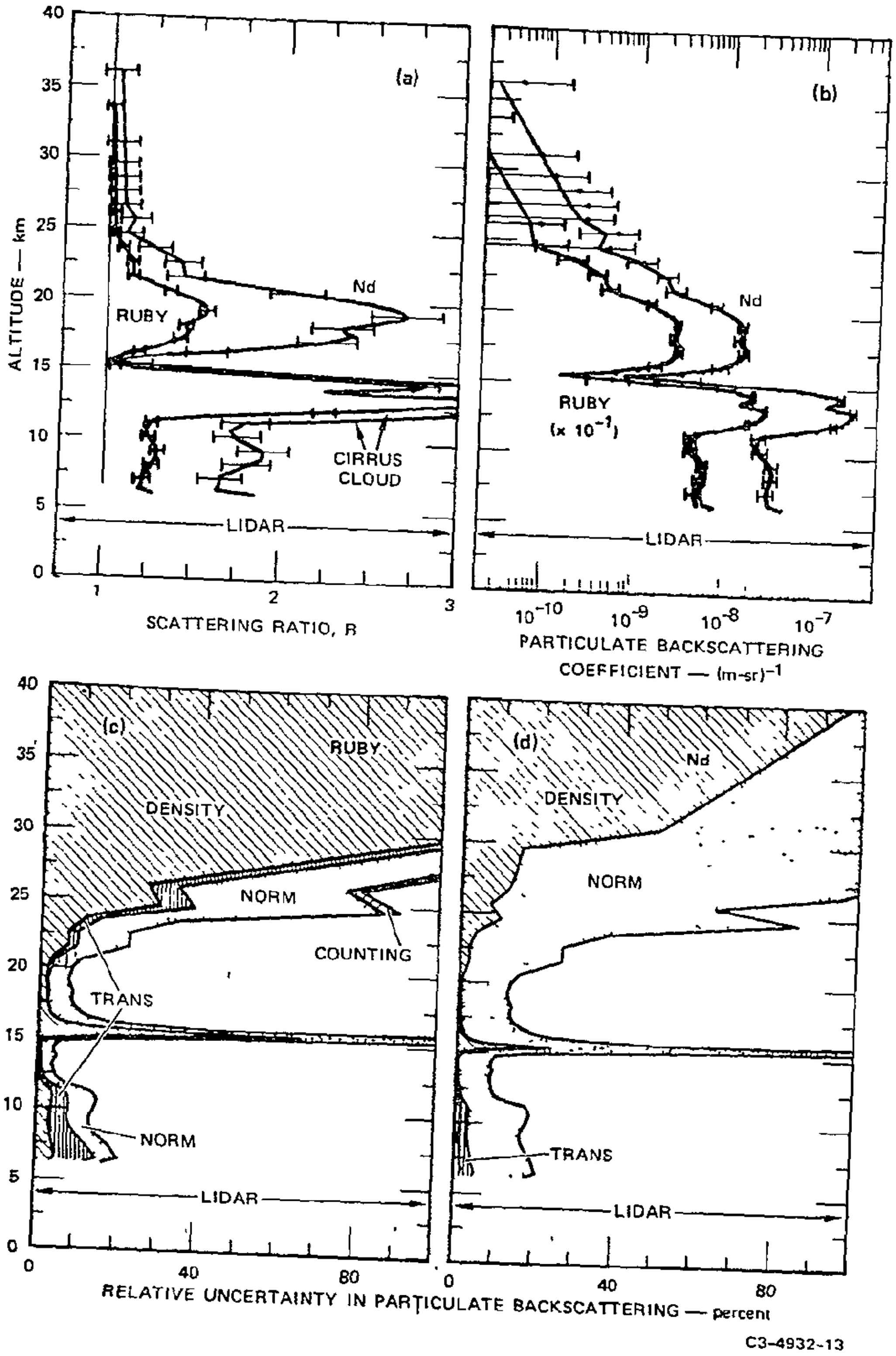


FIGURE 16 LIDAR MEASUREMENT UNCERTAINTIES AND SIMULATED MEASUREMENTS FOR THE ASTP (MIDLATITUDE MODERATE VOLCANIC) MODEL ATMOSPHERE (a) Model scattering ratios and expected error bars. (b) Model backscattering coefficients, simulated measurements (dots), and expected error bars (c), (d) Relative uncertainty in particulate backscattering, showing contributions by source Transmission errors are overestimated, because normalization height is above cirrus cloud See text for discussion

can be expected to yield a backscattering measurement uncertainty that meets the target figure of 10% (cf Section 1 1 ) at the aerosol peak and that is less than 20% for all heights of interest below 20 km On the other hand, the measurement errors for the ruby system can be expected to exceed those of the Nd system by about a factor of two, for such high-latitude nonvolcanic conditions. For midlatitude moderate volcanic conditions, as represented by the ASTP model, both lidars are expected to satisfy the desired 10% criterion at all heights of interest (see Figure 16)

At this point it is worth emphasizing that the advantages of airborne lidar listed in Section 1.2 make either ruby or Nd lidar measurements an essential part of the ground-truth program, even though ruby measurement accuracies may be somewhat less than desired for high-latitude nonvolcanic aerosol conditions It should also be borne in mind that for immediate postvolcanic or moderate volcanic conditions the ruby lidar measurement accuracy for particulate backscattering is reduced to a few percent at all altitudes of interest, as was shown in Figure 16. Moreover, the mobility and fine-scale horizontal and vertical resolution of airborne lidar make it an unsurpassed sensor for such conditions, because marked spatial inhomogeneities in aerosol concentration are then the rule rather than the exception

*Conversion to Particulate 1 0-μm Extinction Profiles*

Lidar-measured particulate backscattering coefficients can be converted to particulate 1 0-μm extinction coefficients by using an assumed refractive index and particle size distribution. Figure 17 shows the dependence of the conversion ratio on optical model properties (cf. Figure 8 and accompanying discussion) (The size distributions and compositions shown have been derived from measurements by various investigators -- e g. Hofmann et al, 1975, Pinnick et al, 1976; Shettle and Fenn, 1976, Deirmendjian, 1969, Toon and Pollack, 1976, Harris and Rosen, 1976; Swissler and Harris, 1976 ) In a given lidar measurement the optical model can in general only be estimated on the basis of previous or simultaneous (e g dustsonde) measurements Numerous dustsonde measurements have shown a preferred height dependence for the channel ratio, $N_{15}/N_{25}$, and that, for nonvolcanic conditions, the range of values within the major aerosol mixing ratio peak is usually bounded by 3 and 5 (Hofmann et al , 1975). Thus the uncertainty in conversion ratio is given by the vertical spread of data points in Figure 17 above the appropriate range of $N_{15}/N_{25}$ values. The mean and standard deviation of appropriate subsets of conversion ratios is shown in Table 6

Figure 17 and Table 6 show that when recent or nearby dustsonde measurements (or other measurements) indicate that $N_{15}/N_{25}$ falls in the range 3-5, the uncertainty (standard deviation) in the conversion ratio is about ±10% for both ruby ($\lambda$ = 0 694 μm) and Nd ($\lambda$ = 1 06 μm) measurements The slightly larger uncertainty for ruby measurements shown in Table 6 arises mainly from composition uncertainty (aqueous sulfuric acid vs silicate), to which the Nd conversion ratio is not so sensitive (presumably because the Nd wavelength is close to 1 0 μm). If the particle composition can be ascertained by some other measurement(s), then the uncertainty in the ruby conversion ratio is slightly reduced--to about ±8%, which is about equal to the uncertainty in the Nd ratio

### 2.2.2. Dustsondes

NASA Langley Research Center has contracted with the University of Wyoming (Professors David Hofmann and James Rosen) to make three dustsonde flights during the practice comparative experiment and the November 1978 Sondrestrom experiment The University of Wyoming has tentatively agreed to support the 1979 Sondrestrom experiment, and that support will be contracted for at a later data In addition, the University of Wyoming has agreed to make available any dustsonde data collected in Antarctica which may be useful in validating the SAM-II data (See paragraph 2.1.1.) These dustsondes will all be two-channel instruments, with design, resolution, and accuracy as described in Section 2 1 1 The accuracy of conversion to 1.0-μm extinction is also discussed in that section

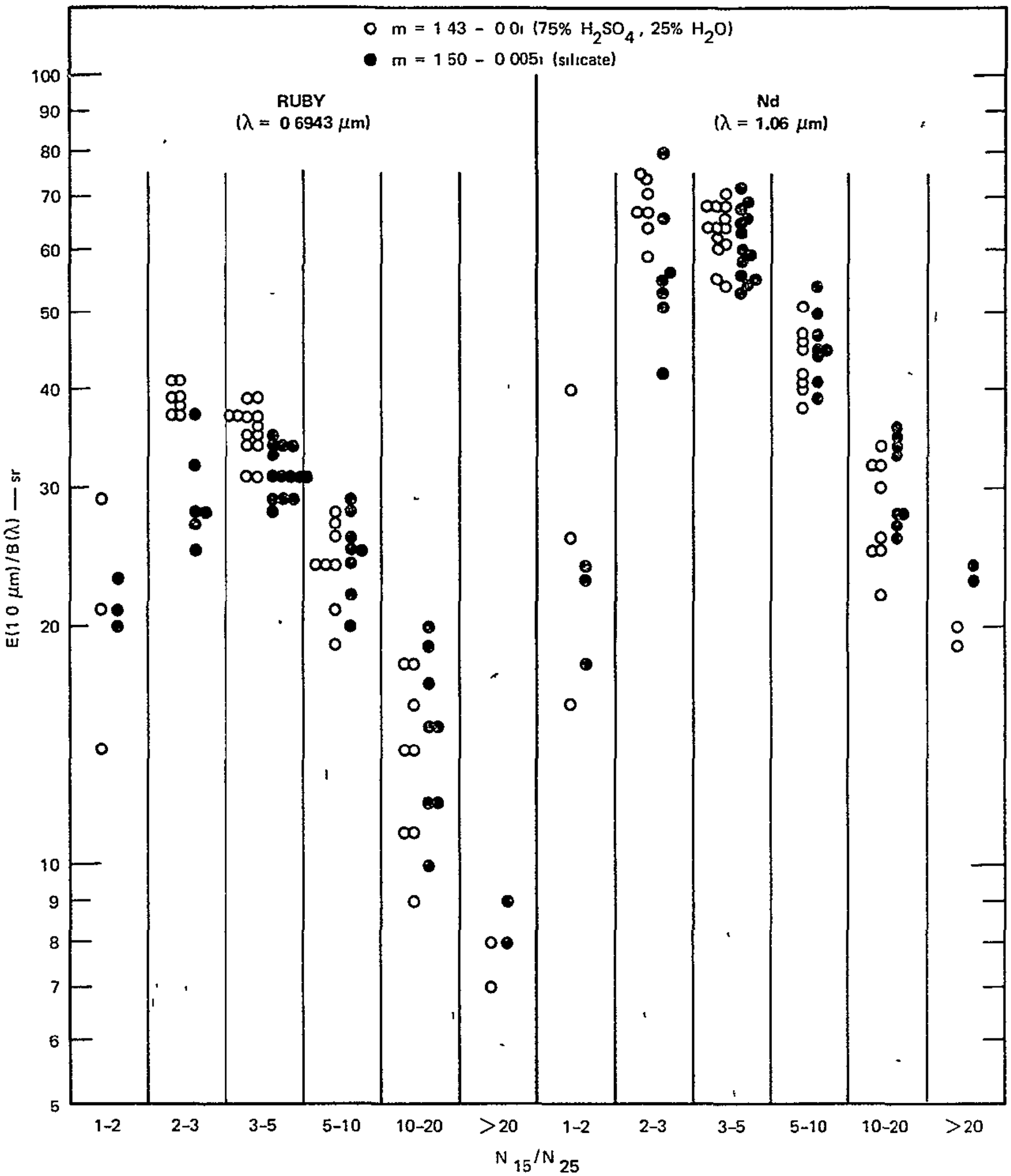


FIGURE 17 EXTINCTION-TO-BACKSCATTER RATIOS, E(1 0μm)/B(λ), COMPUTED FOR RUBY AND Nd WAVELENGTHS λ, SILICATE AND AQUEOUS SULFURIC ACID COMPOSITIONS, AND A WIDE RANGE OF SIZE DISTRIBUTIONS Size distributions are grouped according to their value of the integral number ratio $N_{15}/N_{25}$ See Table 6 and text for discussion of observed regions and frequency of $N_{15}/N_{.25}$ values

Table 6

MEAN AND STANDARD DEVIATION OF EXTINCTION-TO-BACKSCATTER RATIO, E(1.0μm)/B(λ), FOR TWO LIDAR WAVELENGTHS λ AND VARIOUS GROUPS OF SIZE DISTRIBUTIONS

| | Lidar | RUBY (λ=0.6943μm) | | | | | | | Nd - YAG (λ=1.06μm) | | | | | | |
|---|---|---|---|---|---|---|---|---|---|---|---|---|---|---|---|
| Composition | $N_{.15}/N_{.25}$ | 1-2 | 2-3 | 3-5 | 3.5-4.5 | 5-10 | 10-20 | >20 | 1-2 | 2-3 | 3-5 | 3.5-4.5 | 5-10 | 10-20 | >20 |
| 75% $H_2SO_4$-25% $H_2O$ | Mean (sr) | 30 | 38 | 35 | 35 | 23 | 14 | 8 | 44 | 70 | 63 | 63 | 43 | 28 | 21 |
| | σ/Mean | 33% | 6% | 8% | 5% | 21% | 24% | 25% | 46% | 9% | 8% | 3% | 18% | 14% | 13% |
| SILICATE | Mean (sr) | 23 | 29 | 31 | 32 | 23 | 15 | 9 | 32 | 61 | 61 | 61 | 45 | 31 | 23 |
| | σ/Mean | 22% | 13% | 8% | 6% | 20% | 24% | 12% | 51% | 22% | 10% | 6% | 18% | 12% | 5% |
| BOTH | Mean (sr) | 26 | 34 | 33 | 33 | 23 | 14 | 8 | 38 | 65 | 62 | 62 | 44 | 29 | 22 |
| | σ/Mean | 31% | 16% | 10% | 7% | 21% | 24% | 20% | 50% | 17% | 9% | 5% | 18% | 14% | 12% |

### 2.2.3. Balloonborne Sunphotometer

Professor Theodore Pepin of the University of Wyoming is now developing a balloon-borne sunphotometer with a 1.0-$\mu$m channel that is spectrally equivalent to that on SAM-II While in flight on the balloon gondola, the photometer will lock onto the sun and view it through the atmosphere during sunrise or sunset events, thus providing a measurement of 1.0-$\mu$m extinction along the viewed path.

*Resolution and Accuracy*

The sunphotometer has the capability to measure the intensity of the sun as viewed through the atmosphere with a precision of $\pm$0 1%. The calibration of the photometer is accomplished during the extinction balloon flight by observing the sun at high elevation angles from the balloon platform and extrapolating the observed signal to outside of the atmosphere Observations will be made to less than 0 01 airmass

The sunphotometer makes use of the total solar disc rather than the partial disc which is observed by the scan system employed in SAM-II. Since the sunphotometer is used at balloon altitude rather than spacecraft altitude, it achieves vertical resolution of the same order as SAM-II, but it does not require high pointing accuracy and it is less sensitive to refraction.

*Conversion to Particulate 1.0-$\mu$m Extinction Profiles*

The sunphotometer measurements will be converted to 1 0-$\mu$m extinction profiles by several methods of inversion, as outlined by Pepin (1970,1977)

## 3. MEASUREMENT SITES AND SCHEDULE

Table 7 summarizes the sites and schedule of the practice and ground-truth comparative experiments that the SAM-II NET has chosen after detailed consideration of a number of tradeoffs. The nature of these tradeoffs and the rationale for the selections made are described in the following subsections.

### 3.1. Practice Comparative Experiment

The Practice Comparative Experiment (scheduled for mid-August 1978) will include flights by the airborne lidar, a dustsonde, and the balloonborne sunphotometer Its purpose is to develop multisensor and multiplatform coordination procedures and to test data reduction and comparison techniques, as mentioned previously in Section 1 2

Laramie, Wyoming, was chosen as the preferred site for the Practice Comparative Experiment because of its proximity to the University of Wyoming. This proximity will reduce the cost and simplify the logistics of both the dustsonde and sunphotometer balloon flights, and will maximize chances of instrument recovery. It should also maximize chances of success on what will be the first flight of the balloonborne sunphotometer.

As can be seen from Table 7, the Laramie Practice Comparatice Experiment does not include a ground-based lidar for direct comparisons with the airborne lidar However, during the development of the airborne lidar, data from it and the Langley 48-inch ground-based lidar will be compared in a number of experiments at Langley Research Center (37° 4' N, 76° 20' W).

### 3.2. Postlaunch Ground Truth Measurements

Seven potential balloon-launch and aircraft-staging sites in the Northern Hemisphere, and six in the Southern Hemisphere, were actively considered in developing the ground-truth plan shown in Table 7. Table 8 summarizes important characteristics of each of these sites More detailed consideration of these characteristics, and of the tradeoffs among them, follows below

The selection of optimum sites and dates was made after careful consideration of SAM-II and balloon-borne sunphotometer viewing geometries, surface and upper-air meteorology at sites and dates acceptable for balloon photometer observations (see below), airfield characteristics and services, logistics and costs of transporting personnel and materials, costs of personnel billeting, and special site restrictions. The primary driver in the site and date selection process is the time-dependent locus of SAM-II tangent points Figure 2 shows how this locus depends on the time of Nimbus G's first equator crossing--an orbit parameter that might be altered by changing the launch time or other launch conditions (duration of burn, etc.) As can be seen by comparing Table 7 and Figure 2, the sites and dates chosen for ground-truth experiments tend to occur when and where the tangent location and time are relatively insensitive to equator crossing time Table 9 lists tangent dates for each Northern Hemisphere site and for each of three different equator crossing times The probabilities of achieving an equator crossing time within the ±15-minute range shown is greater than 99%, on the basis of past launch vehicle performance.

A second driver in determining acceptable sites and dates is the range of sun elevation angles available to the balloonborne sunphotometer at an altitude of 28 km For the sunphotometer to scan the atmosphere from 0 to 40 km, the solar elevation angle (viewed from 28 km) must range from -5° to +10° with respect to local horizontal Plots showing the dependence of (balloon-viewed) solar elevation angle on time and date for each potential site are given in Appendix E Consideration of these plots greatly reduces the number of acceptable intercept dates for SAM-II/balloonborne photometer comparisons, yielding the list shown in Table 10 As can be seen, of the seven Northern Hemisphere sites actively considered, only four (Barrow, Cambridge Bay, Sondrestrom, and Fairbanks) are acceptable for SAM-II/balloonborne sunphotometer comparisons, and of these only Cambridge Bay and Sondrestrom are acceptable for the nominal equator crossing time

Table 7

OVERVIEW OF SAM II GROUND TRUTH EXPERIMENT SCHEDULE

| Observation | 1[1] | 2 | 3 | 4[2] |
|---|---|---|---|---|
| Approximate Date | 14-16 August 1978 | Late November 1978 | Mid-December 1978 | Late May-Early July 1979 |
| Site | Laramie, WY | Sondrestrom, Greenland | Palmer, Antartica | Sondrestrom, Greenland |
| Lat. | $41^\circ$ 18' N. | $67^\circ$ 01' N. | $64^\circ$ 46' S. | $67^\circ$ 01' N. |
| Long. | $105^\circ$ 42' W. | $50^\circ$ 43' W. | $64^\circ$ 03' W. | $50^\circ$ 43' W. |
| Airborne Lidar | 1 flight | 8 flights | 7 flights | 8 flights |
| Staging Site | Laramie | Sondrestrom | Rio Grande, Argentina | Sondrestrom |
| Dustsonde | 1 flight | 2 flights | -- | 2 flights |
| Balloon Sunphotometer | 1 flight | 1 flight | -- | 1 flight |
| Radiosonde | 2 flights | 16 flights | -- | 16 flights |
| Airborne In Situ Observations | 1 flight | 8 flights | -- | 8 flights |

[1] Practice Comparative Experiment
[2] SAM II - SAGE comparison (partially funded by SAGE).

# Table 8

## POTENTIAL SAM II GROUND TRUTH SITES

| Balloon & Aircraft Staging Site | Geographic Location | | Aircraft Facilities | SAM II Coincidence |
|---|---|---|---|---|
| | Latitude | Longitude | | |
| Alert, Canada (Canadian) | $82^{\circ}$ 31' N | $62^{\circ}$ 17' W | Limited | No opportunities |
| Thule, Greenland (Danish-USAF) | $77^{\circ}$ 30' N | $69^{\circ}$ 29' W | Unlimited | Late August, mid-October, late February, mid-April |
| Resolute Bay, Canada (Canadian) | $74^{\circ}$ 43' N | $94^{\circ}$ 58' W | Unlimited | Mid-August, late October, mid-February, late April |
| Point Barrow, Alaska (USN) | $71^{\circ}$ 20' N | $156^{\circ}$ 38' W | Limited | Early August, early November, early February, early May |
| Cambridge Bay, Canada (Canadian-USAF) | $69^{\circ}$ 06' N | $105^{\circ}$ 08' W | Unlimited | Mid-November, late January, mid-May, late July |
| Sondre Stronfjord, Greenland (Danish-USAF) | $67^{\circ}$ 01' N | $50^{\circ}$ 43' W | Unlimited<br>9,200 ft runway | Late November, mid-January, early June, early July |
| Fairbanks, Alaska | $64^{\circ}$ 50' N | $147^{\circ}$ 37' W | Unlimited | Mid-December, early January |
| Palmer, Antarctica (USA) | $64^{\circ}$ 45' S | $64^{\circ}$ 05' W | Ski-equipped A/c only | Mid-December, mid-June, early July |
| Siple, Antarctica (USA) | $75^{\circ}$ 56' S | $84^{\circ}$ 15' W | Ski-equipped A/C only | Late August, late October, mid-February, mid-April |
| McMurdo, Antarctica (USA) | $77^{\circ}$ 51' S | $166^{\circ}$37' E | Ski-equipped A/A except Oct. to Dec. | Early September, mid-October, late February, early April |
| Punta Arenas, Chile | $53^{\circ}$ 05' S | $71^{\circ}$ 00' W | Limited | A/C staging for measurements over Palmer, Antarctica ($\sim$ 700 nautical miles) |
| Ushuaia, Argentina | $54^{\circ}$ 49' S | $68^{\circ}$ 19' W | 4,600 ft runway | |
| Rio Grande, Argentina | $53^{\circ}$ 47' S | $67^{\circ}$ 46; W | 6,500 ft runway | |

Table 9

SAM-II TANGENT DATES FOR POTENTIAL GROUND-TRUTH SITES

| | | I | II | III | IV |
|---|---|---|---|---|---|
| ALERT (82.5N) | B+ | Mar 16.5 | | Sept 13 | - |
| | Bo | | - | - | - |
| | B- | - | - | - | - |
| THULE (76.7N) | B+ | Feb 22 | April 9 | Aug 20 | Oct 20 |
| | Bo | Feb 25 | April 17.5 | Aug 26 | Oct 16 |
| | B- | Mar 2.5 | April 22 | Sept 3 | Oct 11 |
| RESOLUTE (74.8N) | B+ | Feb 16 | April 29 | Aug 14 | Oct 26 |
| | Bo | Feb 18 | April 25 | Aug 18 | Oct 23 |
| | B- | Feb 22 | April 18 | Aug 25 | Oct 19.5 |
| PT. BARROW (71.5N) | B+ | Feb 4 | May 12 | Aug 1 | Nov 6 |
| | Bo | Feb 6 | May 8 | Aug 5 | Nov 4.5 |
| | B- | Feb 9 | May 2 | Aug 11 | Nov 2 |
| CAMBRIDGE (69.2N) | B+ | Jan 26.5 | May 22.5 | July 21 | Nov 15.5 |
| | Bo | Jan 28 | May 18.5 | July 25 | Nov 14 |
| | B- | Jan 30 | May 12 5 | July 31.5 | Nov 12 |
| SONDRESTROM (67.0N) | B+ | Jan 16 | June 8 | July 5 | Nov 26 |
| | Bo | Jan 17.5 | June 1 | July 11 | Nov 24.5 |
| | B- | Jan 19.5 | May 24 | July 19 | Nov 23 |
| FAIRBANKS (65.0N) | B+ | Jan 1 | - | - | Dec 11.5 |
| | Bo | Jan 3 | - | - | Dec 9 |
| | B- | Jan 5 | June 11.5 | July 1 | Dec 7 |
| PALMER ($64^0.8^0$S) | B+ | Dec 27 | June 8 | July 4.5 | Dec 25 |
| | Bo | - | June 11 | July 1.5 | - |
| | B- | - | June 13.5 | July 28.5 | - |

Note: $B_o$ designates dates for Nimbus G equatorial crossing time as specified in current launch plans. $B^+$ and $B^-$ designate dates for orbit with first equator crossing time changed by ±15 minutes. Columns I, II, III, IV show tangent dates for 1st, 2nd, 3rd, and 4th satellite crossings of station latitude during a given calencar year.

Table 10

SUMMARY OF INTERCEPT DATES THAT GIVE ACCEPTABLE BALLOON GEOMETRY
Based on Results of Figure 2 and Table 9, Plus Balloon Look Angles of Appendix E.

| STATION | | I | IV |
|---|---|---|---|
| ALERT | B+ | Mar. 16.5 | -- |
| Thule | B+ | Feb. 22 | Oct. 20 |
| | $B_o$ | Feb. 25 | Oct. 16 |
| | B- | Mar. 2.5 | Oct. 11 |
| Resolute | B+ | Feb. 16 | -- |
| | $B_o$ | Feb. 18 | Oct. 23 |
| | B- | Feb. 22 | Oct. 19.5 |
| Pt. Barrow | B+ | Feb. 4 | Nov. 6 |
| | $B_o$ | Feb. 6 | Nov. 4.5 |
| | B- | Feb. 9 | Nov. 2 |
| Cambridge | B+ | Jan. 26.5 | -- |
| | $B_o$ | Jan. 28 | Nov. 14 |
| | B- | Jan. 30 | Nov. 12 |
| Sondrestrom | B+ | Jan. 16 | Nov. 26 |
| | $B_o$ | Jan. 17.5 | Nov. 24.5 |
| | B- | Jan. 19.5 | Nov. 23 |
| Fairbanks | B+ | -- | Dec. 11.5 |
| | $B_o$ | -- | Dec. 9 |
| | B- | -- | Dec. 7 |

Perhaps the next most important factor in site and date selection is expected meteorological conditions and services. These are important both because of (1) the need for a high probability of data capture within a window of several days duration and (2) the need for atmospheric density profiles to be used in data reduction Table 11 summarizes available meteorological and support services. Another characteristic of importance to experiment operations is the duration of daylight at each site and date The variability of this quantity is shown in Figure 18

The meteorology for the sites under consideration has been reviewed for the November period with regard to cloud cover, surface wind, precipitation, and visibility period Historically, the surface conditions at Sondrestrom, Greenland during November indicate that balloon operations can be conducted from that site with a high probability of success during this period On the other hand, the meteorology at a number of other sites is marginal for conducting successful operations.

The remaining factors in site and date selection are airfield characteristics and services, air transportation costs, and personnel billeting costs and special restrictions. Tables 12-14 summarize these factors, and Appendix H provides approach plates for each airfield

### 3.3. Coordination with SAGE Ground-Truth Program

As indicated by Table 7, the second SAM-II ground-truth experiment at Sondrestrom (Experiment No. 4, late May-July 1979) will be a joint SAM-II/SAGE grount-truth experiment Table 15 gives more detail regarding the operations at Sondrestrom for both the 1978 and 1979 experiments (referred to as Experiments I and II in Table 15) In addition, Figure 19 shows a typical day of overlapping SAM-II and SAGE coverage in the northern hemisphere in May 1979, assuming a SAGE orbital inclination of 50° (Note that current plans call for a slightly higher inclination for SAGE, so the results in Figure 19 are illustrative, rather than definitive. Mission analyses for currently planned SAGE orbit parameters are now being run, and will appear in SAGE ground-truth planning documents) Figure 20 shows similar results for the southern hemisphere, generated under a previous assumption of a SAGE launch in late November, 1978 The possibility of southern-hemisphere coordinated SAM-II/SAGE ground-truth experiments is now being investigated for SAGE's currently planned launch date of late January 1979.

Table 11

Meteorological and Support Services

| Station | SYNOPTIC OBSERVATION Surface | Rad-Sond | Roc-Sond. | RELATED SUPPORT Spec. Bal. | Rad. Trac. | Spec. Fax/Data |
|---|---|---|---|---|---|---|
| Alert | X | X | | X | | X |
| Thule | X | X | X | X | X | X |
| Resolute Bay | X | X | (X)(1) | X | | X |
| Barrow | X | | | | (X)(1) | X |
| Cambridge Bay | X | X | | X | X | X |
| Sonderstrom | X | (2) | | | | X |
| Fairbanks | X | X | (X) (1) | X | (X)(1) | X |

NOTES: (1) Rocket-Sondes are from Poker Flats, AK.

(2) Meteorological support (including radiosondes and ozone rocketsondes) at Sondrestrom will be provided by the Wallops Flight Center.

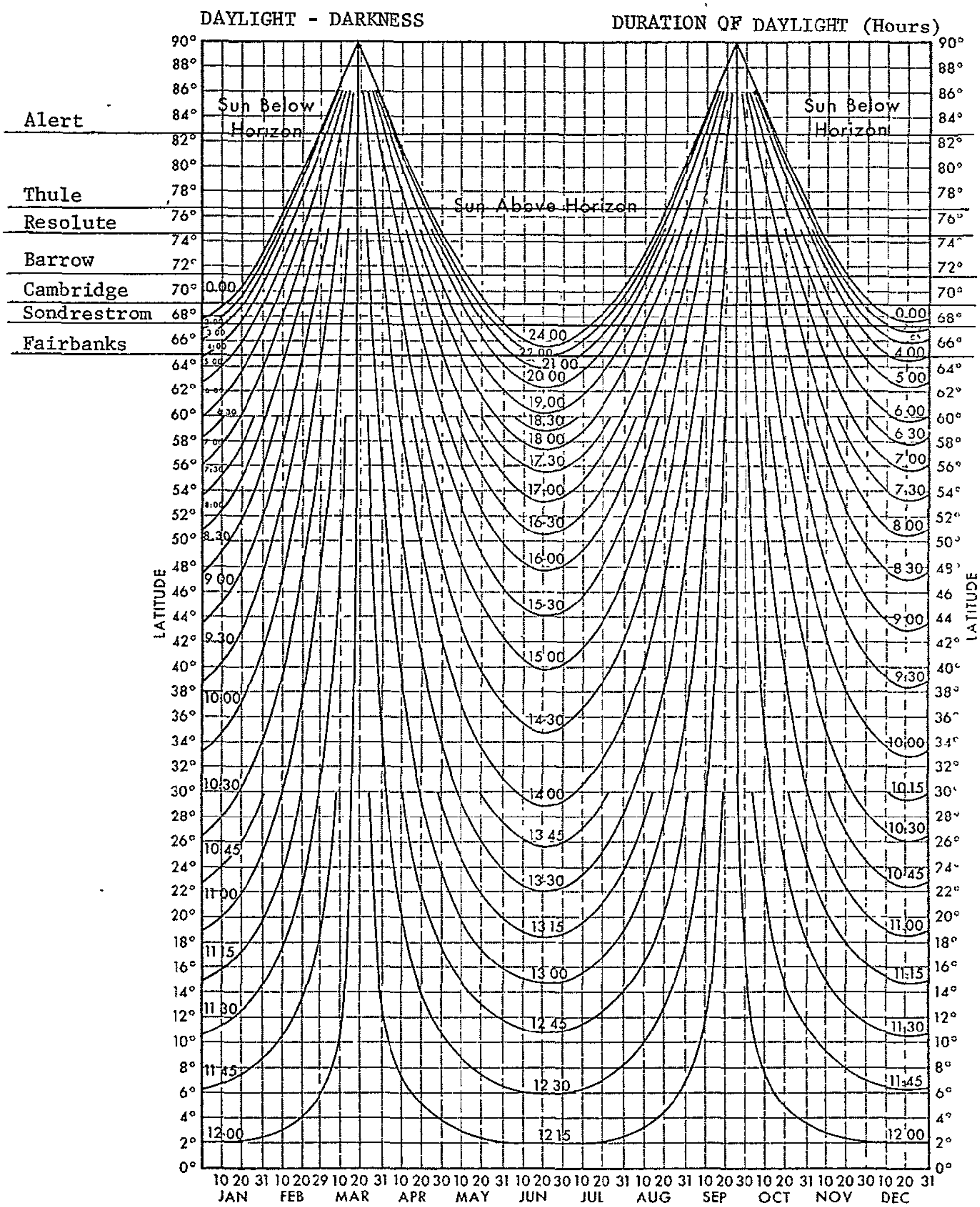


FIGURE 18 DURATION OF DAYLIGHT AT POTENTIAL NORTHERN HEMISPHERE GROUND TRUTH SITES



ORIGINAL PAGE IS OF POOR QUALITY

Table 12

SUMMARY OF AIRFIELD CHARACTERISTICS & SERVICES

| Station (Call) | N. Lat. | W. Long | (Z) | Elev. | Runway Length | Weight | Approach | Fuel/Svc | Agency |
|---|---|---|---|---|---|---|---|---|---|
| Fairbanks (FAF) | 64-50 | 147-37 | (+10) | 545' | 14,500 | H - OK | VOR/PAR | OK | USAF/(USA) |
| Sondrestrom (GSF) | 67-01 | 50-43 | (+3 ) | 165' | 9,200 | H - OK | TAC/PAR | OK | USAF/Danish |
| Cambridge Bay (CYCB) | 69-06 | 105-08 | (+7 ) | 90' | 5,000 | U - OK | VOR/DME | OK | MOT/USAF |
| Barrow (BRW) | 71-20 | 156-38 | (+10) | 44' | 6,500 | H - OK? | VOR/TAC-DME | NONE | USN |
| Resolute (CYRB) | 74-43 | 94-58 | (+6 ) | 65' | 6,500 | U - OK | VOR/ILS ** | OK | MOT |
| Thule (GTL) | 76-32 | 68-42 | (+4 ) | 251' | 10,000 | H - OK | VOR/PAR | OK | USAF/Danish |
| Alert (CYLT) | 82-31 | 62-17 | (+4 ) | 100' | 5,500 | U - OK? | TAC/NDB * | NONE | DND/AES |

* TACAN Unreliable
** Magnetic Compass Unreliable
? OK for C-130, P-3 Type, uncertain

Note: Using published terrain clearance minimum radio horizon from station elevation is calculated to be in excess of 200 n. mi. for all stations.

Z indicates hours difference from Greenwich

H indicates heavy aircraft

U indicates unloaded aircraft

Table 13

ESTIMATED AIR TRANSPORTATION COSTS

a. Non-helium

| Destination | Orig. | Carrier | Fare (R/T) | Average (1 way/lb) |
|---|---|---|---|---|
| Fairbanks | Seattle | (VAR) | $262.00 | $0.15 |
| Sondrestrom | McGuire(N.J.) | MAC | $174.00 | $1.13 |
| Cambridge Bay | Edmonton | Pac. Western | $310.00 | $0.78 |
| Barrow | Fairbanks | Wien | $155.00 | $0.39 |
| Resolute | Winnipeg (Montreal) | Transair (Nordair) | $490.00 ($584.00) | $1.23 ($1.46) |
| Thule | McGuire | MAC | $174.00 | $1.44 |
| Alert | Thule (Trenton, Ont.) (Thule) | CANFORE (Bradley, Air) | $120.00 (charter) | $0.50 (Negot.) |

b. Helium

Fxcept for Alert, NWT, and providing that one surface re-supply season is available prior to its use, cost of helium, delivered and including return of bottles is a flat $0.12 per cubic foot, ~~or~~ approximately $2.00 per pound of lift. This price includes capped bottles only. Manifolding equipment, gages, diffusers, etc. must be supplied seperately.

Cost to Alert is unclear at this time. It is probable that helium could be taken there via RCAF air for only slightly more than the above prices.

Table 14

PERSONNEL BILLETING COSTS AND SPECIAL RESTRICTIONS

| SITE | QUARTERS | MEALS | SPECIAL RESTRICTIONS |
|---|---|---|---|
| Sondrestrom | $12.00 | Incl. | Orders |
| Thule | $15.00 | Incl. | Orders |
| Alert (1) | $20.00 | $52.00 | Orders, Facilities limited License req'd. |
| Resolute | $22.00 | $24.00 | Orders, License req'd. |
| Cambridge Bay | $24.00 | Incl. | Orders, License req'd. |
| Fairbanks | $ 5.30 | Incl. | Orders |
| Barrow | $35.00 | $33.00 | Orders |

(1) Possibly arrangements may be made to go under orders to RCAF at, greatly reduced cost.

## Table 15

### PRELIMINARY DESCRIPTION OF POTENTIAL SAM-II/SAGE GROUND-TRUTH EXPERIMENTS AT SONDRESTROM, GREENLAND

| Gnd Truth Exp | Measurement | Measurement Coordinator(s) | Support Personnel Req'd | Flight (flt) Schedule | Flight Duration | Maximum Altitude | Maximum Diameter | Load Train Length | Payload Weight | Antenna Length | Transmitter | | Support Required |
|---|---|---|---|---|---|---|---|---|---|---|---|---|---|
| | | | | | | | | | | | Frequency | Power | |
| I & II | Airborne Lidar | William H Fuller (NASA-LaRC) Samuel Sokol (NASA-LaRC) | 11 | 8 flts (1 flt/day) | 4 hrs | 30,000 ft | | | | | | | |
| I & II | Dustsonde | David T Hoffman (U Wyo ) James M Rosen (U Wyo ) | 3 | 2 flts | 3 hrs | 100,000 ft | 50 ft | 320 ft | 20 lbs | 320 ft | 1 68 GHz | 300 mw | GMD Recovery desired 80 lbs He/flt |
| I & II | Balloon Sunphotometer | Theodore J Pepin (U Wyo ) | 3 | 1 flt | 9 hrs | 100,000 ft | 60 ft | 20 ft | 100 lbs | 320 ft | 1 68 GHz 1.67 MHz | 300 mw 10 watts | GMD Recovery Desired 160 lbs He/flt |
| II Only | Rocket Ozonesonde | Tom Perry (NASA-WFC) | 4* | 3 flts | 2 hrs | 250,000 ft | 16 ft | 18 ft | 2 lbs | -- | 1 68 GHz | 250 mw | GMD Recovery not required Tracking desired radar Rocket launcher |
| II Only | Balloon Ozonesonde | Tom Perry (NASA-WFC) | 2* | 3 flts | 2 hrs | 100,000 ft | 9 ft | 50 ft | 4 lbs | 6 in | 1 68 GHz | 250 mw | GMD No recovery 9 lbs He/flt |
| I & II | Radiosonde | Tom Perry (NASA-WFC) | 2* | 16 flts (2 flts/day) | 2 hrs | 100,000 ft | 6 ft | 50 ft | 2 lbs | 6 in | 1 68 GHz | 250 mw | GMD No recovery 9 lbs He/flt |
| I & II | Airborne In Situ Observations | Gerald W Grams (Ga Tech ) | 7 | 8 flts (1 flt/day) | 3 hrs | 40,000 ft | | | | | | | |

*Only five people are required to support these three measurements

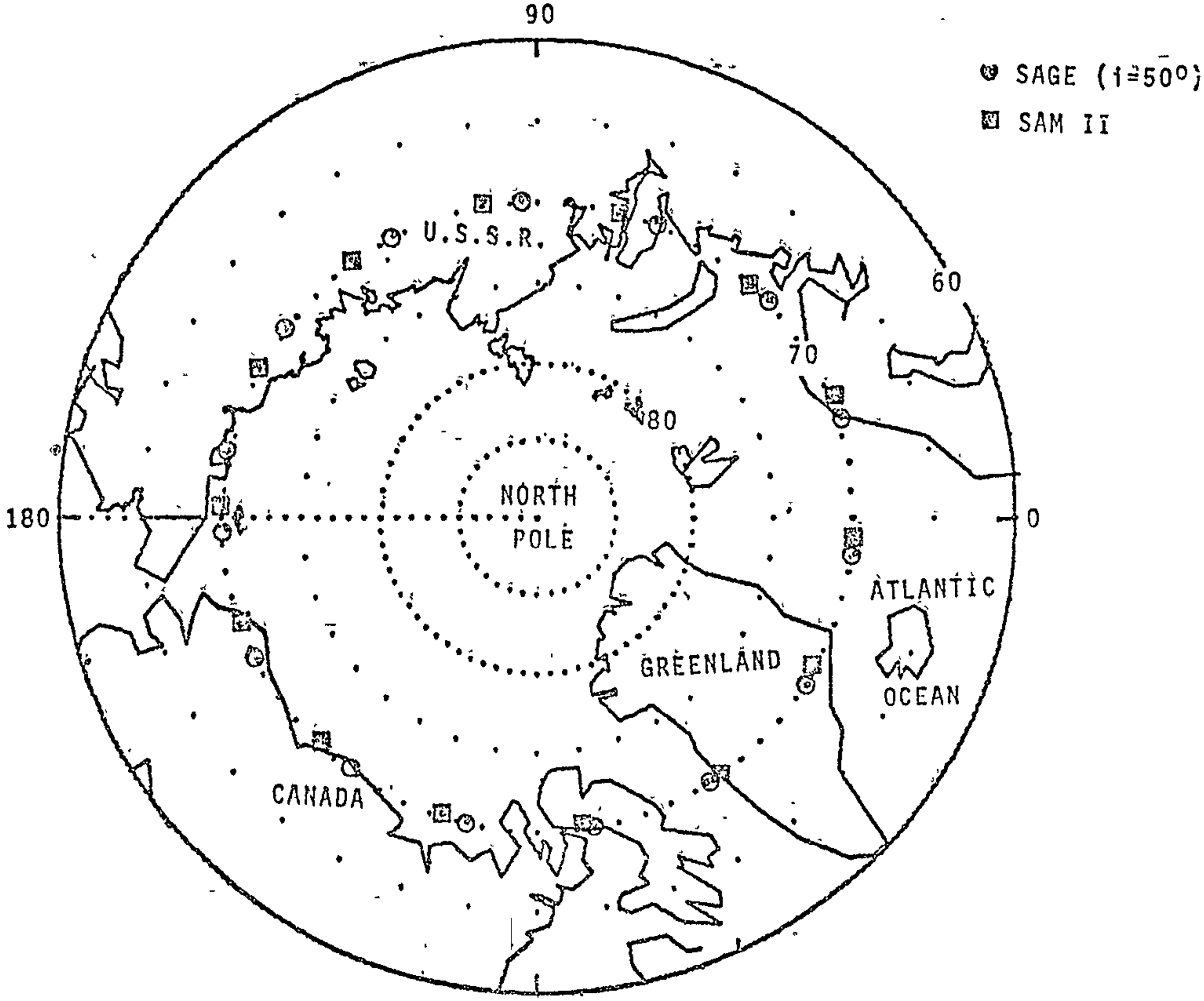


FIGURE 19 TYPICAL DAY OF OVERLAP OF SAM-II AND SAGE COVERAGE NORTHERN HEMISPHERE. Predicted locations are for May 19, 1979.

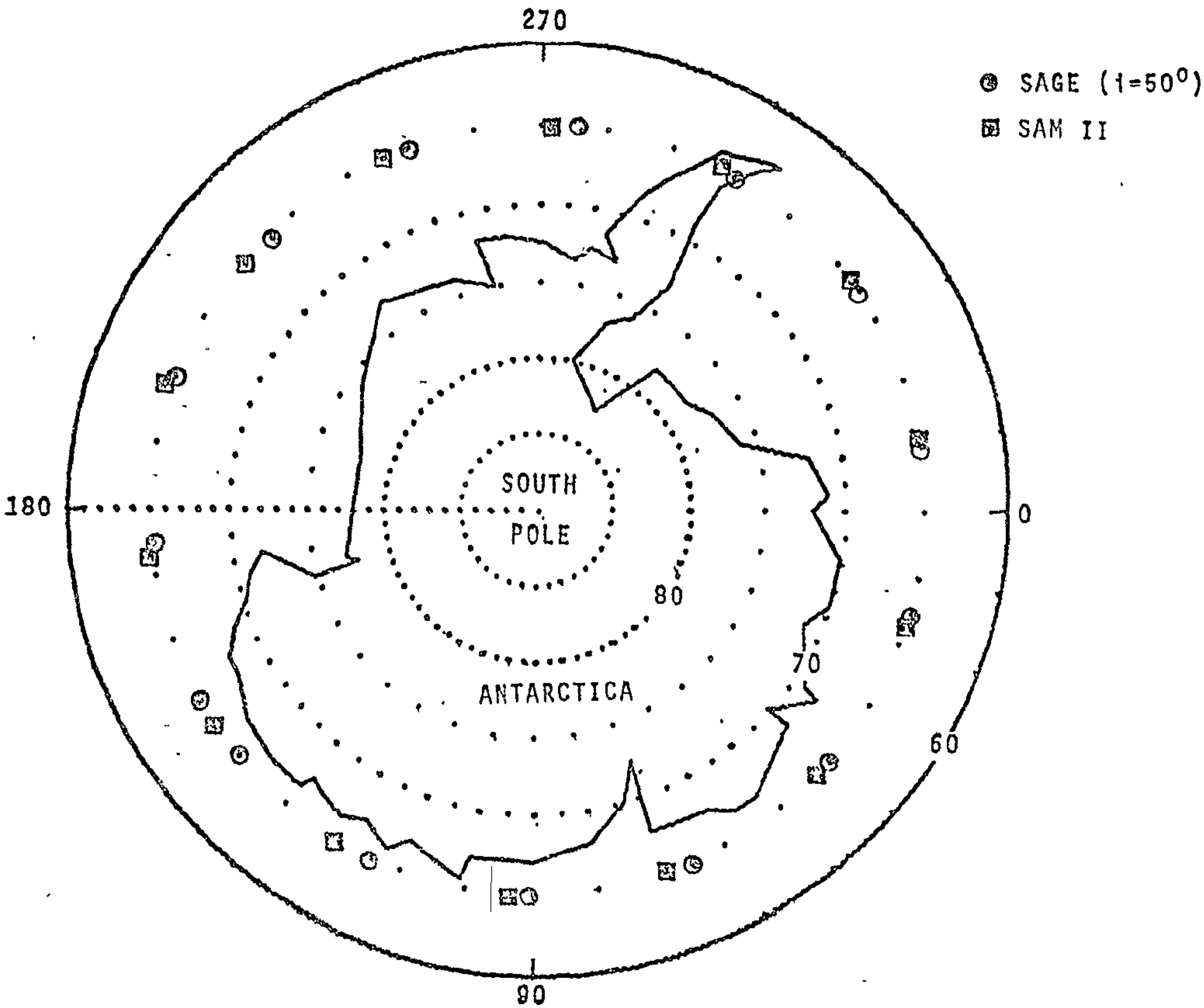


FIGURE 20 TYPICAL DAY OF OVERLAP OF SAM-II AND SAGE COVERAGE: SOUTHERN HEMISPHERE. Predictions are for December 21, 1978

## 4. DATA PROCESSING

Procedures for reducing ground-truth data to formats that are readily comparable to SAM-II extinction and number profiles will be established and tested prior to launch, so that data comparisons can be carried out in the shortest time possible For example, Figure 21 shows the data processing flow established for the airborne lidar

### 4.1. Ancillary Data

Both the lidar and sunphotometer data require a molecular density profile for separation of gaseous from particulate optical coefficients. In addition, the lidar data (especially ruby data) require an estimated ozone and particulate extinction profile A two-step process will be used to incorporate these ancillary data into the data analysis

#### 4.1.1. Model Atmospheres

Prior to launch, model profiles of atmospheric density and of ozone and particulate extinction (at the lidar wavelengths) will be developed for the location and month of each ground-truth site (see Table 7). These profiles will be stored on cards or another medium that can be computer-read as input to the lidar and sunphotometer data reduction algorithms (see Section 4 2). They will be used for first-cut reduction of the lidar and balloon photometer data.

#### 4.1.2. Measured Atmospheres

Each northern hemisphere ground-truth experiment will include dustsonde flights, which provide temperature-vs-pressure profiles in addition to the aerosol data These profiles will be converted to density profiles and stored in the same format as the model density profiles, so they can be readily substituted for the model profiles in the data reduction In addition, as a routine part of SAM-II data reduction, estimated density profiles for the time and location of each SAM-II scan will be interpolated from gridded 12-hour WMO analysis data. (The sources of these gridded data are rawinsondes, rocketsondes, and satellite radiometers ) These interpolated density profiles will be extracted from the SAM-II data tapes and stored in the same format as the model and dustsonde-measured density profiles Model, dustsonde-measured, and interpolated density profiles will be plotted for each ground-truth experiment when available In this manner differences in density profiles can be highlighted, and, by sequentially using each profile in the data analysis, effects of density differences on derived aerosol properties (both SAM-II and ground-truth) can be explored and understood

During each Sondrestrom experiment, two standard rawinsonde flights will be made each day These will be used as appropriate to obtain best-estimate density profiles for reducing ground-truth data

Carefully chosen model ozone profiles are probably adequate for lidar data reduction (certainly for Nd lidar), but nevertheless, measured ozone profiles near the time and location of lidar flights will be compared to the model profiles and substituted if necessary Likewise, particulate extinction profiles (at the lidar wavelength) derived from the lidar and SAM-II measurements will be compared to the model profiles and iteratively substituted whenever appropriate

### 4.2. Conversion to Particulate 1-$\mu$m Extinction Profiles

#### 4.2.1. Airborne Lidar

The lidar data will be reduced to vertical profiles of particulate backscattering coefficient (at the lidar wavelength) by using data reduction techniques similar to those routinely employed by SRI and NASA Langley in many previous measurements (See, e.g Russell et al., 1976a,b.) The reduction algorithm will include automatic computation of error bars that include contributions from uncertainties in: (1) signal measurement, (2) density estimation, (3) transmission estimation, and (4) normalization (See Figure 9 ) In addition, scattering ratio profiles will be normalized to force the minimum scattering ratio to equal the value expected on

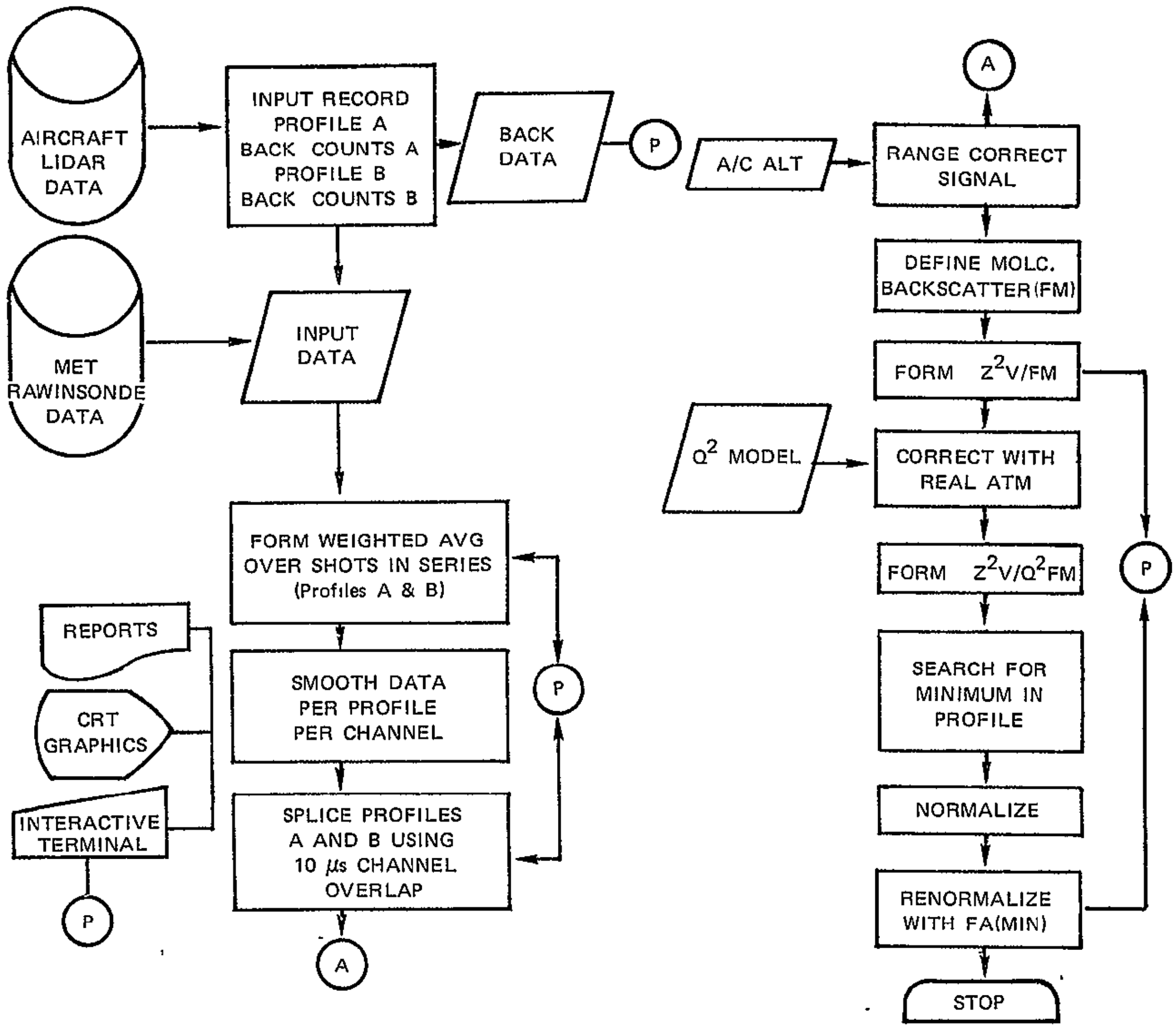


FIGURE 21 SAM-II AIRCRAFT LIDAR DATA PROCESSING FLOW

the basis of previous dustsonde measurements and optical models (e g , Russell et al., 1976b), rather than the value of unity that has customarily been assumed in the past. (This procedure has the effect of symmetrizing the expected normalization error and reducing it by about one-half )

The derived profiles of particulate backscattering coefficient will be converted to profiles of 1.0-$\mu$m extinction coefficient by using an appropriate conversion factor from Figure 17. Extinction error bars will also be computed, based on the particulate backscattering error bars and the uncertainty in the conversion factor (See discussion accompanying Figure 17 and Table 6 )

Both the backscattering and extinction profiles will be plotted on scales that permit easy comparison with the SAM-II extinction profiles provided as standard output products (GSFC, 1975, 1976) Figure 22 shows the specifications of these profiles. All plots of lidar output data products will show error bars at 1-km intervals. In addition to the plots shown in Figure 22, both SAM-II and lidar data will be plotted with more sensitive horizontal scales, so that all features of interest in the particular measurement are clearly displayed

The lidar-measured backscattering coefficient profile (Figure 22a) will be superimposed on the SAM-II extinction coefficient profile (similar to Figure 22b) to derive a cross-wavelength extinction-to-backscatter ratio (which may be height-dependent) Conversion ratios derived in this manner will be compared with the values in Figure 17 to help in selection of appropriate optical models and subsequent aspects of data validation and reduction.

#### 4.2.2. Dustsondes

The dustsonde data will be reduced to vertical profiles of $N_{15}$ and $N_{15}/N_{25}$ by using the data reduction techniques routinely employed by the University of Wyoming for many years ($N_x$ is the number of particles with radius $\geqslant$ x $\mu$m; cf. Figure 7 ) The derived profiles of $N_{15}$ and $N_{15}/N_{25}$ will be converted to profiles of 1.0-$\mu$m extinction coefficient by using an appropriate conversion factor from Figure 8 Extinction error bars will also be computed, based on the uncertainties in $N_{15}/N_{25}$ and the conversion ratio.

Number and extinction profiles derived from the balloon data will be plotted on scales as shown in Figure 23 The extinction (Figure 23b) will be directly compared to the corresponding lidar (Figure 22b) and SAM-II results In addition, the particle number profile (Figure 23a) will be used to derive a (possibly height-dependent) extinction-to-number ratio for comparison with Figure 8, and will be directly compared with the particle number profile derived from the SAM-II extinction profile

#### 4.2.3. Balloonborne Sunphotometer

The sunphotometer data will be reduced to vertical profiles of particulate 1.0-$\mu$m extinction using algorithms now being developed by T Pepin at University of Wyoming These results will be plotted as in Figures 22b and 23b Error bars will be plotted at 1-km intervals

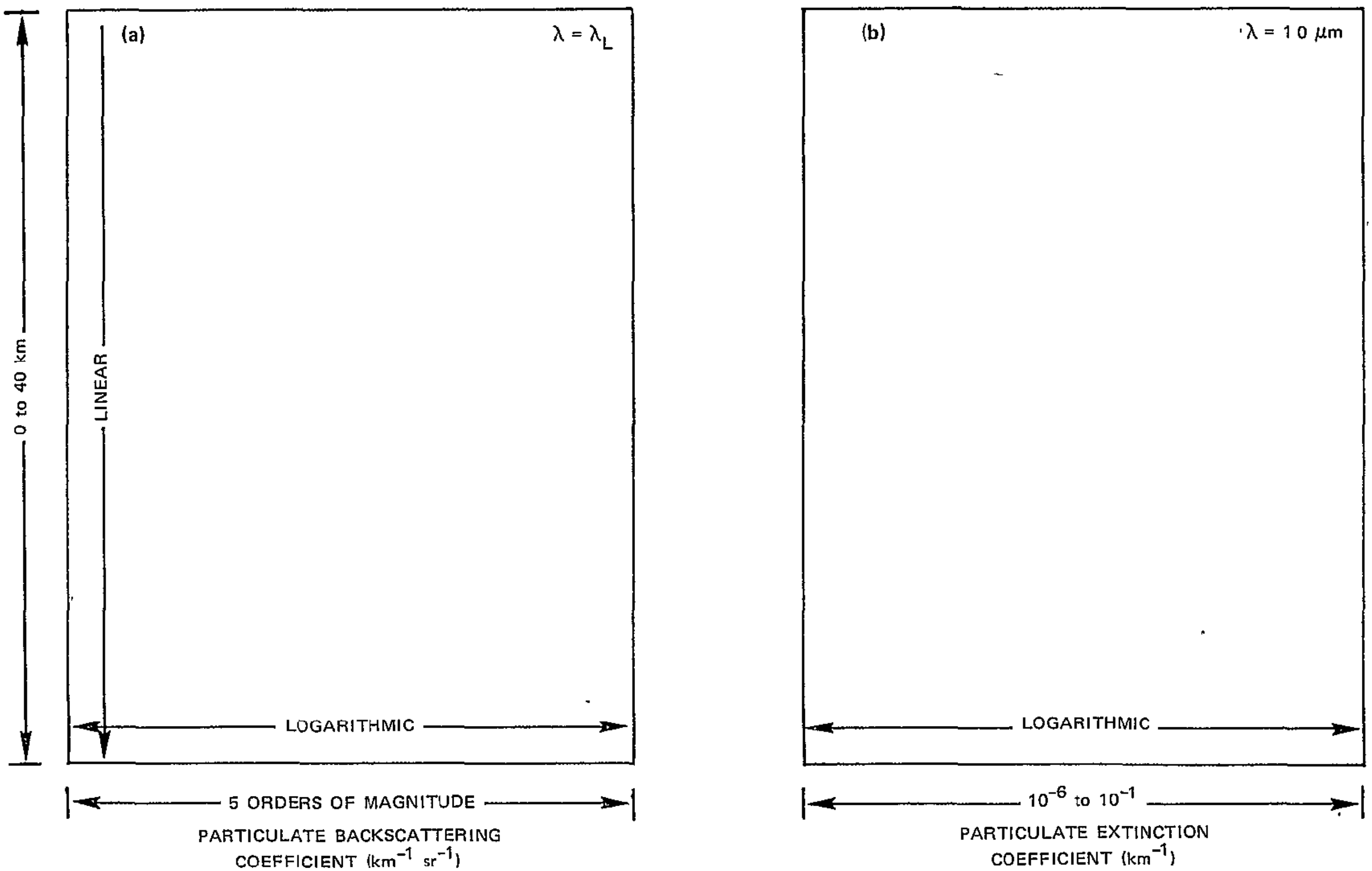


FIGURE 22 PLOTTING SPECIFICATIONS FOR LIDAR OUTPUT DATA PRODUCTS
$\lambda_L$ is lidar wavelength. Plots will also be prepared with more sensitive horizontal scales, to clearly display all profile features of interest Frames shown are not to scale Actual frames should be *square*, to match shape of microfilm data frames.

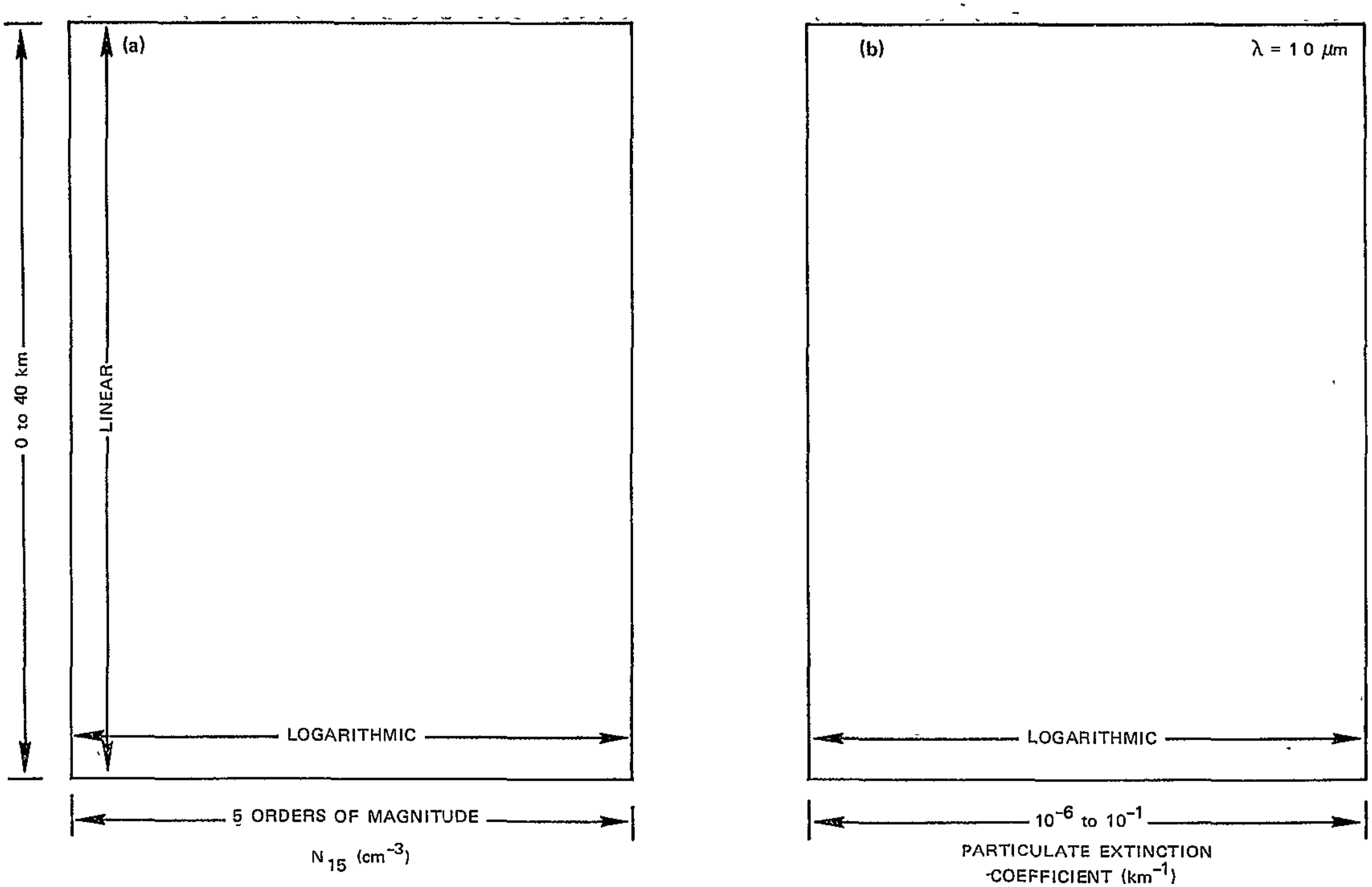


FIGURE 23 PLOTTING SPECIFICATIONS FOR DUSTSTONDE OUTPUT DATA PRODUCTS Plots will also be prepared with more sensitive horizontal scales, to clearly display all profile features of interest Frames shown are not to scale Actual frames should be *square*, to match shape of microfilm data frames.

## REFERENCES


Bronshten, V.A., and N I Grishkin, 1975. *Noctilucent Clouds,* Keter Publications, Jerusalem, 288 pp.

Chu, W.P., T.J Swissler, and M.P. McCormick, 1977 Theoretical analysis of the retrieval of stratospheric aerosol vertical profiles from spacecraft measurements of solar extinction in the 0 3-1.0 μm region *Proc. Symp. Rad. in Atmos.,* pp 138-140, H J Bolle, Ed , Science Press, Princeton, N J

Deirmendjian, D , 1969· *Electromagnetic Scattering on Spherical Polydispersions,* Elsevier, New York.

Evans, W E., 1977· Design of an Airborne Lidar for Stratospheric Aerosol Measurements. Final Report 5557, SRI International, Menlo Park, CA 94025.

Evans, W.E , 1978 Evaluation of a near-infrared photomultiplier for airborne lidar applications. Draft Final Report, Contract NAS1 15114, SRI Project 6919, March 1978, to NASA Langley Research Center, Hampton, VA.

Fuller, W.H , T.J. Swissler, and M P McCormick, 1976: Comparative analysis of red-blue lidar and rawinsonde data Paper TuC2 of Atmospheric Aerosols Their Optical Properties and Effects. NASA CP-2004, available from NASA Langley Research Center, Hampton, VA 23665

GSFC, 1975, 1976. Nimbus Observation Processing System (NOPS) Design Study Report, Main Volume and Appendix D. NASA Goddard Space Flight Center, Greenbelt, MD 20771, October 1975 and January 1976.

Harris, F.G., and J.M. Rosen, 1976· Measured and analytic distributions of stratospheric aerosols A review and commentary *Atmospheric Aerosols Their Optical Properties and Effects* NASA CP-2004, pp. MA2-1 to MA2-4. National Aeronautics and Space Administration, Langley Research Center, Hampton, VA 23665.

Hofmann, D.J , J M Rosen, T J Pepin, and R G. Pinnick, 1975 Stratospheric aerosol measurements I: time variations at northern mid-latitudes *J Atmoc. Sci., 32,* 1446-1456

Hofmann, D.J. and J M Rosen, 1977: Balloon observations of the time development of the stratospheric aerosol even of 1974-1975 *J Geophys Res., 82,* 1435-1440

Hoxit, L R , and R M Henry, 1973· Diurnal and annual temperature variations in the 30-60 km region as indicated by statistical analysis of rocketsonde temperature data *J Atmos Sci , 30,* 992-932

Lenhard, R W., 1973 A revised assessment of radiosonde accuracy *Bull Amer Meteor. Soc., 54,* 691-693

McCormick, M P , H.B Edwards, L.E Mauldin, III, and L R McMaster, 1976 Satellite Solar Occultation Measurements SAM-II and SAGE *Atmospheric Aerosols. Their Optical Properties and Effects,* NASA CP-2004, pp TuB2-1 to TuB2-4. Available from National Aeronautics and Space Administration, Langley Research Center, Hampton, VA 23665

Pinnick, R G and D J. Hofmann, 1973· Efficiency of light-scattering aerosol particle counters. *Appl Opt., 12,* 2593-2597

Pinnick, R G., J M Rosen, and D J Hofmann, 1976· Stratospheric aerosol measurements III optical model calculations *J Atmos. Sci ,* 33, 304-314

Pepin, T J., 1970 The use of extinction from high altitude balloons as a probe of the atmospheric aerosols Ph D Thesis, Part II, Dept of Physics and Astronomy, University of Minnesota

Pepin, T.J , 1977 Inversion of solar extinction data from the Apollo-Soyuz Test Project Stratospheric Aerosol Measurement (ASTP/SAM) *Inversion Methods in Atmospheric Remote sounding,* NASA CP-2004, available from NTIS

Pepin, T.J., and T.A. Cerni, 1977 Definition of Model Atmospheres for Application in Preliminary Studies of the Stratospheric Aerosol Experiment (SAM-II) Aboard the Nimbus-G Spacecraft Report APP-11, Dept. of Phys and Astron , Univ. of Wyoming, Laramie, WY 82070.

Pepin, T.J. and T.A. Cerni, 1978 High-latitude model atmospheres for application to the SAM-II experiment, SAGE experiment, and associated ground-truth measurements Report APP-20, Dept of Phys and Astron., Univ of Wyoming, Laramie, WY 82070

Rosen, J M , 1964: The vertical distribution of dust to 30 km. *J. Geophys Res., 69,* 4673-4676.

Rosen, J.M., D J. Hofmann, and J. Laby, 1975 Stratospheric aerosol measurements II. the worldwide distribution. *J. Atmos Sci , 32,* 1457-1462

Russell, P B , and R D Hake, 1977 The post-Fuego stratospheric aerosol: lidar observations with radiative and thermal implications *J. Atmos. Sci , 34,* 163-177.

Russell, P B , W. Viezee, R D. Hake, Jr., and R T.H Collis, 1976a Lidar measurements of the stratospheric aerosol: California, October 1972 - February 1974 *Quart. J. Roy. Meteor Soc., 102,* 675-695.

Russell, P B , W Viezee, R.D. Hake, Jr , and R T.H Collis, 1976b. Lidar measurements of the stratospheric aerosol summary of results and a calibration error assessment Proc Fourth Conf. Climatic Impact Assessment Prog., U S Dept of Transportation Report DOT-TSC-OST-75-38, August 1976, Available from NTIS

Shettle, E S., and R.W. Fenn, 1976. Models of atmospheric aerosols and their optical properties. AGARD Optical Propagation in the Atmosphere, 27-31 Oct., Conf. Proc., GP-183, pp 2-1 to 2-16.

Swissler, T J , and F S Harris, Jr., 1976 Comparison of Extinction and Backscattering Coefficients for Measured and analytic stratospheric aerosol size distribution. Atmospheric Aerosols Their Optical Properties and Effects, NASA CP-2004, MC11-1 to MC11-4

Toon, O.B., and J.B. Pollack, 1976 A global average model of atmospheric aerosols for radiative transfer calculations. *J. Appl. Meteor., 15,* 225-246.

Wu, M -F , 1973: Observation and Analysis of Trace Constituents in the Stratosphere Report No ERT P-93 DOT-TST-74-7, Available from NTIS, Springfield, VA 22151

## Appendix A

## THE SAM-II INSTRUMENT AND EXPECTED MEASUREMENT ERRORS

## THE SAM-II INSTRUMENT AND EXPECTED MEASUREMENT ERRORS

Figures A1 and A2 show exterior and cross-sectional views of the SAM-II instrument. The instrument uses the sun as a constant radiant source and measures the radiation that reaches the spacecraft after penetrating the earth's atmosphere during spacecraft sunrise and sunset events The instrument's passband, centered at a wavelength of 1 $\mu$m (see below) is in a window region of the atmosphere, where gaseous absorption is negligible Hence, any attenuation of refracted radiation beyond that caused by gaseous Rayleigh scattering can be attributed to suspended aerosol particles.

*Instrument Configuration.* The SAM-II instrument package consists of optical and electronic subassemblies mounted side by side (see Figure A1). The optical subassembly (Figures A2 and A3) consists of gimbals, a flat entrance window, Cassegrain optics, a flat scanning mirror, sun acquisition sensors, and a detector package The entire optical subassembly is gimballed in azimuth The azimuth servo employs sun sensors driven to null on the center of the sun to a tolerance of ±2 arc minutes

*Operating Sequence.* At the beginning of a sunrise or sunset event, the optical subassembly slews in azimuth to a position to acquire the sun (approximately 180° from the last event or as determined by commands) Upon acquisition in azimuth, the mirror servo scans in elevation until the sun is acquired. The scan range is then reduced to scanning back and forth across the solar image only. Edge detectors on the detector package (Figure A2) monitor solar limb crossings. Time is recorded for each detected limb crossing, both going on and going off the sun Also, each time a limb is crossed going off the sun, a servo timer is triggered to reverse scan mirror direction in a fixed time increment The scan sequence is also reinitiated again

The science data stream is read at a constant 50 samples per second synchronized with the main frame pulse of the Versatile Information Processor (VIP) of the Nimbus G Spacecraft Data points can be correlated with position on the solar image by extrapolating edge crossing times, linear scan rates, and spacecraft ephemeris data in coordination with a model of solar refraction by the earth's atmosphere The data are digitized to 10 bits for a science data rate of 500 bits per second

*Spectral Parameters* The flat entrance window filters out the UV component of the solar spectrum Thereafter, an interference filter rejects all but the 1-$\mu$m passband, resulting in the response curve shown in Figure A4

*Spatial Parameters.* The instrument scans the vertical center of the solar disk with a 0 177 mrad IFOV Angular rate of the scan mirror is 2.18 ± 0 011 mrad/sec

*View Axis.* 0.44 rad azimuth perpendicular to orbit plane, approximately 0 40 rad to 0 58 rad depression from horizontal (pitch) in forward and rearward directions

*Radiometric Parameters*

| | |
|---|---|
| Dectector | = Pin Photodiode Type |
| Dynamic Range | = 100 |
| Accuracy | = 0 3% of Full Scale |

PRECEDING PAGE BLANK NOT FILMED

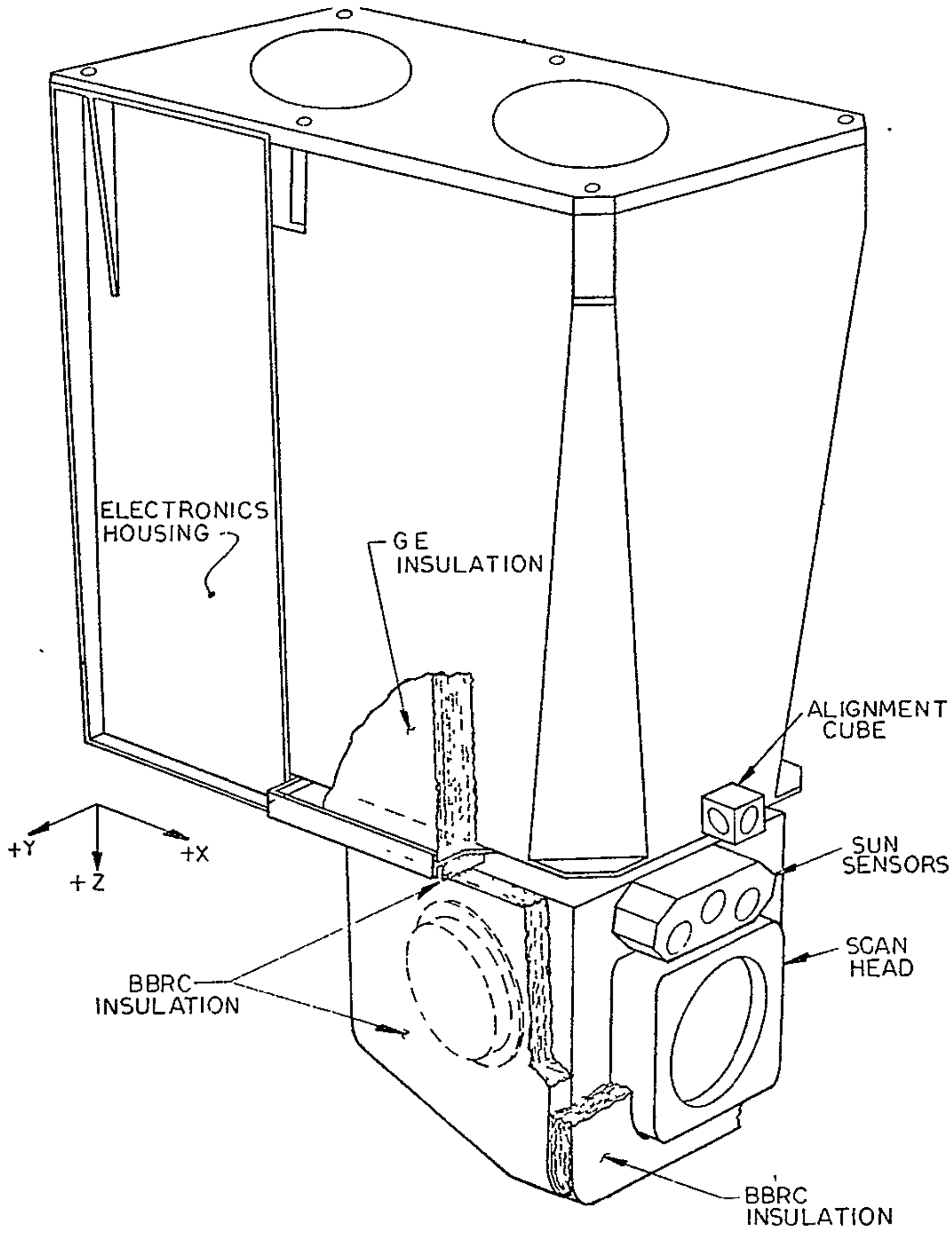


FIGURE A1 SAM-II INSTRUMENT MOUNTED IN INTERFACE STRUCTURE

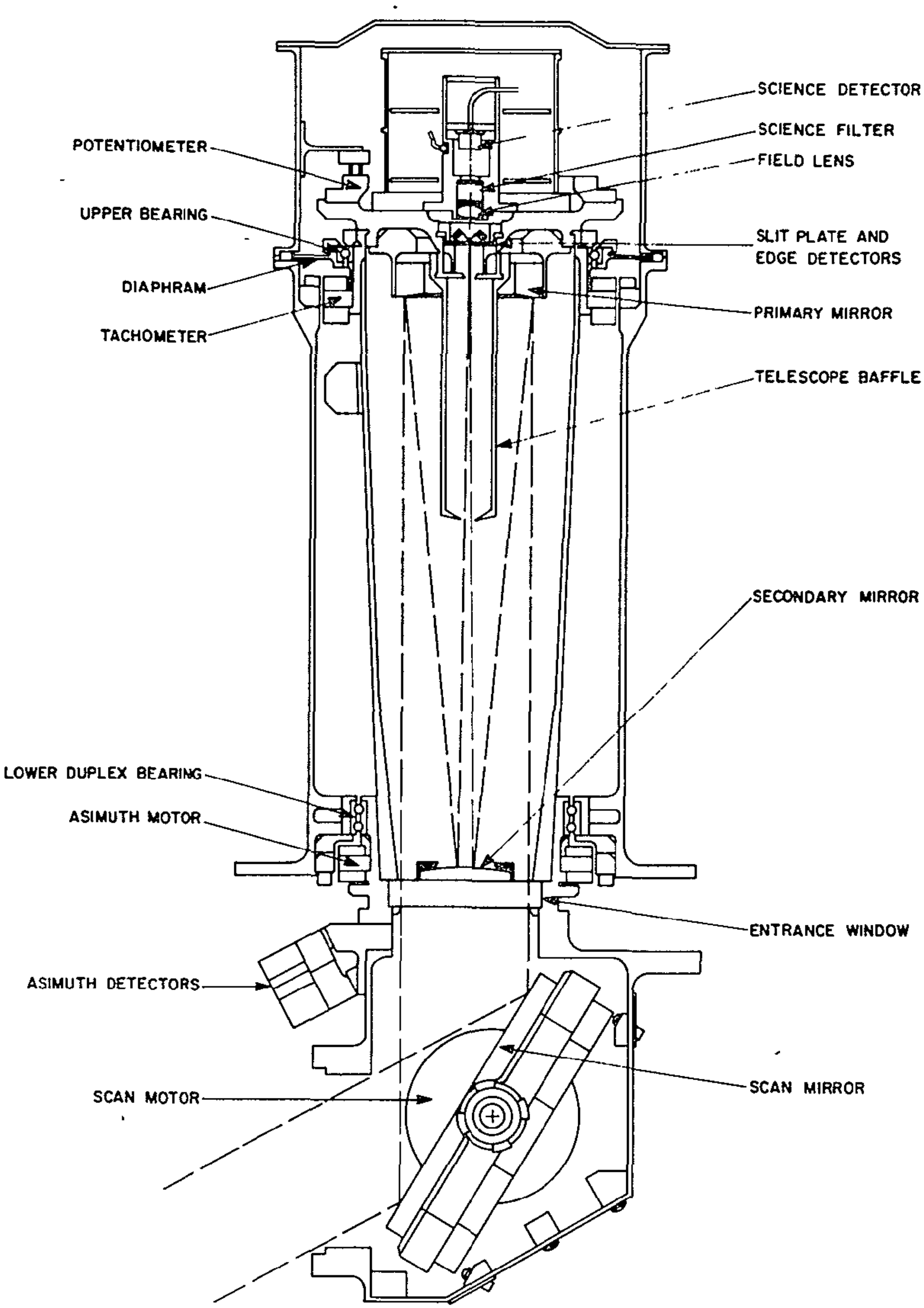


FIGURE A2 SAM-II POINTING SYSTEM CROSS SECTION

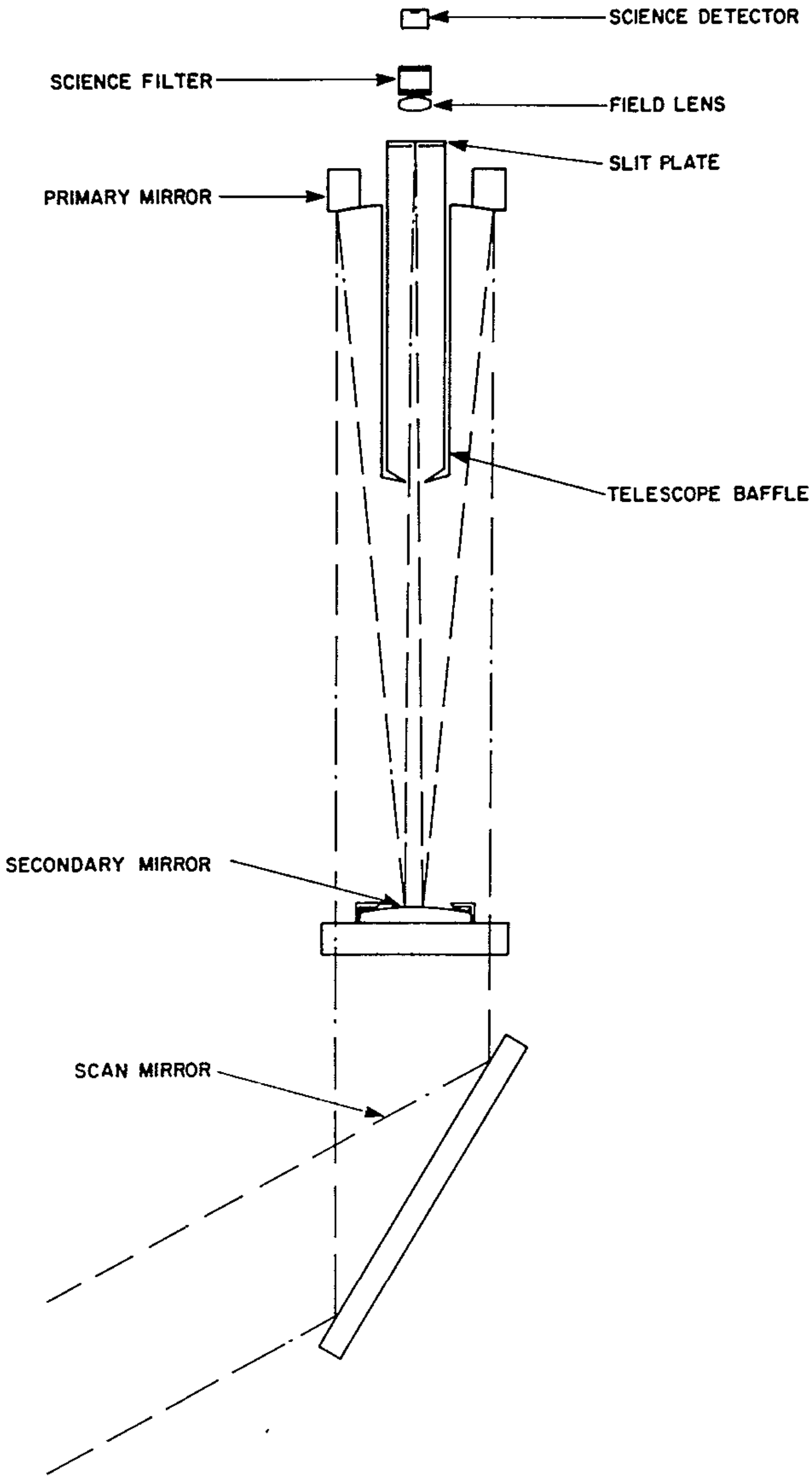


FIGURE A3 SAM-II OPTICAL SYSTEM

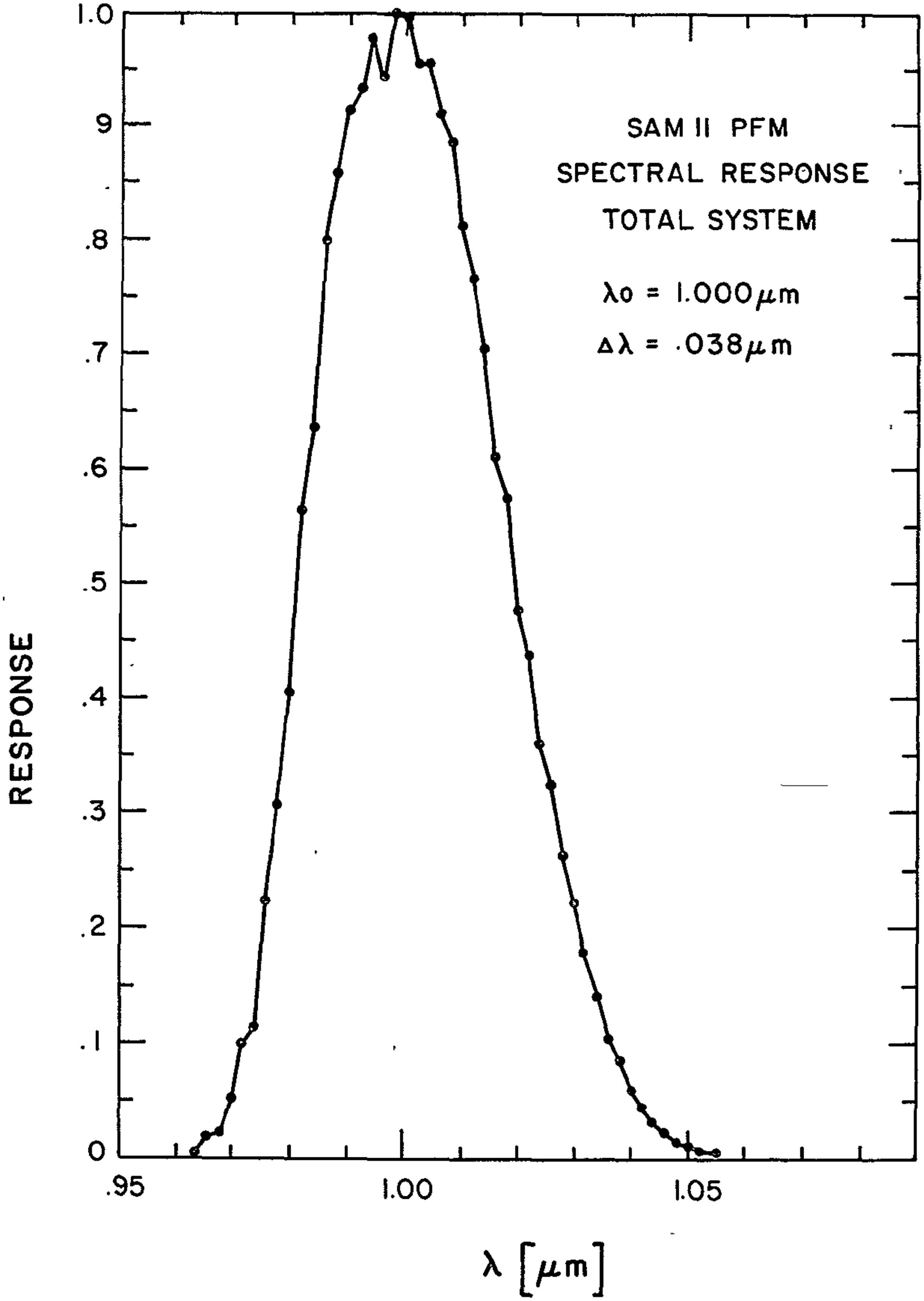


FIGURE A4 SAM-II SCIENCE DETECTOR RESPONSE CURVE

*Instrument Error.* The two sources of instrumental error are (1) radiometric measurement and digitization, and (2) pointing. Table A1 summarizes the radiometric errors as determined by measurements and calculations up to September 1977 The uncertainty in pointing is estimated at 4 sec or 1.9 x 10-5 rad, based on latest tests, October 1977 The effect of these expected instrumental errors, in combination with expected errors in the molecular density profile, on the accuracy and resolution of inverted particulate extinction profiles is discussed in Section 1.1. of the main text. (See Figures 3 and 4 and accompanying discussion.)

Table A1.

SAM-II ERRORS - RADIOMETRIC MEASUREMENT AND DIGITIZATION

| ERROR SOURCE | ERROR % | MEASURED | CALCULATED |
|---|---|---|---|
| ELECTRICAL SYSTEM | | | |
| A/D System | | | |
| Encoding Error | ±.05 | X | |
| D/A Converter Zero | ±.005 | | X |
| D/A Accuracy | ±.04 | | X |
| +15 Supply Drift Rejection | ±.005 | | X |
| -15 Supply Drift Rejection | ±.015 | | X |
| LMIII | | | |
| Offset Voltage | ±.007 | | X |
| Offset Current | ±.0002 | | X |
| Sample Hold | | | |
| Gain Error | ±.03 | | X |
| Droop | -.02 | | X |
| Total Electrical System | ±.16 | | X |
| Total Electrical System | ±.12 | X | |
| DETECTOR SYSTEM | | | |
| Temperature Stability | ±.01 | X | |
| Detector Linearity | ±.05 | | X |
| Detector Linearity | ± \|<.1\| | X | |
| Total Detector System | ±.06 | | |
| OPTICAL SYSTEM | | | |
| Polarization | ±.004 | | X |
| Above Band Rejection | ±.01 | X | |
| Below Band Rejection | +.0001 | X | |
| Scan Mirror Non-Uniformity | ± \|<.01\| | X | |
| Scattered Light | +.1 | X | |
| Total Optical System | +.12 | | |

Worst Case:

| | |
|---|---|
| Electrical | ±.12 |
| Detector | ±.06 |
| Optical | +.12 |
| Total Worst Case | .30 |
| RSS | ±.12 |
| | ±.01 |
| | ±.05 |
| | ±.004 |
| | +.01 |
| | +.0001 |
| | ±.01 |
| | +.1 |
| Total RSS | .16 % |

# Appendix B

## SURVEY OF POTENTIAL GROUND TRUTH SUPPLIERS

PAGE _____ INTENTIONALLY BLANK

STANFORD RESEARCH INSTITUTE
MENLO PARK, CALIFORNIA 94025
(415) 326-6200

PRECEDING PAGE BLANK NOT FILMED

21 July 1976

The Nimbus-G Spacecraft will be launched by the National Aeronautics and Space Administration in October, 1978. It will carry highly advanced meteorological, oceanographic, and earth-surface-sensing instruments to obtain a variety of environmental information. One of these is the Stratospheric Aerosol Measurement (SAM-II) instrument, which will measure vertical profiles of aerosol extinction in the upper troposphere, the stratosphere, and above.

SAM-II is a one-channel photometer that measures the intensity of sunlight (at wavelength 1 μm) traversing the earth's limb during spacecraft sunrise and sunset events. In this manner it will measure vertical profiles of aerosol extinction in arctic and antarctic regions, at the rate of about 28 profiles per day. The latitude bands 64° to 80° N and S will be covered during each 3-month period of observations. The resulting data will constitute the first systematic atlas of stratospheric and mesospheric aerosol extinction measurements. They will be archived and made available to the scientific community for use in a variety of studies.

A very important step in making these data available to the scientific studies is to validate them by making comparisons between the SAM-II measurements and other aerosol measurements made nearby in space and time. This validation is a primary function of the SAM-II Nimbus-G Experiment Team, which consists of Dr. M. P. McCormick (Team Leader), Dr. T. J. Pepin, Dr. G. W. Grams, Dr. B. M. Herman, and me. Our first action is to identify those data available from other measurements that can be used for validation purposes. Not only aerosol measurements *per se*, but also related information, such as volcanic eruption and noctilucent cloud observations, will be useful to us.

We would appreciate your assistance by filling out the enclosed questionnaire and returning it to me at your earliest convenience. Attached to the questionnaire are guidelines for the type of information required for our planning Even if you do not plan to make aerosol measurements during the SAM-II validation period, please answer the Part I regarding possible data use, as this will aid us in our efforts to accelerate data utilization.

We look forward to your support of this very important phase of a major stratospheric research endeavor.

Sincerely,

Phil Russell

Philip B. Russell
Science Coordinator for Data Validation
SAM-II Nimbus-G Experiment Team

PBR:tr

## PART I: POTENTIAL APPLICATIONS OF SAM-II DATA

I would like to use SAM-II data in the following scientific studies

(Check as many as are appropriate)

- ☐ Radiative Transfer
- ☐ Earth Radiation Balance and Climate
- ☐ Pollution Background
- ☐ Pollution Sources and Sinks
- ☐ Atmospheric Chemistry
- ☐ Atmospheric Dynamics and Transport
- ☐ Mesospheric Scattering and Noctilucent Clouds
- ☐ Aerosol Optical and Physical Models
- ☐ Aerosol Effects on Passive Sensors
- ☐ Other (Please Specify) ____________________

Date: ____________________

Name: ____________________

Address: ____________________

____________________

____________________

(Name and Address: May be left blank if following page is filled out.)

Return to:

Dr. Philip B.Russell, K2056
Atmospheric Sciences Laboratory
Stanford Research Institute
Menlo Park, CA 94025

PART II: AVAILABILITY OF DATA TO VALIDATE SAM-II MEASUREMENTS

The following measurements or observations, relevant to SAM-II validation, are contemplated: (see sample responses on following page)

1. Parameter to be measured:
2. Accuracy of measurement:
3. Altutide region:
4. Altitude resolution:
5. Observation period:
6. Frequency of observation:
7. Measurement technique:
8. Instrument type:
9. Measurement platform:
10. Type of data product:
11. Funding authority:
12. Measurement program:
13. Status of prime instrument:
14. Assurance of instrument availability in Oct. 1978-Sept. 1979:
15. Location of measurement:
16. Experimental limitations:
17. Instrumental physical characteristics
18. Experimenter operation experience:

Date: ______________________________

Prepared by: ________________________

Address ____________________________

____________________________

____________________________

Return to:

Dr. Philip B. Russell, K2056
Atmospheric Sciences Laboratory
Stanford Research Institute
Menlo Park, CA 94025

## Guidelines for Part II

The following guidelines are to assist you in supplying the necessary information for Part II of the questionnaire. The completed questionnaires will be evaluated to identify all sources of data, as well as glaring deficiencies, and will be used to establish the validation program which will be part of the Nimbus-G Data Plan.

| Required Parameter | Example of Responses |
|---|---|
| 1. Parameter to be measured: | Aerosol particle number; back-scattering coefficient; noctilucent cloud occurrence |
| 2. Accuracy of measurement: | %, $\pm$ a $m^{-1}sr^{-1}$ |
| 3. Altitude region: | a km to b km |
| 4. Altitude resolution | c km |
| 5. Observation period: | June-August 1979 |
| 6. Frequency of observation· | single flight weekly |
| 7. Measurement technique: | in situ, remote |
| 8. Instrument type: | lidar, sampler |
| 9. Measurement platform: | RB-57 at 20 km altitude |
| 10. Type of data product: | direct, analysis |
| 11. Funding authority: | FAA, COVOS |
| 12. Measurement program: | Atmospheric radiation studies, part of WWW, flight test for specific instrument development, etc. |
| 13. Status of prime instrument: | x years of use, demonstration planned for _____; research stage |
| 14. Assurance of instrument of availability in Oct. 1978 | % probability |
| 15. Location of measurement: | Siberia; Fairbanks, Alaska |
| 16. Experimental limitations: | day-night, duration |
| 17. Instrumental physical characteristics: | weight, size, power requirements |
| 18. Experimenter operation experience: | 10 flights in RB-57 |

## Table B1

### POTENTIAL GROUND TRUTH SENSORS LOCATED BY SURVEY

Part A. Ground-Based

| Scientist (Group) | Type of Instrument | Type of Measurement | Availability in Oct. 1978 | Funding Agency | Measurement Site | Instrument Parameters Size (cm) | Weight (kg) | Power (w) |
|---|---|---|---|---|---|---|---|---|
| McCormick (NASA Langley) | Ruby-Nd lidar | Scattering ratio 6-40 km | 95% | NASA | Hampton, Va (home) or other (movable system) 37° N, 76° W | | | |
| Grams (NCAR) | Dye lidar | Scattering ratio 0-30 km | Medium | NSF | (Mobile System) | | 400 | 3-4kw |
| Frush (NCAR) | Ruby lidar | Scattering ratio 1-50 km | High | NSF | Boulder, Co 40° N; 105° W | | | |
| Isono (Japan WRI) | Ruby-Nd lidar | Scattering ratio 10-40 km | 90% | Japan Min. of Educ. | Nagoya, Japan 35° N, 137° W | | | |
| Reiter (IAUFG, Garmisch-Partenkirchen) | Ruby lidar | Scattering ratio 0-40 km | 100% | FRG | 47°N, 11°E Garmisch-Partenkirchen | | | |
| Derr (NOAA/ERL) | Ruby & dye lidar | Scattering ratio | Medium | NOAA | Boulder, CO | | | |
| Hirono (Kyushu Univ.) | Ruby lidar (may add YAG) | Scattering ratio 10-35 km | 95% | Japan Min of Educ. | 34°N, 131°E Fukuoka, Japan | 300x300x300 | 1000 | 700 |
| Keenliside (UWI) | Two ruby lidars | Molecular density 15-100 km Scattering ratio 15-40 km | 85% | None | Kingston, Jamaica 18° N, 77° W | | | |
| Goldsmith (Met. Office, London) | Dye lidar | Scattering ratio 15-45 km | 75% | U.K. Met. Off. | 51°N, 1°W | | | |

## Table B1 Continued

POTENTIAL GROUND TRUTH SENSORS LOCATED BY SURVEY

Part A. Ground-Based (continued)

| Scientist (Group) | Type of Instrument | Type of Measurement | Availability in Oct 1978 | Funding | Measurement Site | Instrument Parameters Size (cm) Weight (kg) Power (w) |
|---|---|---|---|---|---|---|
| Fegley (NOAA/ARL) | Dye lidar | Scattering ratio 2-25 km | high (planned start summer 1977) | NOAA (GMCC) | Barrow, Alaska (71° N, 156° W) | |
| Fegley (NOAA/ARL) | Ruby lidar | Scattering ratio | high | NOAA | Mauna Loa Hawaii (19° N, 156° W) | |
| Dilley (CSIRO) | Ruby lidar | Scattering ratio 7-40 km | 80% | CSIRO | Aspendale, Australia 38° S, 145° E | |
| Shaw (U. Alaska) | Sunphotometer<br>Twilight Photometer<br>Emis. flux sensor<br>(Navy C-112 flts poss) | Aerosol opt. thck (λ) 10-30km (5-km ver res) | | prop to NASA | Mauna Loa, FAI (?) S. Pole Am Arctic | |
| Porch (L. Livermore L.) | Nephelometer & transmissometer (stellar extinction) | Vert. integrated light scat. coefficient | 50% | LLL | Oakland, Calif | 20-inch telescope |
| Sullivan (U. Victoria) | Birefringent photometer | Twilight-lithium airglow emission 50-150 km | 90% | NRC (Can) U. Victoria | Victoria, B.C., Canada | |

Table B1 Continued

POTENTIAL GROUND TRUTH SENSORS LOCATED BY SURVEY

Part B <u>Airplane-Borne</u>

| Scientist (Group) | Type of Instrument (Aircraft) | Type of Measurement | Availability Oct. 78-Sept. 79 | Funding Agency | Flight Center | Instrument Parameters Size (cm) | Weight (kg) | Power (w) |
|---|---|---|---|---|---|---|---|---|
| Ferry (NASA Ames) | Aerosol sampler (U-2) | Aerosol particle conc, size dist, compos. 15-22 km | 90% | NASA | NASA Ames or Fairbanks | 8x20x60 | 5 | 28V |
| Briehl (NASA Lewis) | CN counter (commercial B 747's) | Aerosol part conc, >00.003 μm diam 6-14 km | 90% | NASA | Pan Am grt cic routes 5 hrs/wk above 64°N | 45x22x58 | 17 | 210 |
| Briehl (NASA Lewis) | Light-scattering particle counter (commerical B 747's) | Aerosol conc, >0.5μm D 6-14 km | 90% | NASA | Pan Am grt cic routes 5 hrs/wk above 64°N | 19x17x53 25x22x51 | 27 | 100 |
| Sedlacek (LASL) | SANDS aitken nuclei det (WB-57F) | Aitken nuclei 15-20 km | 75% | ERDA NASA? | 10°S-75°N | | | |
| Falconer (NOAA/ARL) | (commercial B-747) | 6-12 km | High | NASA | Global | | | |
| Grams (NCAR) | Dye lidar (NCAR Electra or NASA CV-990) | Scattering ratio (25 km above plane) | Medium | NSF | Boulder, Co. or NASA Ames | | | |

Table B1 Continued

POTENTIAL GROUND TRUTH SENSORS LOCATED BY SURVEY

Part C. Balloon-Borne

| Scientist (Group) | Type of Instrument | Type of Measurement | Availability Oct. 78-Sept. 79 | Funding Agency | Launch Site | Instrument Parameters Size (cm) | Weight (kg) | Power (w) |
|---|---|---|---|---|---|---|---|---|
| Iwasaka (Japan WRI) | Impactor | Particle chem. compos. | 40% | Japan Min of Educ. | Sanriku, Japan | | | |
| Rosen (U Wyoming) | Optical counter | Particle no., size dist. | High | NASA | Alaska, Antarctica, & others | | 9 | batteries |
| Rosen (U. Wyoming) | CN counter | CN no. | High | NASA | Alaska, Antarctica, & others | | 12 | batteries |
| Pepin (U. Wyoming) | Solar photometer | Extinction profiles (SAM-II and SAGE wvls) | High | NASA | Alaska, Antarctica, & others | | 6 | batteries |
| Bigg (CSIRO | Impactor<br>Optical counter (Wyo) | Aerosol part, no, size dist, shape, state, chem properties<br>10-30 km | 95% | CSIRO | 34°S<br>142°E | c 40 cm cube | 15 | with batteries |
| Paetzold (U. of Koln) | Optical detector<br>Sampler | Aerosol<br>0-30 km | High | U Cologne | Cologne, BRD | | 15 | |
| Kaselau | Aitken particle | Aitken nuclei<br>4-35 km | 85% | DFG & U. | BRD<br>France<br>USA (one) | 30x30x60 | 10 | 200 |

## Table B1 Continued

### POTENTIAL GROUND TRUTH SENSORS LOCATED BY SURVEY

Part C. Balloon-Borne

| Scientist (Group) | Type of Instrument | Type of Measurement | Availability Oct. 78-Sept. 79 | Funding Agency | Launch Site | Instrument Parameters Size (cm) | Weight (kg) | Power (w) |
|---|---|---|---|---|---|---|---|---|
| Miranda (Epsilon) | Optical counter | Particle no., size dist. 0.1 - 0.5 μm radius | High | None | open (4mcft balloon) | 1.5x2x0.5m | 300 | |
| Bricard (U. Paris) | CN counter | Condensation nuclei 2-25 km | | COVOS | France (and others) | 50x50x41 | 15-20 | |
| Harries (NPL, UK) | Cooled spectrometer | IR emiss. of strat. aer. 15-35 km | High | NPL | France Texas | Being Designed | | |
| Itoh (U. of Tokyo) | Mass spectrometer | Ion number density | 100% | Japan Min of Ed | Sanriku, Japan | $1m^3$ | 150 | 20 |

Part D Spacecraft-Borne

| Scientist (Group) | Type of Instrument | Type of Measurement | Availability Oct. 78-Sept. 79 | Funding Agency | Launch Site | Instrument Parameters Size (cm) | Weight (kg) | Power (w) |
|---|---|---|---|---|---|---|---|---|
| Gray (Draper Lab) | Spectral radiometer (Space shuttle) | Aerosol part. number, size, refractive index 10-70 km | High | NASA | | TBD | | |
| Barnett (Oxford U ) | SAMS (Nimbus G) | Temperature fields, hence motion fields | | | | | | |

## Appendix C

## INFORMATION ON NOCTILUCENT CLOUD OBSERVATIONS

PAGE ____ INTENTIONALLY BLANK

Table C1

DESCRIPTION OF GROUND-BASED PASSIVE NOCTILUCENT CLOUD OBSERVATIONS

1. Parameter to be measured: Noctilucent cloud occurrences; time of display, intensity; forms; extent of azimuth; extent in elevation.
2. Accuracy of measurement: Several degrees in azimuth and elevation.
3. Altitude region: $\sim 83 \pm 10$ km
4. Altitude resolution: Not actually measured, but see attached Fig. C1 from "Noctilucent Clouds" by V.A. Bronshten and N.I. Grishin, Keter Publ., Jerusalem.
5. Observation period: March 1 - October 31, annually.
6. Frequency of observation: Daily
7. Measurement technique: Visual estimation (supplemented by theodolites at some locations); photographic recording of displays at 6 stations.
8. Instrument type: Human eye; 35 mm camera
9. Measurement platform: Surface of the earth.
10. Type of data product: Direct, recorded on forms for punching onto cards; printed in annual publication
11. Funding authority: Atmospheric Environment Service (Canada)
12. Measurement program: International NLC program in cooperation with World Meteorological Organization
13. Status of prime instrument: Operational for many years
14. Assurance of instrument availability in Aug. 1978-Sept. 1979: 100%
15. Location of measurement: 60 stations in Canada; 16, in U.S.A.
16. Experimental limitations: Observations made during pre-sunrise and post-sunset periods when sun's depressional angle is between $6^{\circ}$ and $18^{\circ}$.
17. Instrumental physical characteristics: Normal as to class
18. Experimenter operation experience: Annual regular observations since 1964

Prepared by: Mr. E. J. Truhlar

Address: Atmospheric Environment Service
4905 Dufferin Street
Downsview, Ontario, Canada M3H 5T4

Date: May 18, 1977

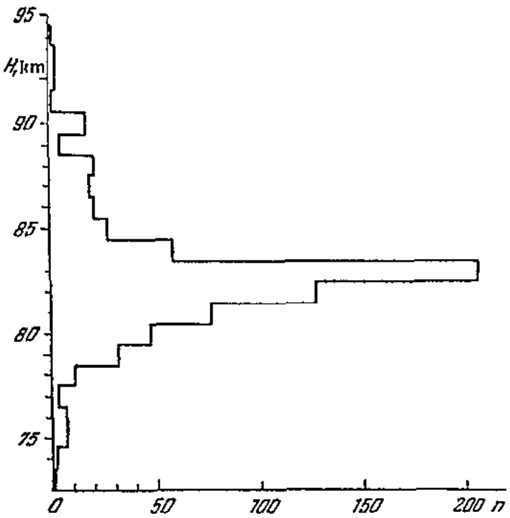


FIGURE C1 DISTRIBUTION OF NOCTILUCENT CLOUD HEIGHTS FROM 695 MEASUREMENTS BETWEEN 1887 AND 1964.

Table C2

EXAMPLE OF LISTING OF NLC SIGHTING DATA PROVIDED BY ENVIRONMENT CANADA

DETAILED INFORMATION ON THE NLC SIGHTINGS REPORTED FROM ALASKA CANADA, GREENLAND AND ICELAND

| DATE | STATION | CODE | LAT. | LONG. | GMT | LST | SDA | I | FORM | AZ. | [illegible] | |
|---|---|---|---|---|---|---|---|---|---|---|---|---|
| 730727 | FORT CHIPEWYAN | YPY | 58.8 | 111.1 | 9.3 | 1.8 | 9.0 | 4 | 25 | 350-100 | 15-50 | A |
| 730727 | FORT CHIPEWYAN | YPY | 58.8 | 111.1 | 9.5 | 2.0 | 8.0 | 3 | 12 | 360-050 | 20-50 | A |
| 730727 | FORT CHIPEWYAN | YPY | 58.8 | 111.1 | 9.8 | 2.3 | 7.0 | 2 | 12 | 360-[illegible]0 | 30 60 | A |
| 730727 | FORT RELIANCE | YFL | 62.7 | 109.2 | 7.5 | 0.1 | 8.0 | 4 | 23 | 300-060 | 35-90 | B |
| 730727 | FORT RELIANCE | YFL | 62.7 | 109.2 | 7.8 | 0.4 | 8.0 | 3 | 23 | 290-060 | 40-90 | B |
| 730727 | FORT RELIANCE | YFL | 62.7 | 10[illegible].2 | 8.1 | 0.7 | 7.5 | 3 | 23 | 300-075 | 20-90 | B |
| 730727 | FORT RELIANCE | YFL | 62.7 | 10[illegible].2 | 8.3 | 0.9 | 7.0 | 3 | 34 | 310-060 | 30 90 | B |
| 730727 | FORT RELIANCE | YFL | 62.7 | 10[illegible].2 | 8.5 | 1.1 | 7.0 | 3 | 13 | 225-090 | 20-45 | B |
| 730727 | FORT RELIANCE | YFL | 62.7 | 10[illegible].2 | 8.8 | 1.4 | 6.0 | 2 | 12 | 270-090 | 20-40 | B |
| 730727 | FORT RELIANCE | YFL | 62.7 | 109.2 | 9.0 | 1.6 | 5.5 | 2 | 12 | 225-090 | 25-40 | B |
| 730728 | FORT SMITH | YSM | 60.0 | 1[illegible].0 | 7.0 | 23.4 | 10.5 | 3 | 13 | 330-040 | 10-45 | B |
| 730728 | FORT SMITH | YSM | 60.0 | 11[illegible].0 | 8.0 | 0.4 | 10.5 | 3 | 13 | 330-040 | 10-45 | A |
| 730728 | FORT SMITH | YSM | 60.0 | 11[illegible].0 | 9.0 | 1.4 | 9.0 | 3 | 12 | 330-040 | 15-60 | A |
| 730729 | WATSON LAKE | YQH | 60.1 | 128.8 | 8.0 | 23.3 | 10.5 | 2 | 2 | -348 | 11- | C |
| 730729 | WATSON LAKE | YQH | 60.1 | 128.8 | 8.3 | 23.6 | 11.0 | 2 | 12 | 309- | -12 | B |
| 730729 | WATSON LAKE | YQH | 60.1 | 128.8 | 8.5 | 23.8 | 11.0 | 2 | 12 | -360 | 10- | B |
| 730729 | WATSON LAKE | YQH | 60.1 | 128.8 | 8.8 | 0.1 | 11.0 | 1 | 12 | 334-357 | 11- | B |
| 730729 | WATSON LAKE | YQH | 60.1 | 128.8 | 9.0 | 0.3 | 11.0 | 1 | 12 | 335-357 | -12 | B |
| 730729 | WHITEHORSE | YXY | 60.7 | 135.1 | 8.0 | 22.9 | 9.0 | 2 | 1 | 360-015 | 20-40 | C |
| 730729 | ENNADAI LAKE | YEI | 61.1 | 100.9 | 6.5 | 23.7 | 10.0 | 3 | 4 | 330-010 | 15-30 | B |
| 730727 | ENNADAI LAKE | YEI | 61.1 | 100.9 | 6.8 | 24.0 | 10.0 | 4 | 24 | 330-010 | 15-30 | B |
| 730729 | FORT RELIANCE | YFL | 62.7 | 10[illegible].2 | 6.0 | 22.6 | 6.5 | 2 | 12 | 340-070 | 10-50 | B |
| 730729 | FORT RELIANCE | YFL | 62.7 | 10[illegible].2 | 6.3 | 22.9 | 7.5 | 3 | 12 | 360-060 | 10-40 | B |
| 730729 | FORT RELIANCE | YFL | 62.7 | 109.2 | 6.5 | 23.1 | 7.5 | 3 | 12 | 010-060 | 15-60 | B |
| 730729 | FORT RELIANCE | YFL | 62.7 | 109.2 | 6.8 | 23.4 | 8.0 | 3 | 12 | 350-070 | 10 60 | B |
| 730729 | FORT RELIANCE | YFL | 62.7 | 109.2 | 7.0 | 23.6 | 8.0 | 3 | 2 | 350-060 | 10-65 | B |
| 730729 | FORT RELIANCE | YFL | 62.7 | 109.2 | 7.3 | 23.9 | 8.5 | 2 | 2 | 340-050 | 15-60 | B |
| 730729 | FORT RELIANCE | YFL | 62.7 | 109.2 | 7.5 | 0.1 | 8.5 | 2 | 23 | 360-080 | 10-70 | B |
| 730729 | FORT RELIANCE | YFL | 62.7 | 109.2 | 7.8 | 0.4 | 8.0 | 3 | 23 | 010-080 | 10-75 | B |
| 730729 | FORT RELIANCE | YFL | 62.7 | 109.2 | 8.0 | 0.6 | 8.0 | 3 | 3 | 350-070 | 20-75 | B |
| 730729 | FORT RELIANCE | YFL | 62.7 | 10[illegible].2 | 8.3 | 0.9 | 7.5 | 3 | 3 | 350-070 | 10-80 | B |
| 730729 | FORT RELIANCE | YFL | 62.7 | 109.2 | 8.5 | 1.1 | 7.5 | 2 | 2 | 340-070 | 10-90 | B |
| 730729 | FORT RELIANCE | YFL | 62.7 | 109.2 | 8.8 | 1.4 | 6.5 | 1 | 2 | 320-085 | 40-90 | B |
| 730730 | FORT RELIANCE | YFL | 62.7 | 109.2 | 6.3 | 22.9 | 7.5 | 1 | 1 | 290-040 | 40-65 | B |
| 730730 | FORT RELIANCE | YFL | 62.7 | 10[illegible].2 | 6.5 | 23.1 | 8.0 | 1 | 1 | 310-070 | 50-60 | B |
| 730730 | BAKER LAKE | YBK | 64.3 | 96.0 | 6.0 | 23.5 | 7.0 | 2 | 2 | 300-070 | 40-90 | A |
| 730730 | BAKER LAKE | YBK | 64.3 | 96.0 | 7.0 | 0.5 | 7.0 | 2 | 2 | 270-030 | 50-90 | A |
| 730802 | GRANDE PRAIRIE | YQU | 55.2 | 11[illegible].9 | 10.0 | 2.0 | 12.5 | 1 | 2 | 340-042 | 25-40 | A |
| 730802 | GRANDE PRAIRIE | YQU | 55.2 | 118.9 | 10.3 | 2.3 | 11.5 | 1 | 2 | 340-042 | 25-40 | A |
| 730803 | YELLOWKNIFE | YZF | 62.5 | 114.5 | 7.0 | 23.3 | 9.5 | 2 | 2 | 330-015 | 10-25 | A |
| 730803 | YELLOWKNIFE | YZF | 62.5 | 114.5 | 7.5 | 23.8 | 9.5 | 2 | 2 | 330-015 | 05-25 | A |
| 730803 | YELLOWKNIFE | YZF | 62.5 | 114.5 | 8.0 | 0.3 | 9.5 | 2 | 2 | 330-015 | 10-25 | A |
| 730803 | YELLOWKNIFE | YZF | 62.5 | 114.5 | 8.5 | 0.8 | 9.5 | 2 | 12 | 330-030 | 10-30 | A |
| 730803 | YELLOWKNIFE | YZF | 62.5 | 114.5 | 9.0 | 1.3 | 8.5 | 2 | 123 | 330-060 | 10-55 | A |
| 730803 | FORT RELIANCE | YFL | 62.7 | 109.2 | 6.0 | 22.6 | 8.0 | 2 | 1 | 300-030 | 10-20 | B |
| 730803 | FORT RELIANCE | YFL | 62.7 | 109.2 | 6.3 | 22.9 | 8.5 | 2 | 1 | 290-030 | 05-20 | B |
| 730803 | FORT RELIANCE | YFL | 62.7 | 109.2 | 6.5 | 23.1 | 9.0 | 2 | 1 | 270-030 | 05-25 | B |
| 730803 | FORT RELIANCE | YFL | 62.7 | 10[illegible].2 | 6.8 | 23.4 | 9.5 | 2 | 1 | 270-015 | 05-15 | B |
| 730803 | FORT RELIANCE | YFL | 62.7 | 1[illegible].2 | 7.0 | 23.6 | 9.5 | 2 | 1 | 290-015 | 05-15 | B |
| 730803 | FORT RELIANCE | YFL | 62.7 | 1[illegible].2 | 7.3 | 23.9 | 9.5 | 2 | 1 | 290-320 | 10-15 | B |
| 730803 | FORT RELIANCE | YFL | 62.7 | 1[illegible].2 | 7.5 | 0.1 | 9.5 | 1 | 1 | 300-320 | 15-20 | B |
| 730803 | NORMAN WELLS | YVQ | 65.3 | 12[illegible].8 | 8.8 | 0.2 | 7.0 | 2 | 23 | 270-120 | 30-90 | A |
| 730803 | NORMAN WELLS | YVQ | 65.3 | 1[illegible].8 | 9.0 | 0.4 | 7.0 | 2 | 23 | 320-100 | 30-90 | A |
| 730803 | NORMAN WELLS | YVQ | 65.3 | 12[illegible].8 | 9.3 | 0.7 | 6.5 | 2 | 23 | 270-100 | 20-90 | A |
| 730803 | NORMAN WELLS | YVQ | 65.3 | 1[illegible].8 | 9.5 | 0.9 | 6.5 | 2 | 12 | 200-080 | 80-90 | A |
| 730803 | NORMAN WELLS | YVQ | 65.3 | 1[illegible].8 | 9.8 | 1.2 | 6.0 | 3 | 12 | 200-070 | 80-90 | A |
| 730803 | NORMAN WELLS | YVQ | 65.3 | 1[illegible].8 | 10.0 | 1.4 | 5.5 | 3 | 1 | 140-110 | -90 | A |

(See next page for key to column headings.)

Environment Canada / Environnement Canada

Atmospheric Environment / Environnement atmosphérique
4905 Dufferin Street
Downsview, Ontario
M3H 5T4

Your file / Votre dossier

Our file / Notre dossier 8061-2 (ARPD)

May 5, 1977

Dr. P.B. Russell
Science Coordinator for Ground Truth
SAM-II Nimbus G Experiment Team
Stanford Research Institute
Menlo Park. Calif. 94025
U.S.A.

Dear Dr. Russell:

This letter will confirm preliminary arrangements made during your recent discussion with Mr. E.J. Truhlar concerning the provision of noctilucent cloud (NLC) observations in support of SAM-II measurements of mesospheric aerosols. Observations of NLC data will be forwarded to you after they have been received from the stations, transferred to cards, processed by computer for quality and listed in tabular format. (See attachment for an example of a regular listing of such data, including the explanatory legend). About a one-month delay should be expected before a listing for a particular data-month is received by your institute.

The following table shows the average monthly distribution of station-night sightings of NLC during the period 1964-1976 inclusive.

| MAR | APR | MAY | JUN | JUL | AUG | SEP | OCT |
|---|---|---|---|---|---|---|---|
| 0.6 | 0.8 | 2.6 | 40 | 71 | 24.5 | 1.2 | 0.6 |

Most occurrences are in the months of June to August, with a peak in July; very few occur from March to May or in September or October. No NLC are observed from November to February during the fall and winter when the sun's elevation is too low to allow the clouds to be illuminated in the pre-sunrise and post-sunset twilight periods.

We would appreciate receiving information on the progress of the arrangements to implement the SAM-II project.

Yours sincerely

B.W.Boville, Director
Atmospheric Processes Research Branch

Table C2.
(continued)

KEY TO COLUMN HEADINGS

| | |
|---|---|
| DATE | - Year, month, night |
| STATION | - Station |
| CODE | - Station Identifier |
| LAT. | - Latitude |
| LONG. | - Longitude |
| GMT | - Greenwich Mean Time |
| LST | - Local Solar Time (or Local Apparent Time) |
| SDA | - Solar depression angle at time or sighting |
| I | - NLC intensity on 5-point scale, from very weak to extremely bright |
| FORM | - Structural forms: 1 veils; 2-bands; 3-billows; 4-whirls; 5-amorphous |
| AZ | - Azimuthal extend of NLC, relative to geographic North |
| EL | - Extent of NLC in elevation, relative to the horizon |
| CL | - Tropospheric cloud cover in twilight section of sky: A-clear; B-scattered; C-broken; D-overcast |

HEAD OF DEPARTMENT
D H McINTOSH, B Sc, M A, D Sc, F R S E
TEL 031-667 1081 Ext 2920

University of Edinburgh

DEPARTMENT OF METEOROLOGY
THE UNIVERSITY
JAMES CLERK MAXWELL BUILDING
KING'S BUILDINGS
EDINBURGH EH9 3JZ

7th October 1977

Dr. P.B. Russell,
Science Coordinator for Ground Truth,
SAM-II Nimbus Experiment Team,
Stanford Research Institute,
Menlo Park,
California 94024,
U.S.A.

Dear Dr. Russell,

Thank you for your letter of 3rd October expressing interest in data relating to noctilucent clouds.

We shall of course be pleased to cooperate with you in any way we can be sending you our data. Observations made here or reported to us are in large measure confined to June and July; only exceptionally are the clouds seen by 'our' observers in August (or May). It seems likely then that our first reports of interest to you will be for 1979.

The latitude belt you refer to ($64^{o}$ - $80^{o}$) is a good deal poleward of our most northerly observers. We shall make enquiries as to how far poleward we may be able to extend our network, perhaps obtaining the cooperation of other observers in Scandinavia or Iceland.

Yours sincerely,

D. H. McIntosh

D.H. McIntosh.

## Appendix D

# AIRCRAFT FLIGHT CALCULATIONS

by

Samuel I. Sokol
NASA Langley Research Center

PAGE ______ INTENTIONALLY BLANK

PRECEDING PAGE BLANK NOT FILMED

# SAM-II GROUND TRUTH FLIGHT PROGRAM CALCULATIONS

The P-3A aircraft stationed at the NASA Wallops Flight Center will be used to support the SAM-II Ground Truth Flight Program. Flight hours, distances, profiles, and costs have been estimated and are presented below. Different routes leading to the same destination are included in the calculations. This should prove helpful in future planning as costs associated with landing and take-off fees become known or alternate routes have to be selected.

## P-3A Characteristics

The aircraft ground speed, ceiling, and actual range are dependent on such factors as aircraft loads, headwinds, and ground controller operations in different zones. Typical aircraft flight characteristics are listed below:

| | |
|---|---|
| Cruise speed at 7,620 meters (25,000 feet) altitude | 555 km/hour (300 knots) |
| Maximum range with 1 hour fuel reserve | 6 flight hours or 3,335 km (1,800 n.m.) |
| Service ceiling | 9,144 m (30,000 ft.) |
| Time to climb to 7,620 meters altitude | 12 minutes |
| Take-off run | 1,160 m (3,800 ft.) |

## Terminal Points and Staging Areas

The potential stopover points or staging terminals for the experiment, elevation of the aircraft above mean sea level, and local time zones relative to GMT are presented.

| CITY (AIRPORT NAME) | LATITUDE DEG | LATITUDE MIN | LONGITUDE DEG | LONGITUDE MIN | ELEVATION, MSL METERS | ELEVATION, MSL (FEET) | TIME FROM GMT - HOURS |
|---|---|---|---|---|---|---|---|
| Barrow, Alaska | 71 | 16N | 156 | 47W | - | | -10 |
| Brasilia, Brazil | 15 | 52S | 47 | 55W | 1060 | (3478) | - 3 |
| Buenos Aires (Ezeiza) Argentina | 34 | 49S | 58 | 32W | 20 | (66) | - 3 |
| Chincoteaque, Virginia (NASA Wallops) | 37 | 56N | 75 | 28W | 13 | (41) | - 5 |
| Fairbanks, Alaska (International) | 64 | 49N | 147 | 51W | 132 | (434) | -10 |
| Goose Bay, Newfoundland, Canada | 53 | 19N | 60 | 26W | 49 | (160) | - 4 |
| Laramie, Wyoming (General Brees Field) | 41 | 19N | 105 | 40W | 2218 | (7276) | - 7 |
| Minneapolis/St. Paul, Minnesota (International) | 44 | 53N | 93 | 13W | 81 | (264) | - 6 |
| Palmer, Antarctica | 64 | 45S | 64 | 05W | - | | |
| Paramaribo, Surinam (Zanderij) | 05 | 28N | 55 | 11W | 17 | (54) | -3.30 |
| San Juan, Puerto Rico (International) | 18 | 26N | 66 | 00W | 3 | (9) | - 4 |
| Quebec, Canada | 46 | 48N | 71 | 24W | 73 | (239) | - 5 |
| Rio DeJaneiro, Brazil (Galeao) | 22 | 49S | 43 | 15W | 3 | (10) | - 3 |
| Seattle, Washington (Boeing Field, International) | 47 | 32N | 122 | 18W | 5 | (17) | - 8 |
| Sandrestrom Air Base, Greenland | 67 | 01N | 50 | 43W | 50 | (165) | - 3 |
| Thule, Greenland | 76 | 32N | 68 | 42W | 77 | (251) | - 4 |
| Ushuaia, Argentina | 54 | 49S | 68 | 19W | 10 | (33) | - 3 |

The primary staging area for the flight qualification test is expected to be in the Laramie area. One data recording flight should confirm the system's readiness. Sondrestrom is the primary staging area for the Northern Hemisphere, but the Fairbanks area is also considered here as an alternate possibility. Eight flights are considered for the Northern Hemisphere coverage and only seven are considered for the Southern Hemisphere. (Southern Hemisphere flights were to have been staged out of Ushuaia. However, Rio Grande, Argentina is now considered the most likely staging site.)

## Flight Profile

A typical data run flight profile is shown below. The distances shown between waypoints W1, W2, W3, and W4 are the maximum expected ranges. The data run would start at Waypoint W1 and continue around the course back to W1 and then return to the staging area terminal. The total data run (maximum) is 700 km and could be completed in 1.26 hours. The distance from the staging terminal to the first waypoint will vary between flights, but the assumed distances will be elaborated upon in the discussion of the calculations.

SAT = Staging Area Terminal
W = Waypoint
V = Variable Distance

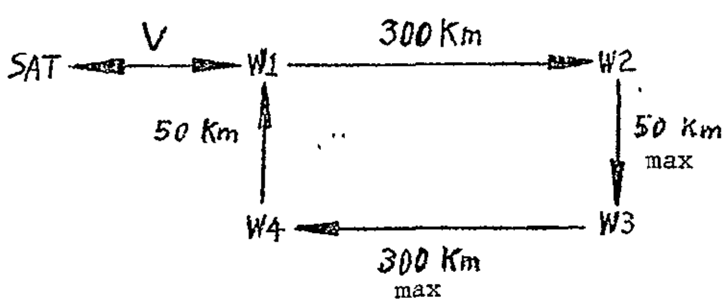

## Estimating Flight Routes, Distances, and Times

All flights are assumed to be at 7,620 m altitude, which is the economical altitude to fly the aircraft. All flight estimates will have a half-hour added to the flight time to account for take-off and landing operations.

## Experiment Qualification/Readiness Flights

A general shakedown and initial readiness flight test will be conducted in the Wallops area. Flight altitude for this test will be at 9,144 meters (30,000 feet). This will consume approximately 1 hour of flight time. A second test will be in the Laramie area to confirm the integrity of the LIDAR system measurements. The Laramie test is expected to follow the outlined data run flight profile. The distances and flight hours for these two tests are expected to be as follows:

| Terminals | Distance, km | Flight Hours |
|---|---|---|
| Chincoteaque (Wallops) | 500 | 1.0 |
| Laramie Operations | | |
| WFC - Laramie | 2,600 | 4.7 |
| Laramie Data Run | 700 | 1.3 |
| Laramie - WFC | 2,600 | 4.7 |
| 1/2 hour flight, 3 flights | -- | 1.5 |
| Total, all flights | 6,400 km | 13.2 hours |

## Northern Hemisphere Flights

Two routes are considered in flying from Wallops to Sondrestrom. One is routed through Goose Bay and the second is routed through Quebec. The Quebec route is slightly shorter, and Quebec has better airport facilities than Goose Bay but the landing fees may be greater than Goose Bay. Some data (such as dustsondes) may be taken at Thule so it may be desirable from the experiment standpoint to have the data run over the Thule area. However, this is expensive since the distance from Sondrestrom to Thule is 1,217 km (2,434 km round trip) and when multiplied by 8 flights it represents a significant portion of the experiment's budget. Therefore, two distances from Sondrestrom to the first waypoint are considered; one to Thule and the other only 555 km north of Sondrestrom at 72°01'N latitude.

The same reasoning applies to staging out of Fairbanks. One consideration has the first waypoint over Barrow (805 km from Fairbanks) and the other consideration has the first waypoint 555 km north of Fairbanks at 69°49'N latitude.

| Terminals | | Distance, km | Flight Hours |
|---|---|---|---|
| ROUTE 1: | WFC - Goose Bay | 2061 | 3.7 |
| | Goose Bay - Sondrestrom | 1609 | 3.0 |
| | 1/2 hour flight | ---- | 1.0 |
| | Subtotal | 3670 km | 7.7 hours |
| | Return Flight | 3670 | 7.7 |
| | Total | 7340 km | 15.4 hours |
| ROUTE 2: | WFC - Quebec | 1040 | 1.9 |
| | Quebec - Sondrestrom | 2545 | 4.6 |
| | 1/2 hour flight | ---- | 1.0 |
| | Subtotal | 3585 | 7.5 |
| | Return Flight | 3585 | 7.5 |
| | Total | 7170 km | 15.0 hours |
| Sondre - Thule Operations | | | |
| | Sondre - Thule | 1217 | 2.2 |
| | Data Run | 700 | 1.3 |
| | Thule - Sondrestrom | 1217 | 2.2 |
| | 1/2 hour flight | ---- | 0.5 |
| | Subtotal | 3134 km | 6.2 hours |
| | 8 Flights | 25072 km | 49.6 hours |
| Sondre - 72°01'N Latitude Operations | | | |
| | Sondrestrom - 72°01' | 555 | 1.0 |
| | Data Run | 700 | 1.3 |
| | 72°01' - Sondrestrom | 555 | 1.0 |
| | 1/2 hour flight | ---- | 0.5 |
| | Subtotal | 1810 km | 3.8 hours |
| | 8 Flights | 14480 km | 30.4 hours |
| Route 1 + Sondrestrom - Thule Operations | | 32412 km | 65.0 hours |
| Route 1 + Sondrestrom - 72°01' Operations | | 21820 km | 45.8 hours |
| Route 2 + Sondrestrom - Thule Operations | | 32242 km | 64.6 hours |
| Route 2 + Sondrestrom - 72°01' Operations | | 21650 km | 45.4 hours |

| | Terminals | | Distance, km | Flight Hours |
|---|---|---|---|---|
| ROUTE 3: | WFC - Minneapolis | | 1664 | 3.0 |
| | Minneapolis - Seattle | | 2242 | 4.0 |
| | Seattle - Fairbanks | | 2452 | 4.5 |
| | 1/2 hour flight | | ---- | 1.5 |
| | | Subtotal | 6358 | 13.0 hours |
| | Return Flight | | 6358 | 13.0 hours |
| | | Total | 12716 km | 26.0 hours |
| Fairbanks - Barrow Operations | | | | |
| | Fairbanks - Barrow | | 805 | 1.5 |
| | Data Run | | 700 | 1.3 |
| | Barrow - Fairbanks | | 805 | 1.5 |
| | 1/2 hour flight | | --- | 0.5 |
| | | Subtotal | 2310 | 4.8 |
| | | 8 Flights | 18480 km | 38.4 hours |
| Fairbanks - 69°49'N Latitude Operations | | | | |
| | Fairbanks - 69°49' | | 555 | 1.0 |
| | Data Run | | 700 | 1.3 |
| | 69°49' - Fairbanks | | 555 | 1.0 |
| | 1/2 hour flight | | --- | 0.5 |
| | | Subtotal | 1810 | 3.8 |
| | | 8 Flights | 14480 km | 30.4 hours |
| Route 3 + Fairbanks - Barrow Operations | | | 31,196 km | 64.4 hours |
| Route 3 + Fairbanks - 69°49' Operations | | | 27,196 km | 56.4 hours |

## Southern Hemisphere Flights

Two routes are considered in flying from Wallops to Ushuaia, one through Brasilia and the other Rio DeJaneiro. The Rio DeJaneiro route is slightly longer than the 6-hour flight criteria, but probably is acceptable. The trip from Wallops to Ushuaia will take a minimum of 3 days, regardless of which route is selected.

| | Terminals | | Distance, km | Flight Hours |
|---|---|---|---|---|
| ROUTE 4: | WFC - Puerto Rico | | 2354 | 4.2 |
| | Puerto Rico - Paramaribo | | 1858 | 3.4 |
| | Paramaribo - Brasilia | | 2501 | 4.5 |
| | Brasilia - Buenos Aires | | 2356 | 4.3 |
| | Buenos Aires - Ushuaia | | 2347 | 4.2 |
| | 1/2 hour/flight | | ---- | 2.5 |
| | | Subtotal | 11416 km | 23.1 hours |
| | Return Flight | | 11416 km | 23.1 hours |
| | | Total | 22832 km | 46.2 hours |
| ROUTE 5: | WFC - Puerto Rico | | 2354 | 4.2 |
| | Puerto Rico - Paramaribo | | 1858 | 3.4 |
| | Paramaribo - Rio DeJaneiro | | 3400 | 6.1 |
| | Rio DeJaneiro - Buenos Aires | | 1992 | 3.6 |
| | Buenos Aires - Ushuaia | | 2347 | 4.2 |
| | 1/2 hour/flight | | ---- | 2.5 |
| | | Subtotal | 11951 km | 24.0 hours |
| | Return Flight | | 11951 | 24.0 hours |
| | | Total | 23902 km | 48.0 hours |
| Ushuaia Operations | | | | |
| | Ushuaia - Palmer | | 1128 | 2.0 |
| | Data Run | | 700 | 1.3 |
| | Palmer - Ushuaia | | 1128 | 2.0 |
| | 1/2 hour/flight | | ---- | 0.5 |
| | | Subtotal | 2956 | 5.8 |
| | | 7 Flights | 20692 km | 40.6 hours |
| Route 4 + Ushuaia Operations | | | 43524 km | 86.8 hours |
| Route 5 + Ushuaia Operations | | | 44594 km | 88.6 hours |

## Flight Costs

Flight costs are based on $500 per flight hour. Landing/take-off fees from the various terminals are unknown at this time but will have to be considered in the future. Also, fuel costs will vary between terminals and between countries, so it is conceivable that the actual costs may be more than $500/hour outside the United States.

| Northern Hemisphere | Flight Hours | Cost, $ |
|---|---|---|
| Wallops Flight | 1.0 | 500 |
| Laramie Operation | 12.2 | 6,100 |
| Route 1 Operation (Sondrestrom - Thule) | 65.0 | 32,500 |
| Route 1 Operation (Sondrestrom - 72°01') | 45.8 | 22,900 |
| Route 2 Operation (Sondrestrom - Thule) | 64.6 | 32,300 |
| Route 2 Operation (Sondrestrom - 72°01') | 45.4 | 22,700 |
| Route 3 Operations (Fairbanks - Barrow) | 64.4 | 32,200 |
| Route 3 Operation (Fairbanks - 69°49') | 56.4 | 28,200 |

| Southern Hemisphere | Flight Hours | Cost, $ |
|---|---|---|
| Route 4 Operation | 86.8 | 43,400 |
| Route 5 Operation | 88.6 | 44,300 |

---

Per Diem Costs

Per diem costs are based on four men from Wallops and three men from Langley receiving per diem. Per diem rates for foreign travel are based on staying in the country for at least 6 hours. The U.S. per diem rate of $35 will be used enroute in these estimates although the rate may actually drop to $6 if the enroute travel exceeds 6 hours. For example, the trip from Wallops to Surinam may include a 2-hour layover in Puerto Rico. However, the whole trip to Surinam may be considered as enroute since the stay in Puerto Rico was less than 6 hours. Car rental is estimated for the U.S. and Greenland; taxi service is considered for the other stations.



C-2

| OPERATIONS/ ROUTE NO. | NO. MEN | PER DIEM | NO.OF DAYS | CAR RENTAL | TAXI FARES | REASON | COSTS |
|---|---|---|---|---|---|---|---|
| Wallops | 3 | 35 | 3 | | | Checkout | $ 315.00 |
| Laramie | 7 | 35 | 3.5 | $ 140 | | Flight Qualification | 997.50 |
| 1 or 2 | 3 | 35 | 1 | | | WFC Flight Preparation | 105.00 |
| | 7 | 35 | 0.5 | | | Enroute to Greenland | 122.50 |
| | 7 | 26 | 10 | 500 | | Greenland Operations | 2320.00 |
| | 7 | 35 | 0.5 | | | Enroute to LaRC/WFC | 122.50 |
| | | | | | | | $2670.00 |
| 3 | 3 | 35 | 1 | | | WFC Flight Preparation | 105.00 |
| | 7 | 35 | 1.5 | | | Enroute to Alaska | 367.50 |
| | 7 | 69 | 10 | 1000 | | Alaska Operations | 5830.00 |
| | 7 | 35 | 1.5 | | | Enroute to LaRC and WFC | 367.50 |
| | | | | | | | $6670.00 |
| 4 | 3 | 35 | 1 | | | WFC Flight Preparation | 105.00 |
| | 7 | 35 | 0.5 | | | Enroute to Surinam | 122.50 |
| | 7 | 44 | 0.75 | | 50 | Rest Stop Overnight | 281.00 |
| | 7 | 35 | 0.5 | | | Enroute to Buenos Aires | 122.50 |
| | 7 | 50 | 1.5 | | 50 | Crew Rest in Buenos Aires | 575.00 |
| | 7 | 35 | 0.25 | | | Enroute to Ushuaia | 61.25 |
| | 7 | 50 | 10 | | 500 | Ushuaia Operations | 4000.00 |
| | 7 | 35 | 0.5 | | | Enroute to Brasilia | 122.50 |
| | 7 | 53 | 0.75 | | 50 | Rest Stop Overnight | 278.25 |
| | 7 | 35 | 0.5 | | | Enroute to Puerto Rico | 122.50 |
| | 7 | 66 | 1 | | 50 | Crew Rest in Puerto Rico | 512.00 |
| | 7 | 35 | 0.25 | | | Enroute to LaRC/WFC | 61.25 |
| | | | | | | | $6463.75 |
| 5 | 3 | 35 | 1 | | | WFC Flight Preparation | 105.00 |
| | 7 | 35 | 0.5 | | | Enroute to Surinam | 122.50 |
| | 7 | 44 | 0.75 | | 50 | Rest Stop Overnight | 281.00 |
| | 7 | 35 | 0.5 | | | Enroute to Rio DeJaneiro | 122.50 |
| | 7 | 63 | 1.25 | | 50 | Crew Rest in Rio | 601.25 |
| | 7 | 35 | 0.5 | | | Enroute to Ushuaia | 122.50 |
| | 7 | 50 | 10 | | 500 | Ushuaia Operations | 4000.00 |
| | 7 | 35 | 0.5 | | | Enroute to Rio DeJaneiro | 122.50 |
| | 7 | 63 | 0.75 | | 50 | Rest Stop Overnight | 380.75 |
| | 7 | 35 | 0.5 | | | Enroute to Surinam | 122.50 |
| | 7 | 44 | 1.5 | | 50 | Crew Rest in Surinam | 512.00 |
| | 7 | 35 | 0.5 | | | Enroute to LaRC/WFC | 122.50 |
| | | | | | | | $6665.00 |

# Appendix E

# GEOMETRY OF SUN ANGLES FOR BALLOONBORNE SUNPHOTOMETER

PAGE ______ INTENTIONALLY BLANK

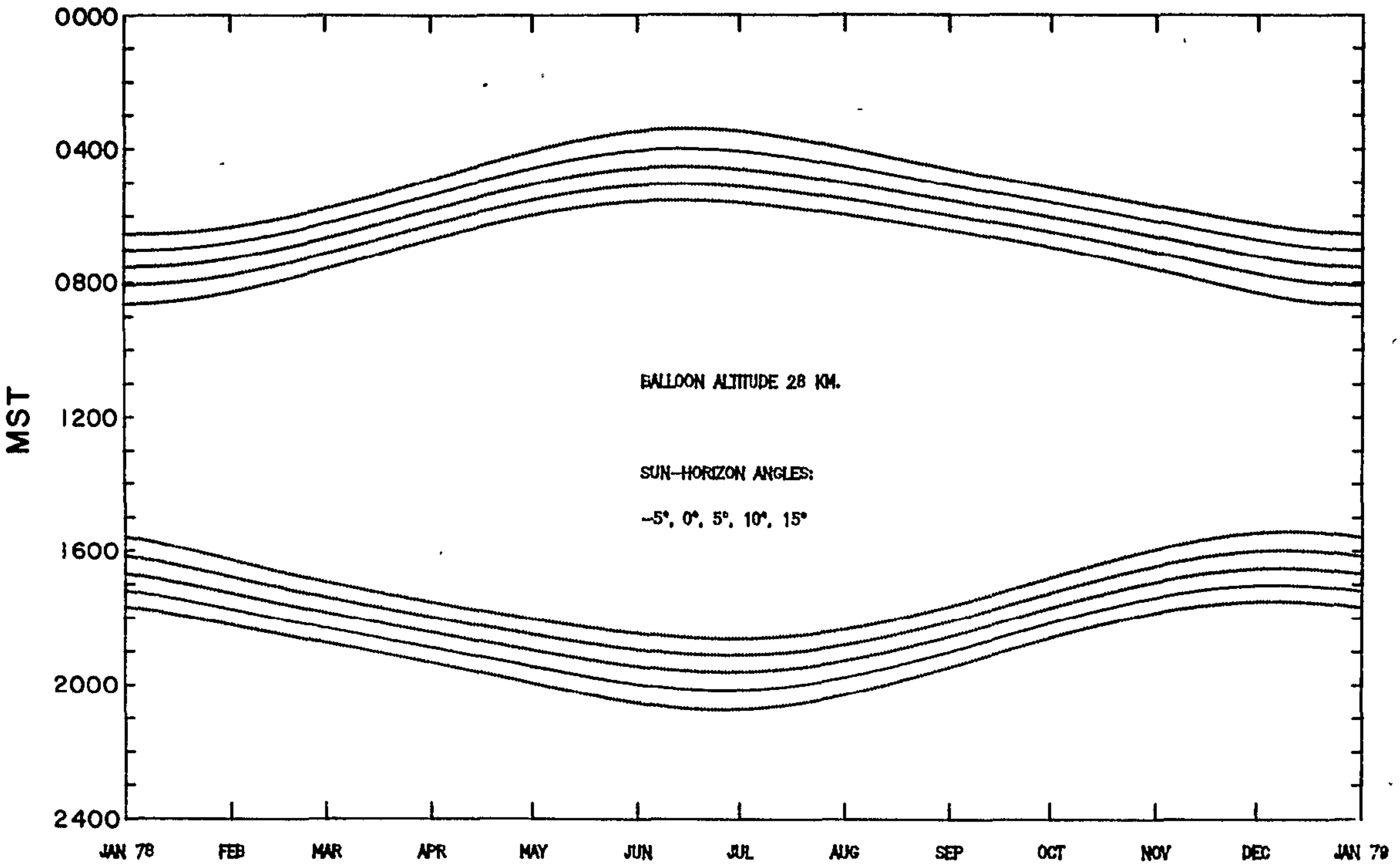


LARAMIE, WYO. (41.3°N, 105.7°W)

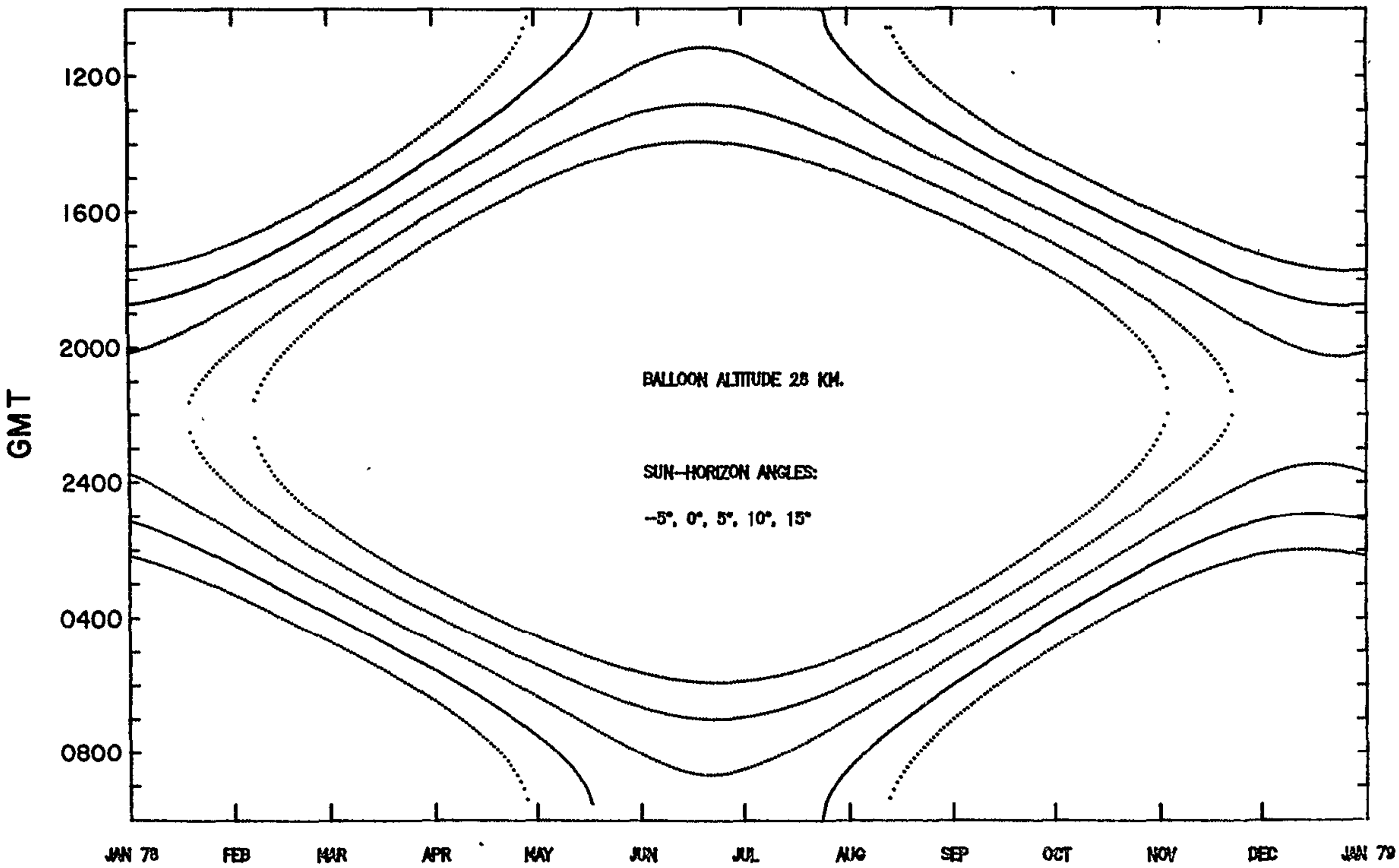


FAIRBANKS, U.S. (65.0°N, 148.0°W)

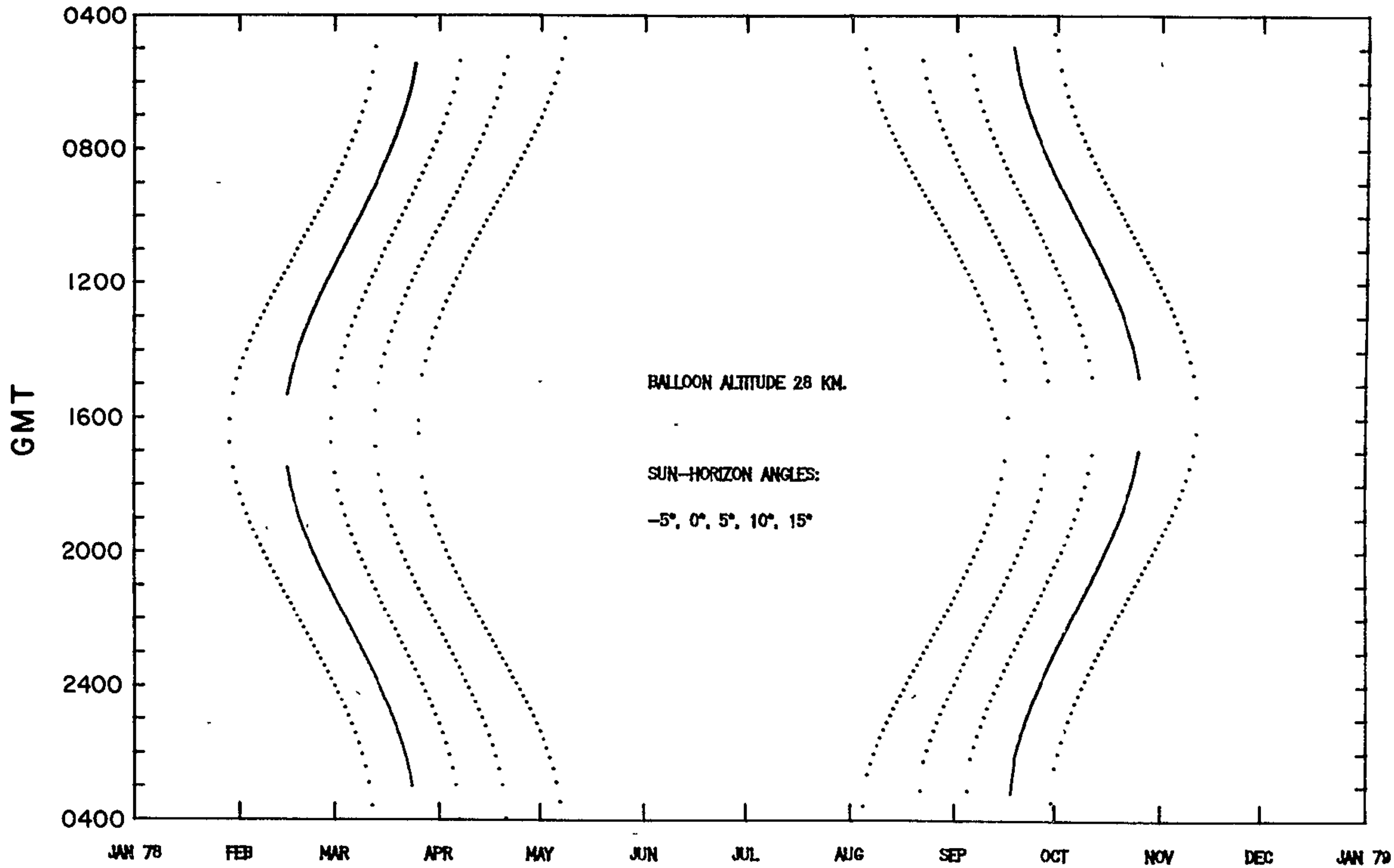


ALERT, CANADA (82.5°N, 62.5°W)

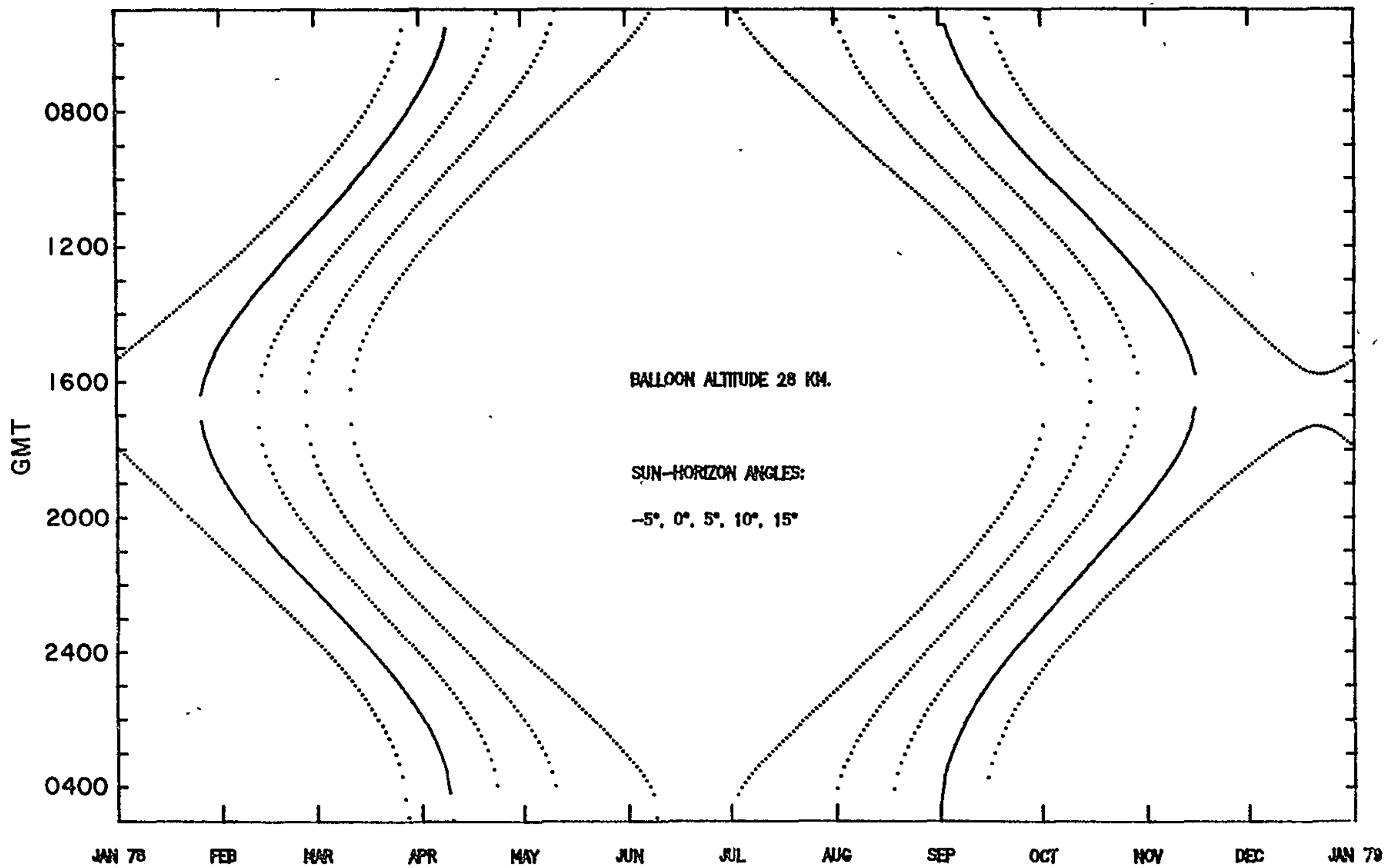


THULE, GREENLAND (76.7°N, 68.5°W)

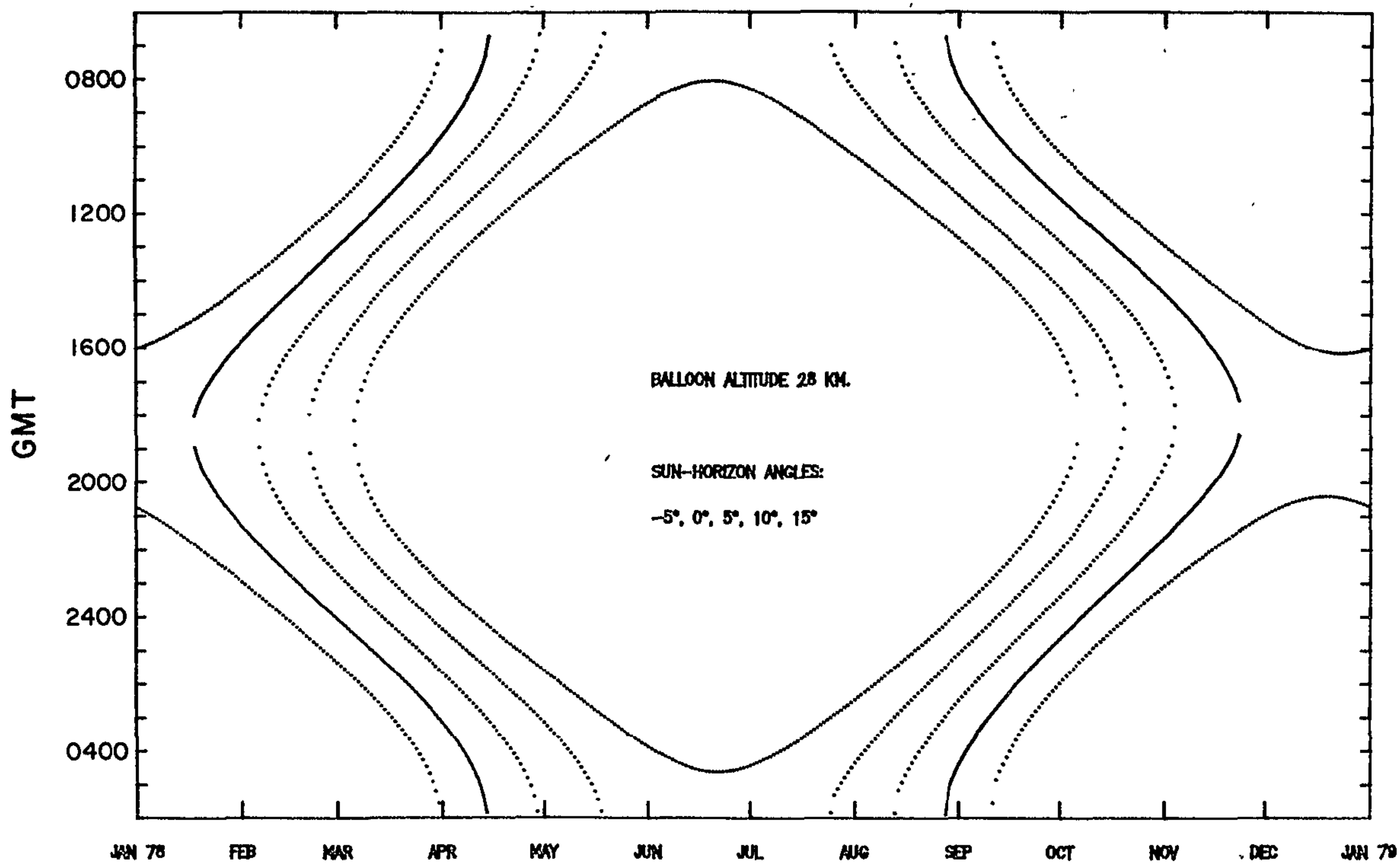


RESOLUTE BAY, CANADA (74.8°N, 94.5°W)

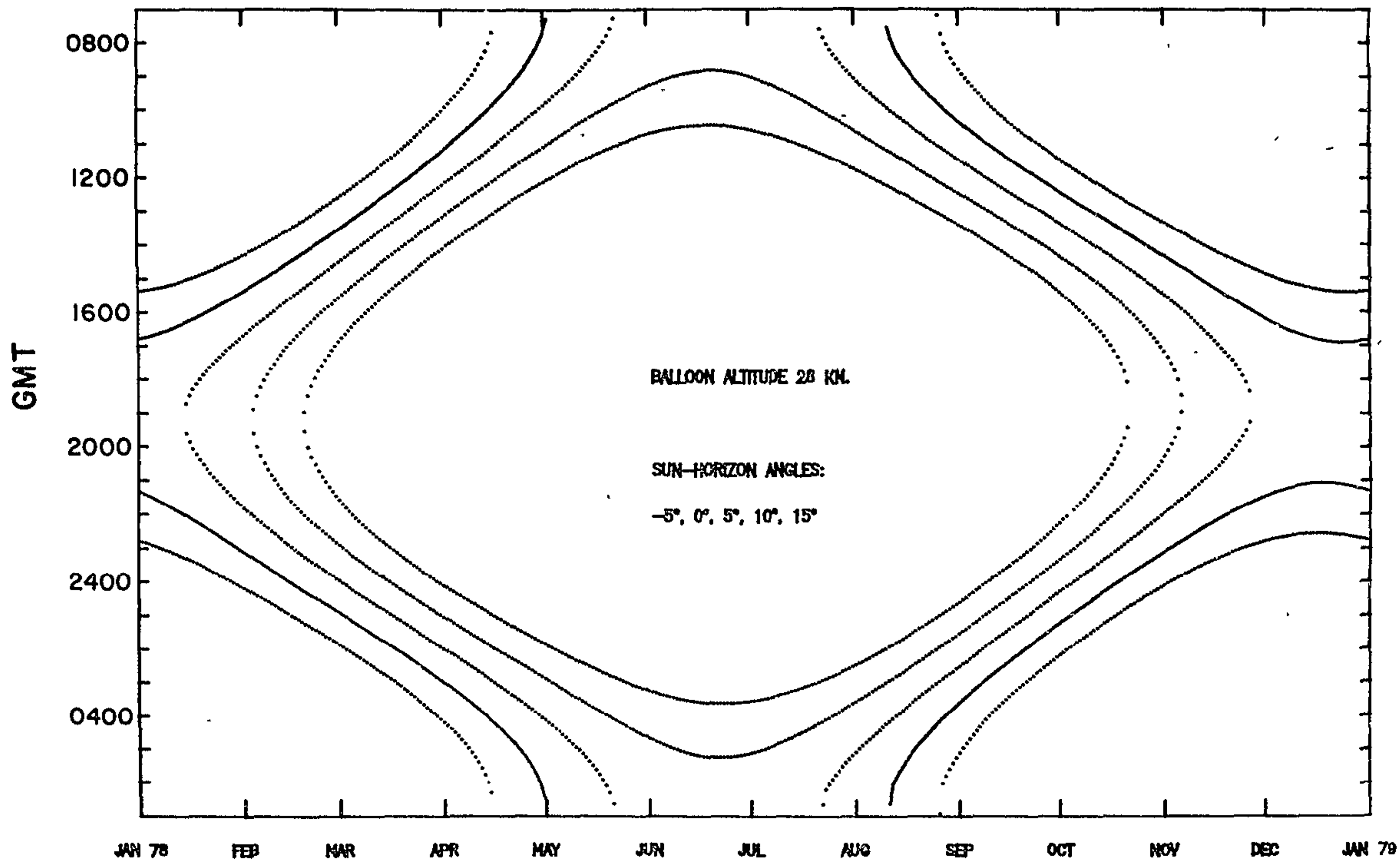


CAMBRIDGE BAY, CANADA (69.2°N, 105.0°W)

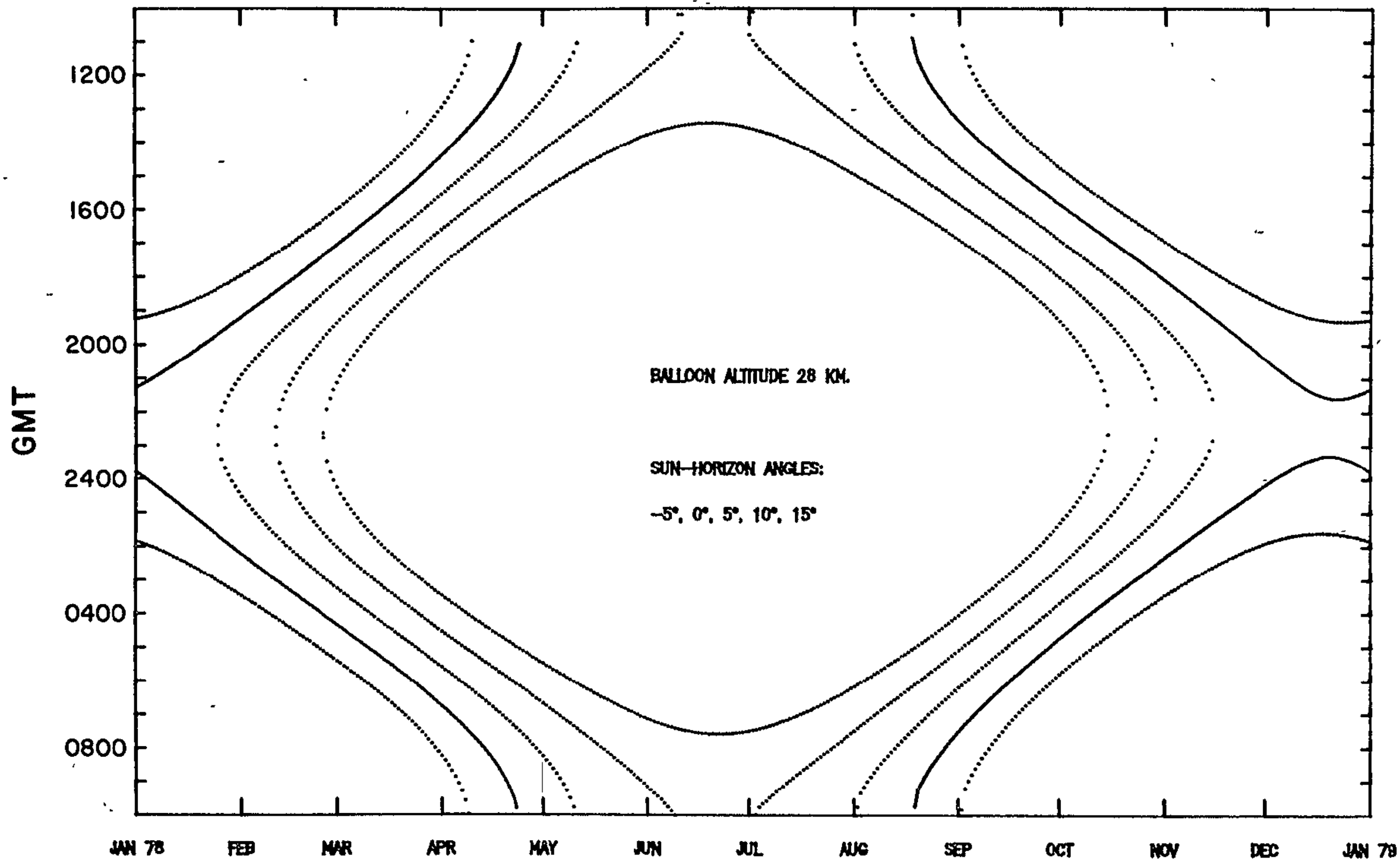


PT. BARROW, U.S. (71.5°N, 157.0°W)

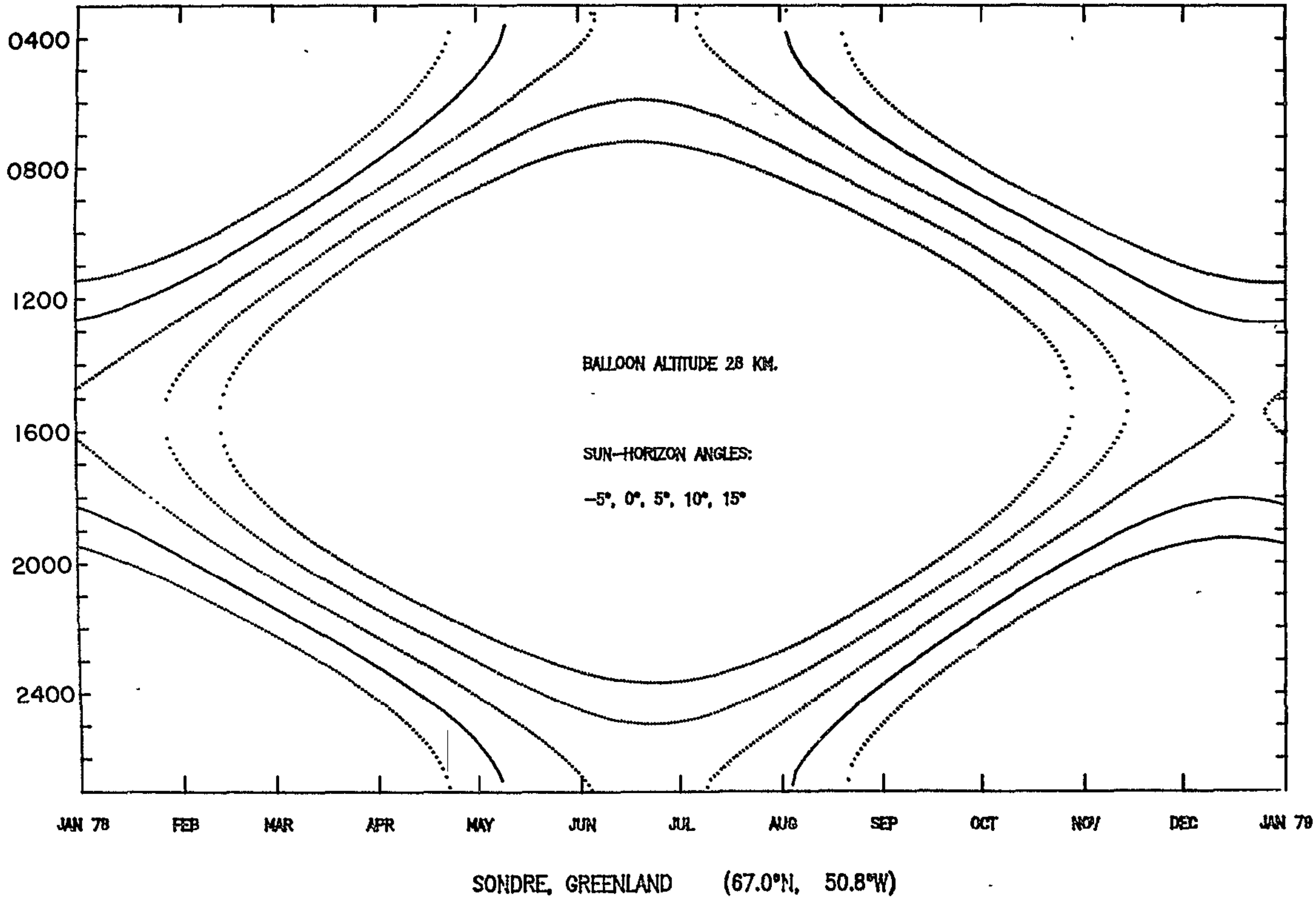
GMT
0400
0800
1200
1600
2000
2400
BALLOON ALTITUDE 28 KM.
SUN-HORIZON ANGLES:
-5°, 0°, 5°, 10°, 15°
JAN 78
FEB
MAR
APR
MAY
JUN
JUL
AUG
SEP
OCT
NOV
DEC
JAN 79
SONDRE, GREENLAND (67.0°N, 50.8°W)

## Appendix F

## AIRFIELD APPROACH PLATES

PAGE ____ INTENTIONALLY BLANK

PRECEDING PAGE BLANK NOT FILMED

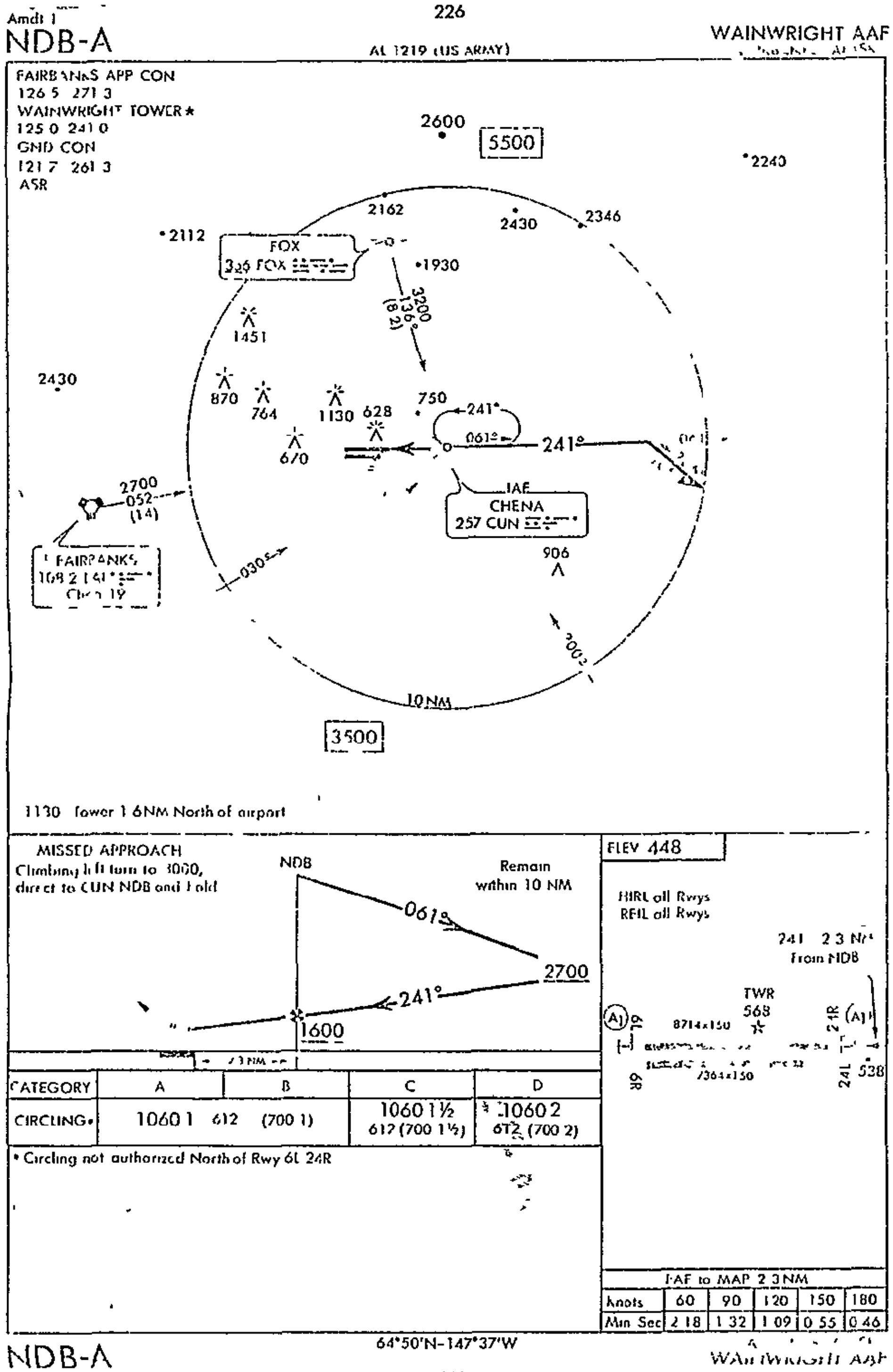


| CATEGORY | A | B | C | D |
|---|---|---|---|---|
| CIRCLING• | 1060 1 612 (700 1) | | 1060 1½ 612 (700 1½) | 1060 2 612 (700 2) |

• Circling not authorized North of Rwy 6L 24R

| Knots | 60 | 90 | 120 | 150 | 180 |
|---|---|---|---|---|---|
| Min Sec | 2 18 | 1 32 | 1 09 | 0 55 | 0 46 |

NDB-A 64°50'N-147°37'W WAINWRIGHT AAF

227

HI-VORTAC RWY 24R



ORIGINAL PAGE IS OF POOR QUALITY

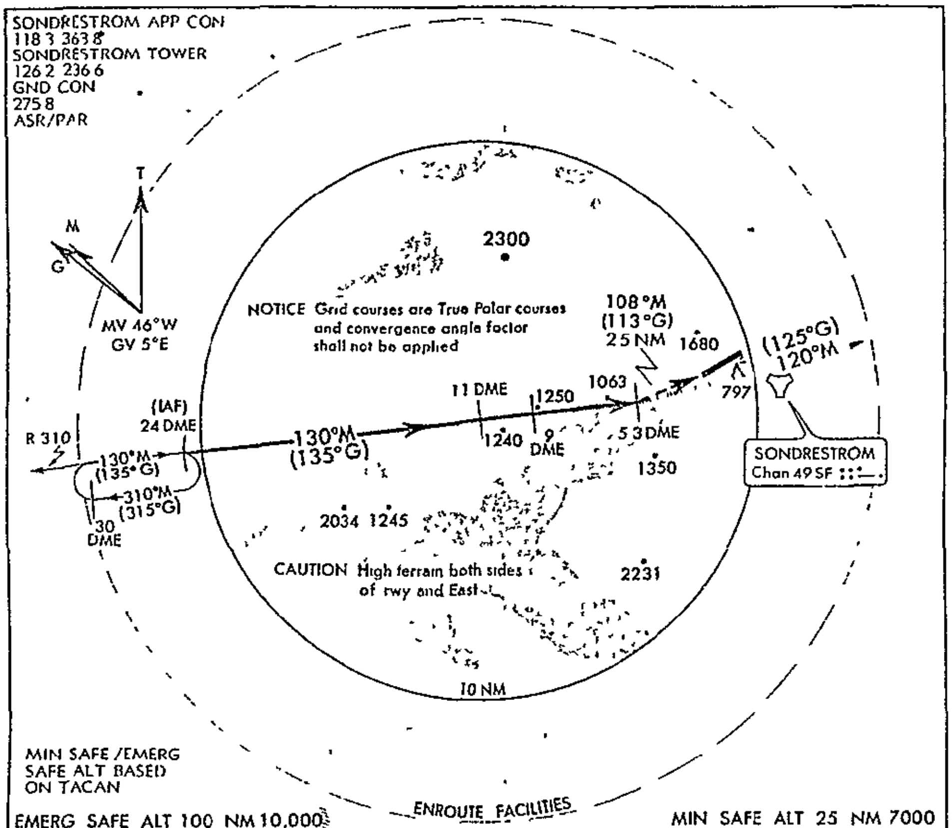


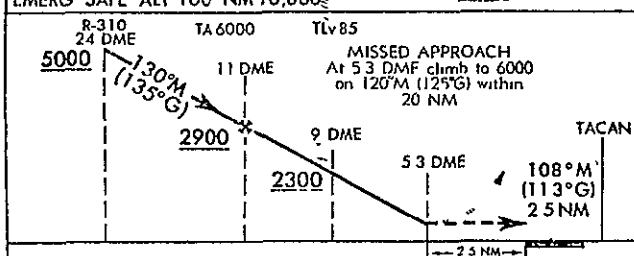


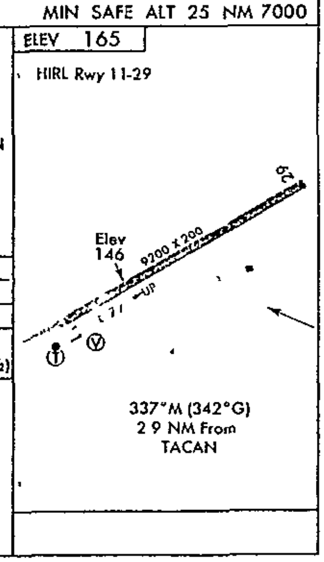


| CATEGORY | A | B | C | D |
|---|---|---|---|---|
| S 11 | 1780-2½ 1634 (1700 2½) | | | |
| CIRCLING * | 1780-2½ 1615 (1700-2½) | | | 1840-2½ 1675 (1700 2½) |

*Circling not authorized north of runway

**TACAN-1 RWY 11**

67°01 N-50°43 W

158

SONDRE STROMFJORD GREENLAND
SONDRESTROM AB

ORIGINAL PAGE IS
OF POOR QUALITY

NDB-1 AL 2051(MOT) CAMBRIDGE BAY
CAMBRIDGE BAY N W T, CANADA

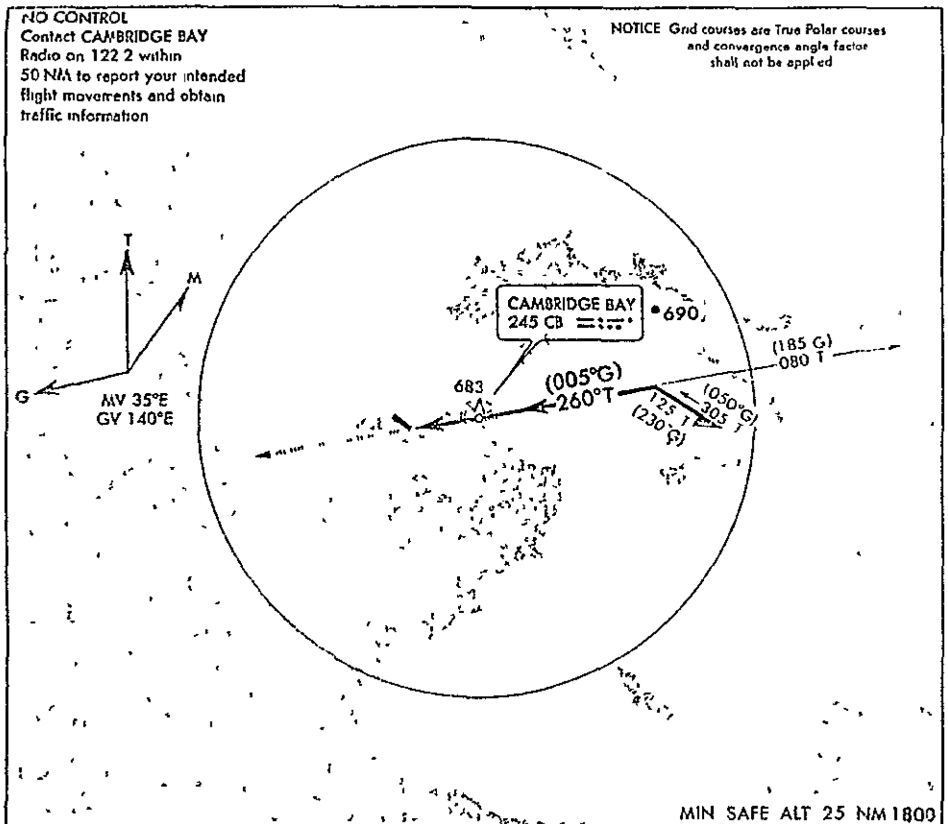


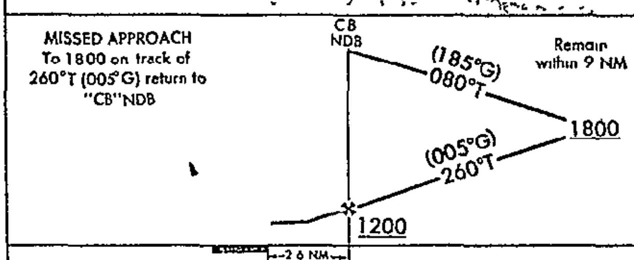


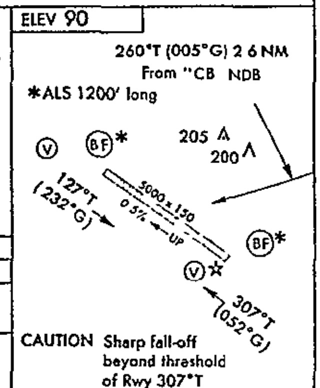


| CATEGORY | A | B | C | D |
|---|---|---|---|---|
| Circling ** | 600-1½ 510 (600 1½) | | 600-2 510 (600-2) | 700-2 610 (700 2) |

** All circling S and W of extended Rwy centerline

REIL Rwys 127°T and 307°T
MIRL Rwy 127°T — 307°T

| FAF to MAP 2 6 NM | | | | | |
|---|---|---|---|---|---|
| Knots | 60 | 90 | 120 | 150 | 180 |
| Min Sec | 2 36 | 1 44 | 1 18 | 1 02 | 0.52 |

NDB-1 69°06'N-105°08'W CAMBRIDGE BAY N W T CANADA
CAMBRIDGE BAY

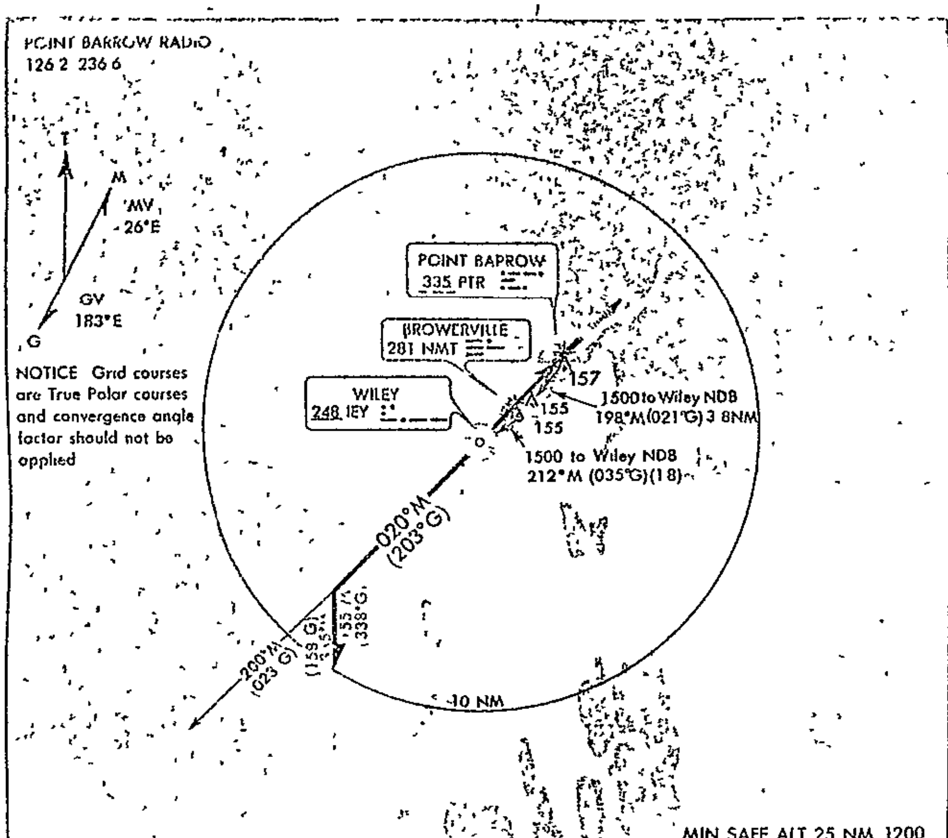


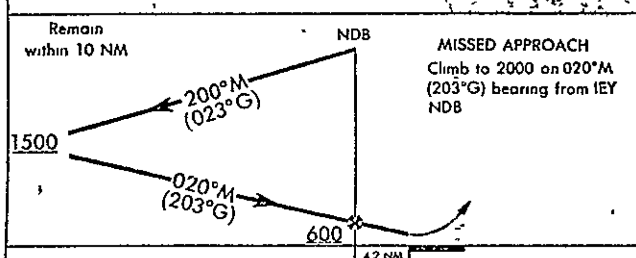


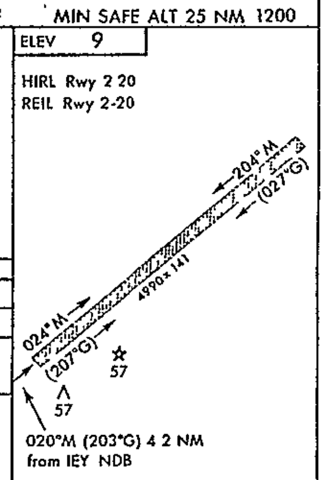


| CATEGORY | A | B | C | D |
|---|---|---|---|---|
| S 2 | 460-1 451 (500-1) | | | |
| CIRCLING | 460-1 451 (500-1) | | 460 1½ 451 (500-1½) | 560 2 551 (600-2) |

| FAF to MAP 4 2 NM | | | | | |
|---|---|---|---|---|---|
| Knots | 60 | 90 | 120 | 150 | 180 |
| Min Sec | 4 12 | 2 48 | 2 06 | 1 41 | 1 24 |

NDB RWY 2

71°20'N-156°38'W

POINT BARROW ALASKA
POINT BARROW NARL

# ILS RWY 35 TRUE

133
AL-2071 (MOT)

RESOLUTE
RESOLUTE BAY, N W T, CANADA

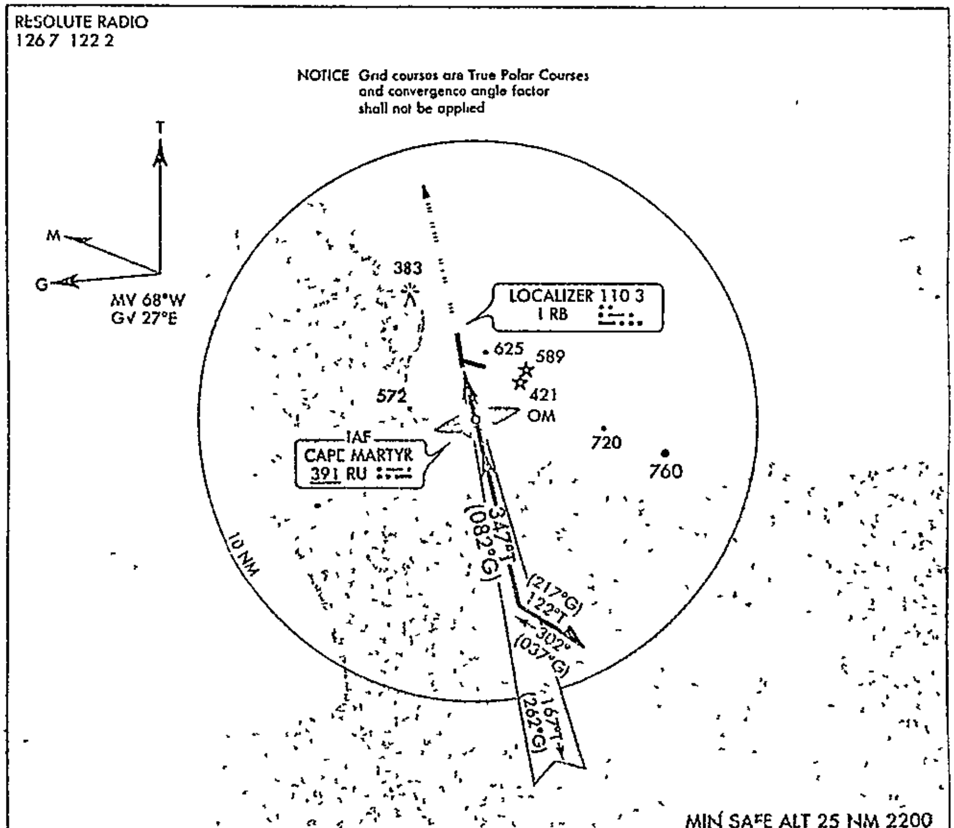


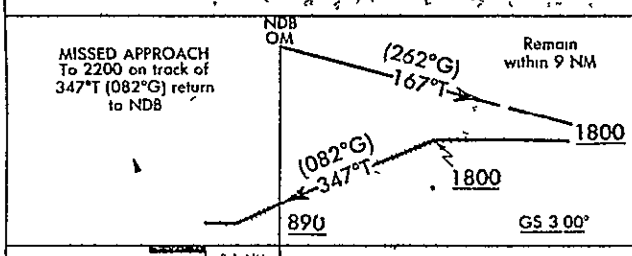


| CATEGORY | A | B | C | D |
|---|---|---|---|---|
| S ILS 35 | 520/26 318 (400-½) | | | |
| S LOC-35 | 520/50 318 (400-1) | | | |
| CIRCLING | 1140-1½ 919 (1000-1½) | | 1140-2 919 (1000 2) | |

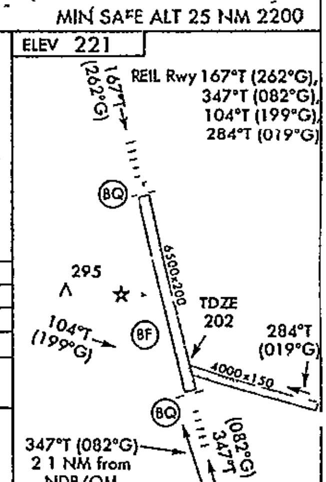


| FAF to MAP 2 1 NM | | | | | |
|---|---|---|---|---|---|
| Knots | 60 | 90 | 120 | 150 | 180 |
| Min Sec | 2 06 | 1 24 | 1 03 | 0 50 | 0 42 |

ILS RWY 35 TRUE 74°43'N-94°58'W RESOLUTE BAY N W T, CANADA

# ILS RWY 16

**THULE AB**
THULE, GREENLAND

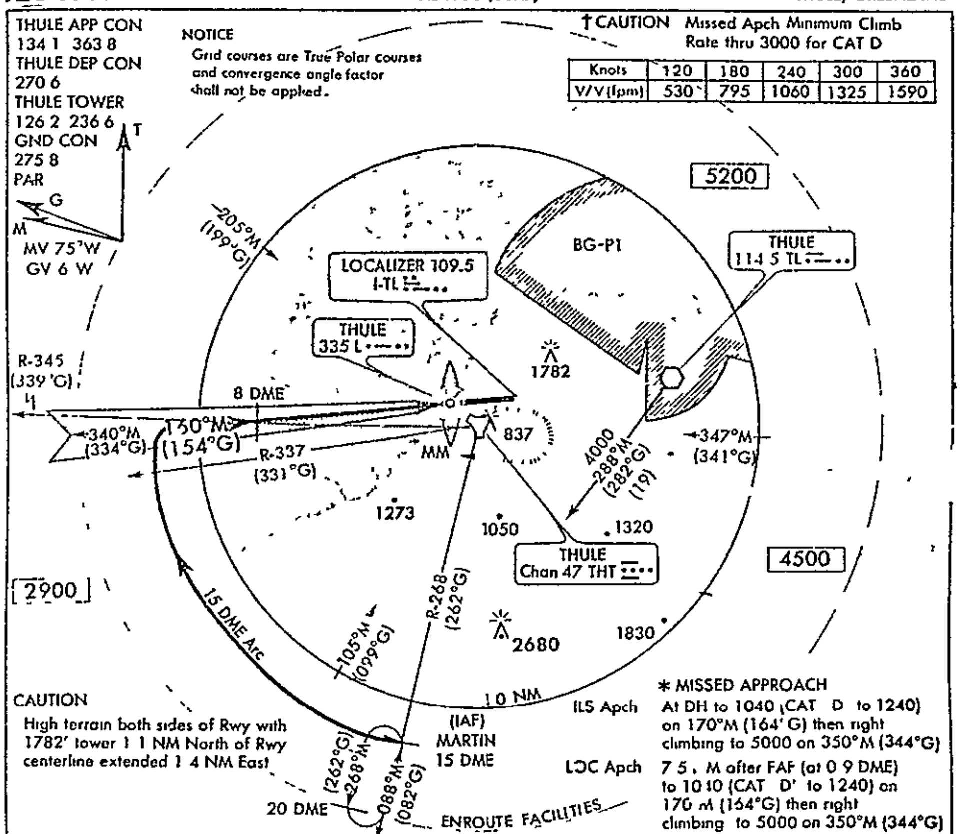


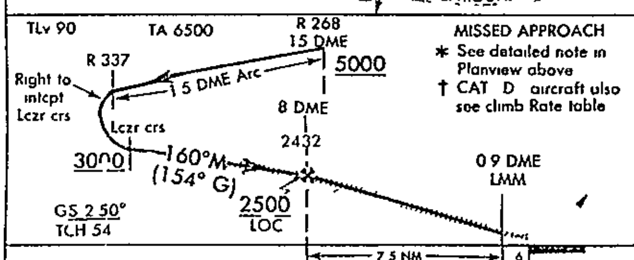


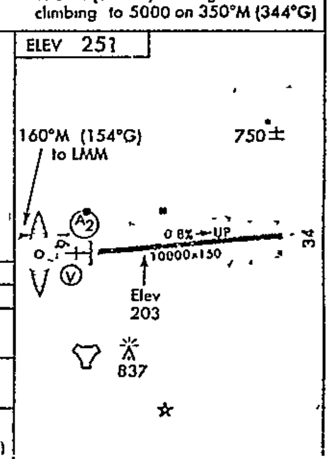


| CATEGORY | A | B | C | D |
|---|---|---|---|---|
| S ILS 16 | 403-½ 200 (200 ½) | | 403-¾ 200 (200 ¾) | |
| S LOC-16 | 440-½ 237 (200 ½) | | 440-¾ 237 (200-¾) | |
| CIRCLING** | 1140-1½ 889 (900 1½) | | 1140-1¾ 889 (900 1¾) | 1140-2 889 (900-2) |

ORIGINAL PAGE IS OF POOR QUALITY



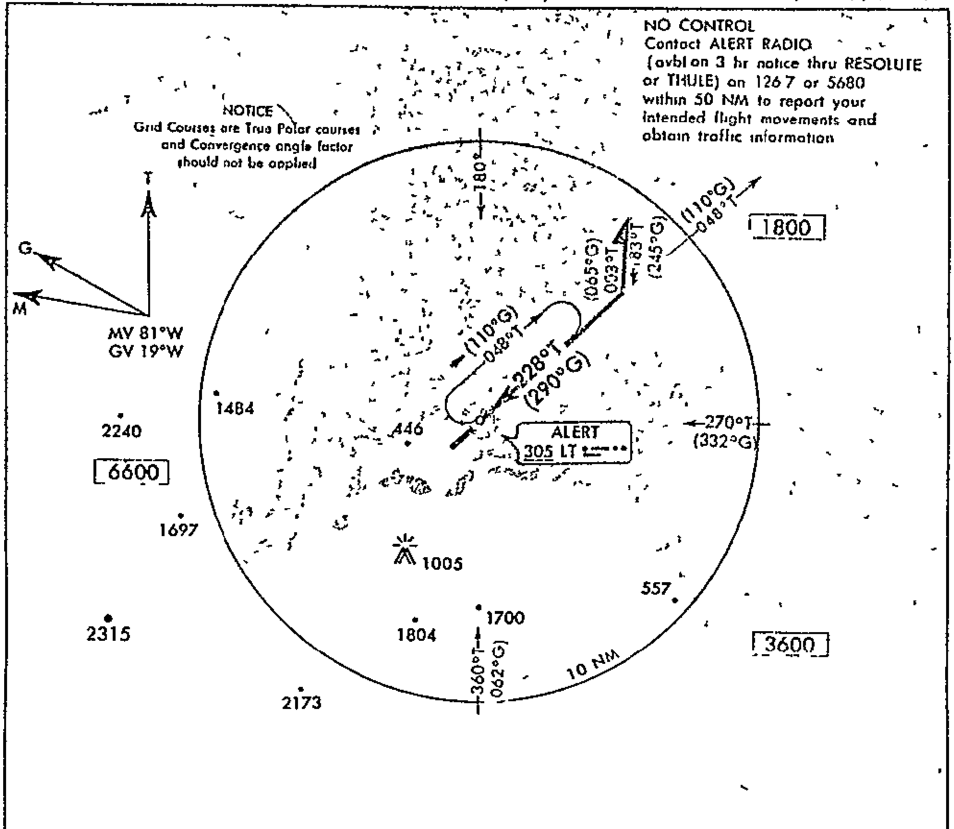


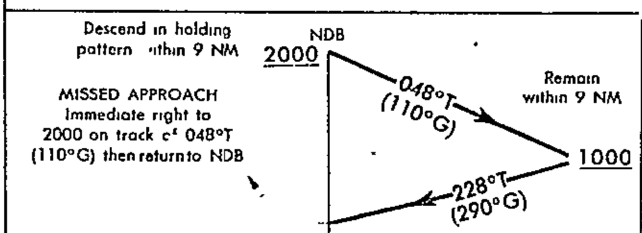


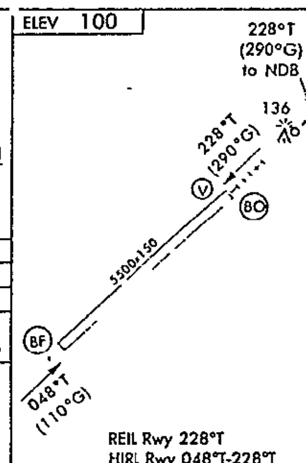


| CATEGORY | A | B | C | D |
|---|---|---|---|---|
| S 228°T | 500-1 400 (400-1) | | | |
| CIRCLING* | 800-1½ 700 (700-1½) | | 800-2 700 (700-2) | 900-2 800 (800-2) |

*All circling Northwest of airport

| 1. Report No. | 2. Government Accession No. | 3. Recipient's Catalog No. |
|---|---|---|
| NASA TM 78747 | | |

| 4. Title and Subtitle | 5. Report Date / 6. Performing Organization Code |
|---|---|
| SAM II GROUND-TRUTH PLAN - CORRELATIVE MEASUREMENTS FOR THE STRATOSPHERIC AEROSOL MEASUREMENT-II (SAM II) SENSOR ON THE NIMBUS G SATELLITE | 5. June 1978<br>6. 1250 |

| 7. Author(s) | 8. Performing Organization Report No. |
|---|---|
| P. B. Russell, M. P. McCormick, L. R. McMaster, T. J. Pepin, W. P. Chu, and T. J. Swissler | |

| 9. Performing Organization Name and Address | 10. Work Unit No. / 11. Contract or Grant No. |
|---|---|
| NASA Langley Research Center<br>Hampton, VA 23665 | 10. 642-14-03-07<br>11. |

| 12. Sponsoring Agency Name and Address | 13. Type of Report and Period Covered / 14. Sponsoring Agency Code |
|---|---|
| National Aeronautics and Space Administration<br>Washington, DC 20546 | 13. Technical Memorandum<br>14. |

15. Supplementary Notes

P. B. Russell, SRI International, Menlo Park, CA, 94025; M. P. McCormick and L. R. McMaster, Langley Research Center; T. J. Pepin, Univ. of Wyoming, Laramie, WY, 82070; W. P. Chu, Langley Research Center; and T. J. Swissler, Systems and Applied Sciences Corporation, Riverdale, MD, 20840

16. Abstract

This document describes the ground-truth plan for correlative measurements to validate the Stratospheric Aerosol Measurement-II (SAM-II) sensor data. SAM-11 will fly aboard the Nimbus-G satellite scheduled for launch in the fall of 1978 and measure stratospheric vertical profiles of aerosol extinction in high latitude bands. The plan gives details of the location and times for the simultaneous satellite/correlative measurements for the nominal launch time, the rationale and choice of the correlative sensors, their characteristics and expected accuracies, and the conversion of their data to extinction profiles. In addition, an overview of the SAM-II expected instrument performance and data inversion results are presented. Various atmospheric models representative of polar stratospheric aerosols are used in the SAM-II and correlative sensor analyses.

| 17. Key Words (Suggested by Author(s)) | 18. Distribution Statement |
|---|---|
| Stratospheric Aerosol, Satellite Measurements, Ground Truth | Unclassified - Unlimited |

| 19. Security Classif. (of this report) | 20. Security Classif. (of this page) | 21. No. of Pages | 22. Price* |
|---|---|---|---|
| Unclassified | Unclassified | 113 | $5.50 |

* For sale by the National Technical Information Service, Springfield Virginia 22161